

Rational Design of Functional Peptide-Gold Hybrid Nanomaterials for Molecular Interactions

Xiaohu Liu, Qingwen Zhang, Wolfgang Knoll,* Bo Liedberg,* and Yi Wang*

Gold nanoparticles (AuNPs) have been extensively used for decades in biosensing-related development due to outstanding optical properties. Peptides, as newly realized functional biomolecules, are promising candidates of replacing antibodies, receptors, and substrates for specific molecular interactions. Both peptides and AuNPs are robust and easily synthesized at relatively low cost. Hence, peptide-AuNP-based bio-nano-technological approaches have drawn increasing interest, especially in the field of molecular targeting, cell imaging, drug delivery, and therapy. Many excellent works in these areas have been reported: demonstrating novel ideas, exploring new targets, and facilitating advanced diagnostic and therapeutic technologies. Importantly, some of them also have been employed to address real practical problems, especially in remote and less privileged areas. This contribution focuses on the application of peptide-gold hybrid nanomaterials for various molecular interactions, especially in biosensing/diagnostics and cell targeting/imaging, as well as for the development of highly active antimicrobial/antifouling coating strategies. Rationally designed peptide-gold nanomaterials with functional properties are discussed along with future challenges and opportunities.

1. Introduction

Although gold nanoparticles (AuNPs) have been scientifically utilized over one century,^[1] it is not until the last two decades that we have seen a dramatic increase in applications of AuNP

Dr. X. Liu, Dr. Q. Zhang, Prof. Y. Wang
School of Biomedical Engineering
School of Ophthalmology & Optometry
Wenzhou Medical University
Xueyuan Road 270, Wenzhou 325027, China
E-mail: wangyi@wibe.ac.cn

Dr. X. Liu, Dr. Q. Zhang, Prof. Y. Wang
Wenzhou Institute
University of Chinese Academy of Sciences
Xinsan Road 16, Wenzhou 325001, China

Prof. W. Knoll
Austrian Institute of Technology
Giefinggasse 4, Vienna 1210, Austria
E-mail: wolfgang.knoll@ait.ac.at

Prof. B. Liedberg
Centre for Biomimetic Sensor Science
School of Materials Science and Engineering
Nanyang Technological University
50 Nanyang Avenue, Singapore 639798, Singapore
E-mail: bliedberg@ntu.edu.sg

 The ORCID identification number(s) for the author(s) of this article can be found under <https://doi.org/10.1002/adma.202000866>.

DOI: 10.1002/adma.202000866

in biosensing development.^[2] In the early twentieth century, the first report of bioassay based on AuNPs for diagnosis of syphilis was presented,^[3] though there was an obvious lack of selectivity due to the use of unmodified AuNPs. As the technology and knowledge of surface chemistry/biology developed over the years, AuNPs were modified with antibodies providing improved selectivity for a series of sensing/diagnostic applications (e.g., home pregnancy test).^[4–6] However, at that time, AuNPs were employed only as colorimetric labels. The relatively large size of the antibody prevented the observation of sufficiently optical shifts resulting from AuNP aggregation. In 1996, Mirkin and colleagues reported on the use of functionalized AuNPs for the detection of target nuclei acids,^[7] which was an important milestone in the era of AuNP-based biosensing. Novel functionalized AuNPs with relevant biomolecules have since then enabled a vast number of strategies targeting metal ions,

organic molecules, oligonucleotides, and proteins.^[8] Peptide as a newly realized bio-functional candidate has played an important role in recent years for targeting numerous biological and chemical molecules. The pros and cons derived from the intrinsic properties of peptide-AuNP conjugates, which are employed by most of the applications, are summarized in **Table 1**.

Several excellent reviews have thoroughly described AuNP-based biosensors categorized either by their targets or detection methods.^[1,8] There is, however, a few that reviews the peptide-gold hybrid nanomaterial as an interactive biotechnological tool.^[9] Hence in this review, we focus on works based on peptide-gold (mainly AuNPs) hybrid nanomaterials from the aspect of peptide functionalities and discuss their bio-applications, including biosensing, cell targeting, and imaging as well as antimicrobial and antifouling coating development (**Figure 1**). In order to chronologically illustrate the development of peptide-gold based applications over the last 25 years, important remarks have been highlighted in **Figure 2**. After almost one decade since the well-known DNA-AuNPs assembling^[7] (1996, purple broken frame, **Figure 2**), peptides designed for molecular recognition^[10] and assembled with AuNPs were intensively studied^[11,12] and applied to various approaches such as in vitro enzymatic assays^[13,14] (2002–2006, blue-green frames, **Figure 2**). Cellular targeting related assays such as cellular imaging,^[15] cell binding,^[16,17] penetration and nuclear targeting,^[18] brain-blood barrier (BBB) translocation,^[19] and cancer therapies^[20] were then developed in the following decade

Table 1. Pros and cons of peptide and gold nanoparticles for bio-applications.

Peptide	AuNPs
Pros:	
Relatively small and robust	Chemically inert
Excellent biocompatibility	High surface to volume ratio
Minimal antigenicity	Great optical properties
Easy to chemically synthesize and modify	Strong gold-sulfur linkages for functionalization
Potential high-affinity to target molecules	Excellent microscopic probes
Chromatographic purity	Plasmonic interactive nanomaterial
Cons:	
Lack of complimentary components (vs nucleic acids)	Lack of fluorescence [vs quantum dots (QDs), etc.]
Low binding affinity generally (vs antibody)	Lack of energy conversion ability (vs QD, graphene, etc.)
Fast digestion rate in vivo (vs protein)	Not porous normally (vs Metal organic frameworks)
Possible self-aggregation	Possible steric hindrance

and are still attractive (2009–2016, light green-dark red frame, Figure 2). Most recently, emerging functions/applications of peptide-AuNPs were presented such as catalysts,^[21] antimicrobial,^[22] assisting multi-photon microscopy,^[23] and formation of chiral AuNPs structures,^[24] which offered new directions of this subject (2012–2018, circles, Figure 2).

2. Interactive Peptide and AuNP Conjugates

2.1. Functional Synthetic Peptide

Peptide is one of the most important and basic materials that bridges chemistry and biology, influencing important

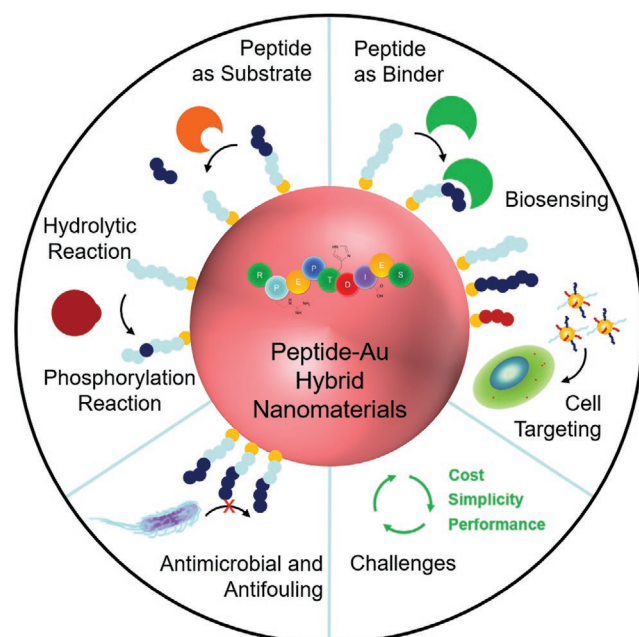


Figure 1. Schematic illustration of the structure of this review.



Wolfgang Knoll earned a Ph.D. degree in biophysics from the University of Konstanz in 1976. From 1991 to 1999, he was the laboratory director for Exotic Nanomaterials in Wako, Japan, at the Institute of Physical and Chemical Research (RIKEN). From 1993 to 2008, he was director of the Materials Science

Department at the Max Planck Institute for Polymer Research in Mainz, Germany. Since April 1, 2008, he is the scientific managing director of the AIT Austrian Institute of Technology. In 2012, he received an honorary doctorate from the University of Twente, The Netherlands.



Bo Liedberg is currently a full professor of materials science and the director of the Center for Biomimetic Sensor Science (CBSS), Nanyang Technological University (NTU), Singapore. He was also a full professor of sensor science and molecular physics at Linköping University, Sweden (2012). Prof. Liedberg is heading a research group primarily

devoted to soft materials science including surface chemistry, self-assembly, supramolecular chemistry, and biomimetics. Professor Liedberg is also heavily involved in the development of new biosensor and diagnostic tools for field applications. He is currently serving as the senior executive director for interdisciplinary graduate programs at NTU.



Yi Wang is currently a professor at Wenzhou Medical University and Wenzhou Institute, University of Chinese Academy of Sciences. He obtained his Ph.D. in 2010 from the Max-Planck Institute for Polymer Research in Mainz, Germany. After that, he worked as a research fellow at the Austrian Institute of Technology, Austria, and

Nanyang Technological University, Singapore, from 2011 to 2015. His research interests include the development of plasmonic nanostructure, nanocomposites, novel polymers, and peptide-functionalized materials for optical and electrical biosensors.

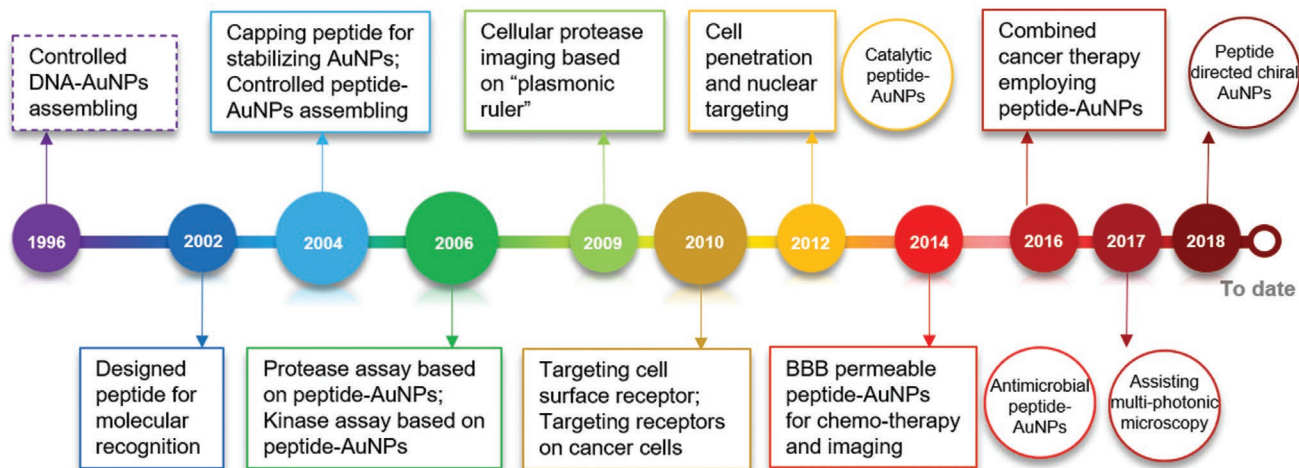


Figure 2. Important remarks in developing applications based on peptide-gold nanoparticles over the last 25 years. (Note that the timeline involves only those representative works to the best of our knowledge, and some might not be included).

physiological functions. They are known to influence the cell-cell communication by receptor bindings and are involved in many biochemical processes such as metabolism, pain, and reproduction.^[25] Besides the physiological functions of natural peptides, rationally designed synthetic peptides or screened peptide libraries are becoming extremely useful as recognition entities,^[26–28] in self-assembling nanostructures^[29–34] and other hybrid materials.^[12,35–37] The major advantages of considering peptides as potential candidates for designing novel recognition entities or receptors are summarized below.

First, theoretically there is nearly an infinite number of chemical combinations leading to a large number of unique peptides. It provides a gigantic peptidyl-reservoir for design and selection of functional peptides. This has paved the way for the development of random combinatorial methods which are based on functional selection via binding affinity.^[38–40] In one of the representative methods, phage display, foreign cDNA library coding a vast polypeptide pool is fused with phage genomes of capsid proteins, followed by the expression of various polypeptides on phage surface. The subsequent screening of peptide of interest is done by cycles of binding (to bait molecule), elution, and amplification (Figure 3A).^[38,40]

Second, functional peptides can be designed and synthesized to mimic protein substrates with specific binding site, taking advantages of natural selection (Figure 3B). The synthesis of peptide has been greatly accelerated by Merrifield's pioneering work on solid phase peptide synthesis,^[41] as large amounts of highly pure peptides since then can be automatically synthesized at a relatively low cost. Additionally, chemical synthesis of peptides also offers opportunities to incorporate an extended spectrum of non-proteinogenic amino acids as well as other building blocks, thus providing a much higher flexibility in obtaining synthetic peptides with unique biological activity and/or structural preference.^[26]

Third, further modification of a selected peptide with small ligands offers a strategy to boost binding affinity between designed peptide receptor and its target.^[10,42] Besides small ligands, discontinuous peptide chains derived from the same binding pocket can be chemically combined through a scaffold

molecule to spatially mimic the 3D-structure for a better interaction against the target protein (Figure 3B).^[43]

Fourth, computational tools have greatly facilitated the rational design of functional peptides by providing key insights toward not only the target-peptide interactions, such as protein-peptide docking methods,^[44] but also surface-peptide interactions when incorporated with nanomaterials (Figure 3C).^[45–50] For instance, peptide/nanowire materials have been designed for the specific recognition of vapors of acetic acid and ammonia.^[47] The mechanism of the binding specificity between acetic acid and its recognition peptide (RVNEWVID) and ammonia with its corresponding recognition peptide (DLESFLD) was investigated theoretically by Becke–Lee–Yang–Parr 3 parameter density functional theory. The calculations revealed that acid/base binding equilibria between the peptides and vapor compounds were significant factors contributing to selectivity. In addition, the secondary structure was important even in these relatively short-chain sequences. Other important interactions, including ionic attraction, also was identified for the acetic binding peptide because of its glutamic acid (Glu) 4-arginine (Arg) 1 “salt-bridge.” The binding energy calculations confirm that the reaction of the acetic acid analyte with the peptide is exothermic ($-5.5 \text{ kcal mol}^{-1}$ of energy) and preferentially bind acetic acid to the Arg1 N-terminus. While for the ammonia-binding peptide, the ammonia reacts favorably ($-7.4 \text{ kcal mol}^{-1}$) with the N-terminal aspartic acid residue to form a unique hydrogen-bond center at the terminal acid and amine groups. Upon exposure to target acetic acid and ammonia, the hybrid peptide/nanowire materials demonstrate the ability to orthogonally sense at low concentration ($\approx 100 \text{ ppm}$) based on the nanowire resistance changes. The advanced molecular dynamics simulations based on reactive force-field (ReaxFF)^[48] or Chemistry at Harvard Macromolecular Mechanics^[50] have been also reported to study the peptide absorption/adaptation on gold surface as well as the peptide effect on nanoparticle motions and interparticle interactions. In these studies, experimental findings have been confirmed and explained in details, providing insights for future design of novel functional peptide-gold nanomaterials.

Fifth, the intrinsic thermal stability of peptides is generally higher as compared to antibodies,^[51,52] which in particular is

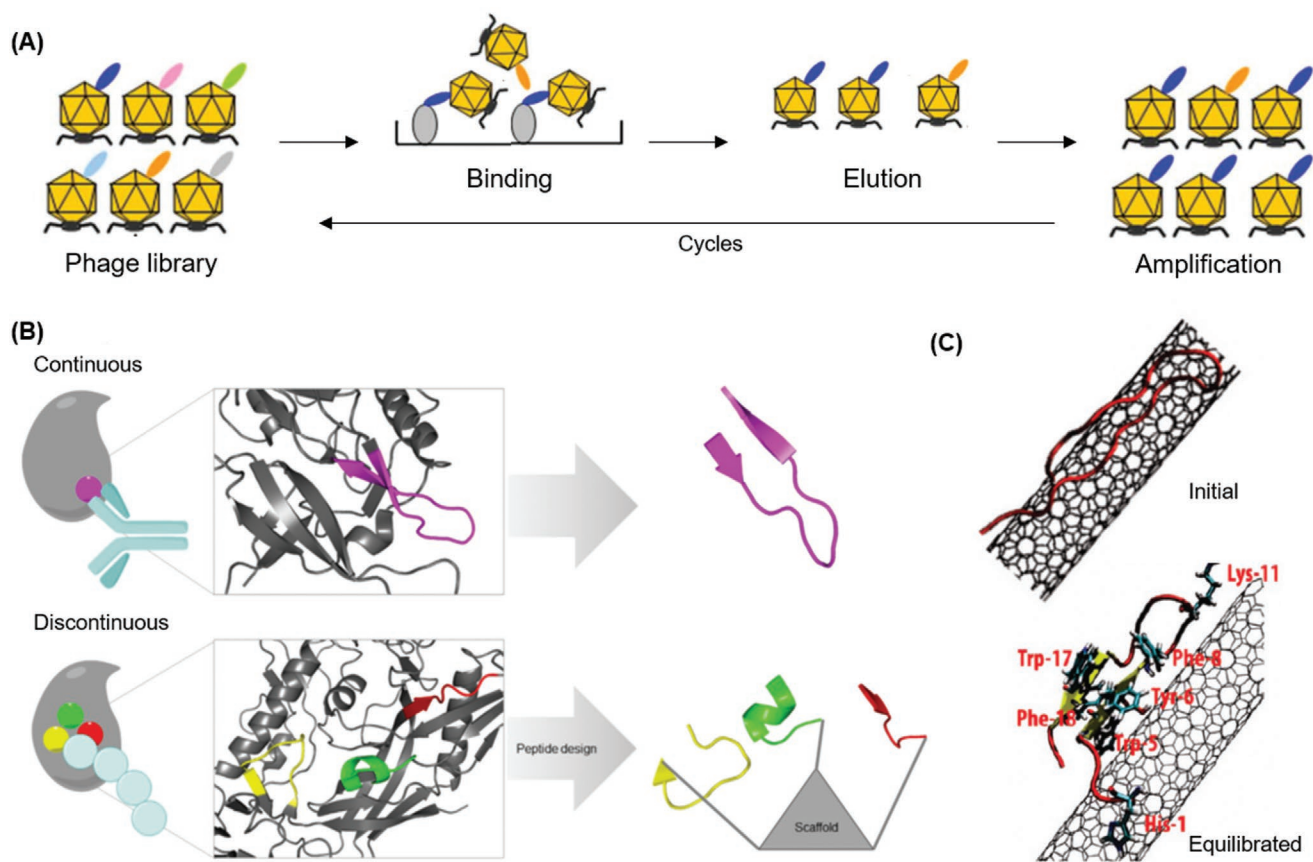


Figure 3. A) Schematic illustration of phage display starting with a phage library (different colors of polypeptides on phages surface). The followed peptide selection is done by cycles of binding (blue), elution (blue and non-specific orange), and amplification. The bait molecule immobilized represents the target. The non-specific peptide (orange) is marginalized by multiple cycles of selection. Reproduced with permission.^[38] Copyright 2009, Springer-Verlag. B) Upper: Peptide design with single continuous sequence (pink) in the binding site as an epitope. Lower: Peptide design with three peptide fragments (yellow, green, and red) in the binding pocket linked by a molecular scaffold to mimic the 3D structure of natural protein. Reproduced with permission.^[26] Copyright 2016, Frontiers Media S.A. C) Molecular dynamics simulations for peptide structure prediction upon binding onto single-wall carbon nanotube (SWNT). Starting with initial parallel configuration (upper), an equilibrated configuration with a β -sheet structure was obtained, suggesting tryptophan (Trp)-5 as a key player for the adsorption of peptide to SWNT. Reproduced with permission.^[46] Copyright 2010, American Chemical Society.

important for detection kits with longer shelf-life and minimal storage requirement. It thus opens up field testing in remote areas where the temperature can be high and standard lab infrastructure such as refrigeration is rare.

2.2. Stabilization of AuNPs by Peptide

There are numerous (bio-)molecules/polymers that can be directly immobilized onto the surface of AuNPs without jeopardizing the colloidal stability which enables further usages with highly specific receptors.^[2] Indirect immobilization can be achieved as well by forming self-assembled monolayer (SAM) which stabilizes the colloidal suspension and facilitates further immobilization. Particularly with peptides, the most common method involves introduction of a terminal cysteine (Cys) whose thiol group on the side chain binds to gold surface via covalent manner^[53,54] leading to an “end-point” anchored peptide on the AuNP surface. This attachment between cysteine and gold surface also has been studied in detail via classical

molecular dynamics simulations such as reactive force fields, ReaxFF.^[48,55] However, due to the chemical versatility of the peptides, the accessibility of the end-point attached peptide might be affected due to multi-point anchoring sites. This is common when using peptides containing positively charged residues [lysine (Lys) and Arg] that are prone to electrostatically interact with the negatively charged citrate-capped AuNP surface, resulting in the colloidal gold suspension collapses. Other methods for the modification of AuNPs with peptides include ligand exchange, chemical reduction, and chemical conjugations such as metal/oxide-binding, the amino-carboxyl coupling, metal coordination, and so forth.^[2,9]

Stable peptide–AuNP conjugation requires optimization of both peptide (e.g., charges, hydrophobicity, length, etc.) and surrounding buffer (e.g., pH, ionic strength, buffer type, etc.).^[11,56] For citrate capped AuNPs, it is crucial to keep the peptide negatively charged or neutral, or at least carrying a minimum of positive charged residues (see discussion about multipoint binding above). Moreover, the curvature of nanoparticles influences surface coverage conformation and accessibility

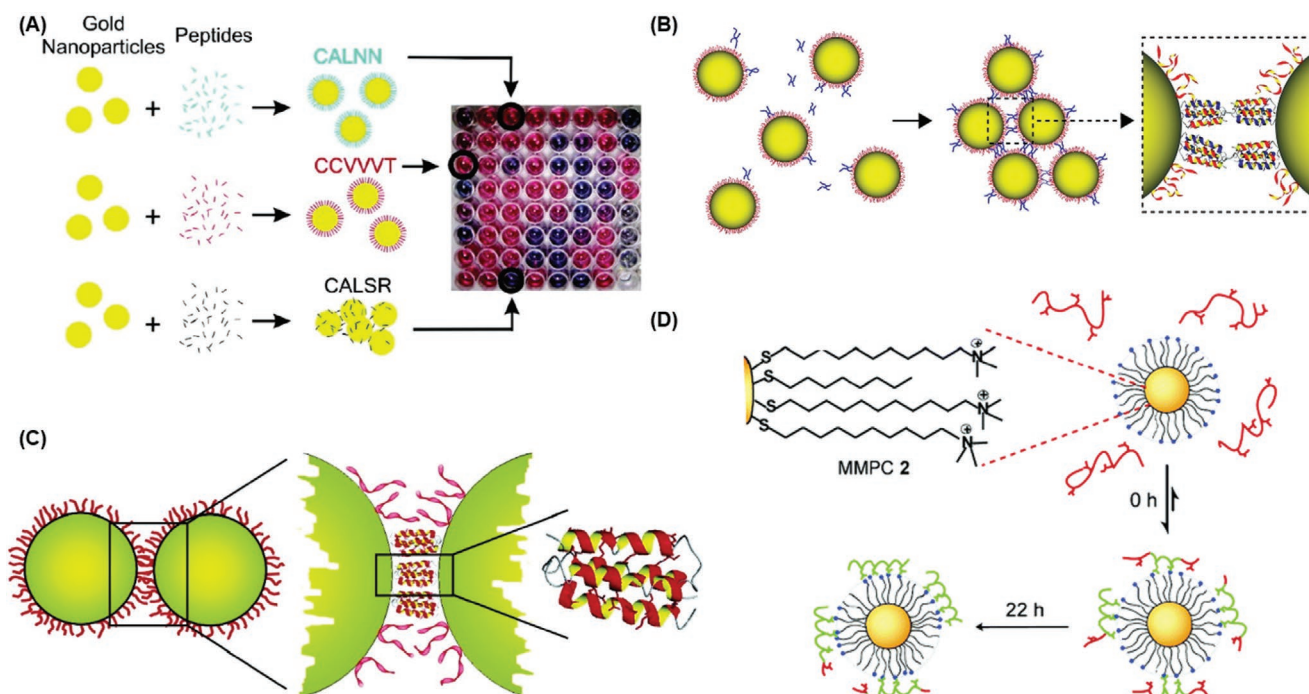


Figure 4. A) The selection of protecting pentapeptide (CALNN) which upon immobilization features extraordinary stability of AuNPs, as compared to two other peptides. Reproduced with permission.^[11] Copyright 2004, American Chemical Society. B) AuNP aggregation induced by folding of complementary peptides: hetero-dimerization. Reproduced with permission.^[58] Copyright 2008, American Chemical Society. C) Peptide folding induced by AuNP aggregation: homo-dimerization. Reproduced with permission.^[59] Copyright 2006, American Chemical Society. D) Functionalized AuNP as template for folding of synthetic peptides into alpha-helices. Reproduced with permission.^[60] Copyright 2007, The Royal Society of Chemistry.

of the immobilized peptides. An excellent example of peptide which offers high stability upon decoration on AuNPs has been reported by Lévy et al. using a pentapeptide (CALNN).^[11] This peptide was selected out of 58 various peptides giving rise to extraordinary colloidal stability when immobilized on AuNPs (i.e., it was found to be stable in 1 M NaCl or in acidic buffer pH = 4). First of all, the N-terminal Cys residue enabled endpoint anchoring of peptide onto the gold surface. The following two hydrophobic residues alanine (Ala) and leucine (Leu) facilitated the monolayer formation via lateral inter-molecular hydrophobic interaction. Last but not least, two asparagine (Asn) residues at un-capped C-terminal provided additional monolayer stability via lateral hydrogen bond interaction and colloidal stability because of negative charges on outer layer at neutral pHs. In addition, the gradually increasing size of side chains on Ala, Leu, and Asn ensured an effective and dense coverage of the curved AuNP surface. As shown in **Figure 4A**, the proposed pentapeptide CALNN and the hexapeptide CCVVVT provided excellent protection and dispersion of AuNPs mainly due to the outer layer charges whereas CALSR resulted in aggregation.

2.3. Controlled Interactions of Peptide-AuNP Conjugates

Opposite to protection, peptide folding may dramatically decrease the stability of gold colloid suspensions.^[57] In the belt and brace model, three pieces of peptide of the coiled-coil Leu zipper was employed. Half fragments were first immobilized on AuNPs that would trigger aggregation upon addition

of a third peptide due to coil-coil folding. Another example of folding induced functionalized AuNPs assembly was demonstrated by Aili et al. employing a complementary pair of de novo designed 42-mer polypeptides which favored heterodimerization to form anti-parallel helix bundles and subsequent aggregation of AuNPs (Figure 4B).^[58] Interestingly, the assembly/aggregation of AuNPs conversely could induce the folding of peptide. The glutamic acid (Glu)-rich polypeptide of the same complementary peptide pair functionalized AuNPs were able to induce the homodimerization of peptides on adjacent particles resulting in the well-structured helix bundles (Figure 4C).^[59] The colloidal stability of the so-formed peptide-AuNP conjugates was controlled by tuning the buffer pH around the calculated pI of the polypeptide (pI ≈ 4.5) due to the loss of charge repulsion. In Rotello's group, pre-structured synthetic peptides were found folding gradually into alpha-helices upon binding to AuNP receptors. It was argued to be due to a surface templating process in which the positively charged surface of the modified AuNPs, as a template, guided and stabilized the peptides folding through noncovalent binding (Figure 4D).^[60,61]

In a summary, peptides can be selected or rationally designed, synthesized, and immobilized on AuNPs directly by terminal cysteine to form interactive conjugates despite many other immobilization methods. However, the stability of colloidal nanoparticles must not be jeopardized during the process. Usually, peptides with negative charges and only one cysteine anchor do not induce any significant change of the colloidal stability. Taking the curvature of nanoparticle surface into consideration, it is better for peptides to have a

conical-like shape to ensure a full coverage of AuNP surface area and hence a better stability of the system. Peptide folding may induce controlled aggregation of AuNPs, providing a promising avenue for the development of colorimetric sensing platforms. Notably, all the activities regarding to peptide–gold nanomaterials such as design of peptide,^[44] preparation/stability of peptide–gold hybrid, and interaction among nanoconjugates can be studied by advanced simulation methods for revealing underneath theoretical details and further improvements.^[55,62,63] The stable and interactive peptide–AuNP conjugates mentioned in this section provides the basis for bio-applications and other functional interaction studies.

3. Targeting Molecules via Peptide–Gold Hybrid Nanomaterials

Novel assembly-folding interactive peptide–gold hybrid nanomaterials have been extensively applied in molecular targeting and biosensing such as medical diagnostics, therapeutics, and environmental monitoring. The peptides are usually designed with specific functionalities such as enzymatically active sites for hydrolytic reactions and phosphorylation reactions (Section 3.1), and peptide binders with specific affinity to biomolecules and targets/receptors on (sub)cellular membranes (Section 3.2).

3.1. Peptide–Gold Substrates for Enzymatic Analysis

It is essential to maintain the physiological homeostasis by optimizing the intrinsic enzyme activities for all beings. In other words, disruptions of any enzymatic reaction will lead to potential pathological outcomes. It is therefore important to monitor (sense) the activities under physiological conditions with/without the presence of either inhibitors or activators. In the sensing process, synthetic peptides are able to mimic natural proteins as substrates for activity detection of various enzymes including hydrolases, transferases, and lyases. Those peptides are usually designed on the basis of known biochemical reactions with functional motifs. By using AuNPs as the sensing platform, numerous assays have been developed over the last decade.^[64,65]

3.1.1. Hydrolytic Reactions

Proteases: Proteases are the most important hydrolases. They hydrolyze the amide bond that links two neighboring amino acids in proteins or peptide substrates. The high specificity is ensured by a particular sequence that the protease recognizes. Proteases play a key role in many physiological processes, including cellular activities such as division, differentiation, migration, aging, death, thermal shock, and morphogenesis, and tissue/system activities such as reorganization of tissues, angiogenesis, immunity, hemostasis, wound healing, ovulation, and fertilization.^[66,67]

Various detection approaches targeting proteases have been developed based on peptide–AuNPs, among which colorimetric assays are the most convenient ones. One of such remark-

able colorimetric assays for the detection of protease thrombin was reported by Scrimin et al.,^[13] illustrating the basic detection principle. They employed free peptide substrate (i.e., non-immobilized peptide substrate) that could cross-link bare AuNPs resulting in aggregation. A peptide containing specific recognition sequence was suitable for thrombin cleavage. As both ends were terminated by Cys, addition of the specific peptide induced immediate aggregation of AuNPs. In the presence of the corresponding protease thrombin, the peptide substrate was cleaved by the target so that it reduced the propensity of aggregation in a concentration-dependent way (Figure 5A). Moreover, a peptide with six positively charged arginine (Arg₆) triggered the aggregation of negatively charged citrate-capped AuNPs due to electrostatic interactions, which resulted in a red-shift of the plasmon absorption peak. However, in the presence of trypsin, the Arg₆ were hydrolyzed into fragments, the electrostatic interactions between AuNPs and arginine residues were weakened, and therefore, no AuNPs aggregation was observed. This feature was used to develop a label-free detection of trypsin with limit of detection 1.6 ng mL⁻¹ and screening inhibitors of trypsin.^[68]

However, the unprotected AuNPs were fragile to other destabilizing molecules that unfortunately lead to aggregation and many false negatives. Recently, matrix metalloproteinase-7 (MMP-7) was detected in Kim's group by employing free peptide substrate in a similar way, but with carboxyl-protected AuNPs (Figure 5B). In their case, the presence of metal ions could coordinate histidine (His)-tagged peptide to AuNPs and induced the aggregation,^[69] whereas the protease MMP halved the peptides resulting in no significant color changes upon mixing (Figure 5C).

Oppositely, a novel colorimetric assay which employed the re-dispersion of pre-aggregated AuNPs was presented by Stevens and her co-workers (Figure 5D).^[70] The particles were first aggregated by immobilization of Cys-containing peptide with Fmoc-protecting groups due to the π - π interactions of aromatic rings (Peptide 1 in Figure 5E). When the target thermolysin was present, the peptide substrates would be cleaved (Peptide 2 in Figure 5E) and the AuNPs re-dispersed with color changing from purple to red in just a one-step process (Figure 5F). The re-dispersion rate of pre-aggregated AuNPs was dependent on the concentrations of thermolysin as indicated in Figure 5G, where 250 ng mL⁻¹ showed an obvious faster rate than 43 ng mL⁻¹. The limit of detection (LOD) was extremely low (90 zg mL⁻¹) due to the fast-catalytic event. The strategy was further developed by redesigning the peptide substrate into a prostate-specific antigen (PSA) biosensor, which demonstrated the versatility. One of the several concerns that must be solved in this case was the issue of steric hindrance that could turn peptide substrates inaccessible to proteases leading to a potential failure of hydrolysis.^[71,72]

More recently Chen et al. utilized the aforementioned peptide-functionalized AuNPs and developed a colorimetric assay for the detection of MMP-7 (Figure 6A).^[73] By spiking MMP-7 into the peptide–AuNPs system, the protease degraded the peptides immobilized on AuNPs, which was proved by ellipsometric contrast images (Figure 6B). As a result, the surface truncated peptides lost too many negative charges leading to the aggregation of AuNPs. The catalytic process was very rapid allowing near real-time detection in minutes with an LOD of 5 nM. On the other hand, from a biologically mimicking point of view,

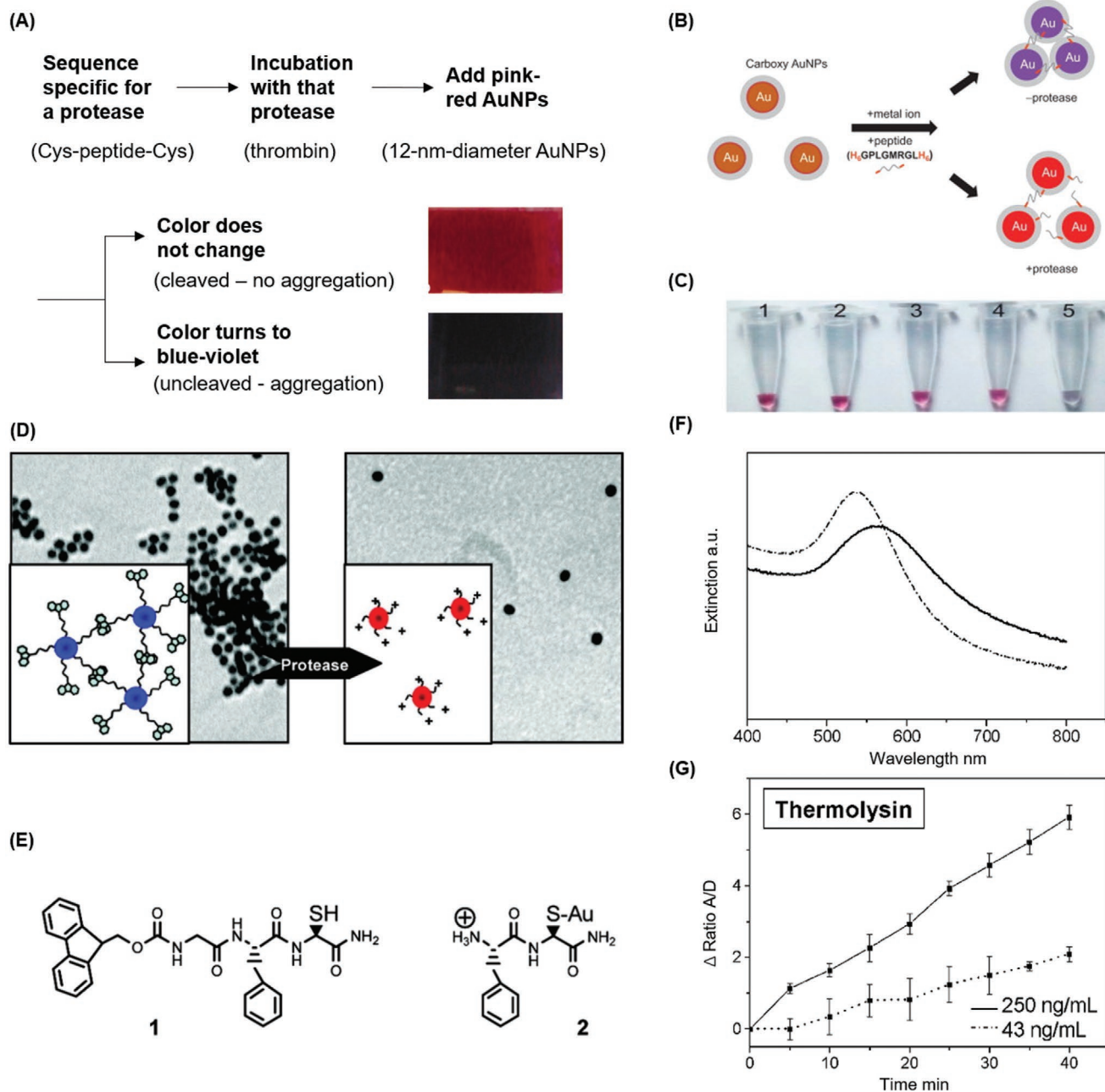


Figure 5. A) Outline of colorimetric protease sensing process by using designed peptides and AuNPs. Reproduced with permission.^[13] Copyright 2006, National Academy of Sciences. B) Schematic illustration of carboxy-protected AuNP-based colorimetric assay for proteases by using designed His₆-ended peptides and metal ions. C) Photograph of the carboxy AuNPs in solution with different peptides in the presence or absence of nickel ions after 60 min incubation (1: AuNP, 2: AuNP/His₆-pep, 3: AuNP/His₆-pep/Ni²⁺, 4: AuNP/His₆-pep-His₆, 5: AuNP/His₆-pep-His₆/Ni²⁺). Reproduced with permission.^[69] Copyright 2013, Elsevier B.V. D) Schematic illustration and corresponding TEM images of the re-dispersion of aggregated AuNPs modified with protease-cleavable Fmoc remaining peptides due to proteolytic removal of terminal hydrophobic groups. E) Designed peptide structures: 1, intact peptide substrate for thermolysin; 2, after cleavage. F) UV-vis spectra of 1-AuNPs before (solid line) and after addition of enzyme for 6 h incubation (dotted line). G) Re-dispersion levels of pre-aggregated 1-AuNPs (indicated by Δ ratio A/D) at 5 min intervals for 250 and 45 ng mL⁻¹ thermolysin. Reproduced with permission.^[70] Copyright 2007, American Chemical Society.

Liu et al. had reported novel biotinylated peptide substrates to mimic synaptosomal-associated protein-25 which were utilized in AuNP-based assays for colorimetric detection of botulinum neurotoxin serotype A light chain (BoLcA).^[72] Two different assay strategies were described in Figure 6C. In these proteolytic assays, biotinylated peptides served as triggers for the

aggregation of AuNPs, while the cleavage of these peptides by BoLcA prevented nanoparticles from aggregation (Figure 6D,E). It demonstrated LODs ranging from 0.1 to 5 nM of BoLcA with an overall assay time of 4 h. These hybrid enzyme-responsive nanomaterials provided rapid and sensitive detection for one of the most toxic substances known to human.

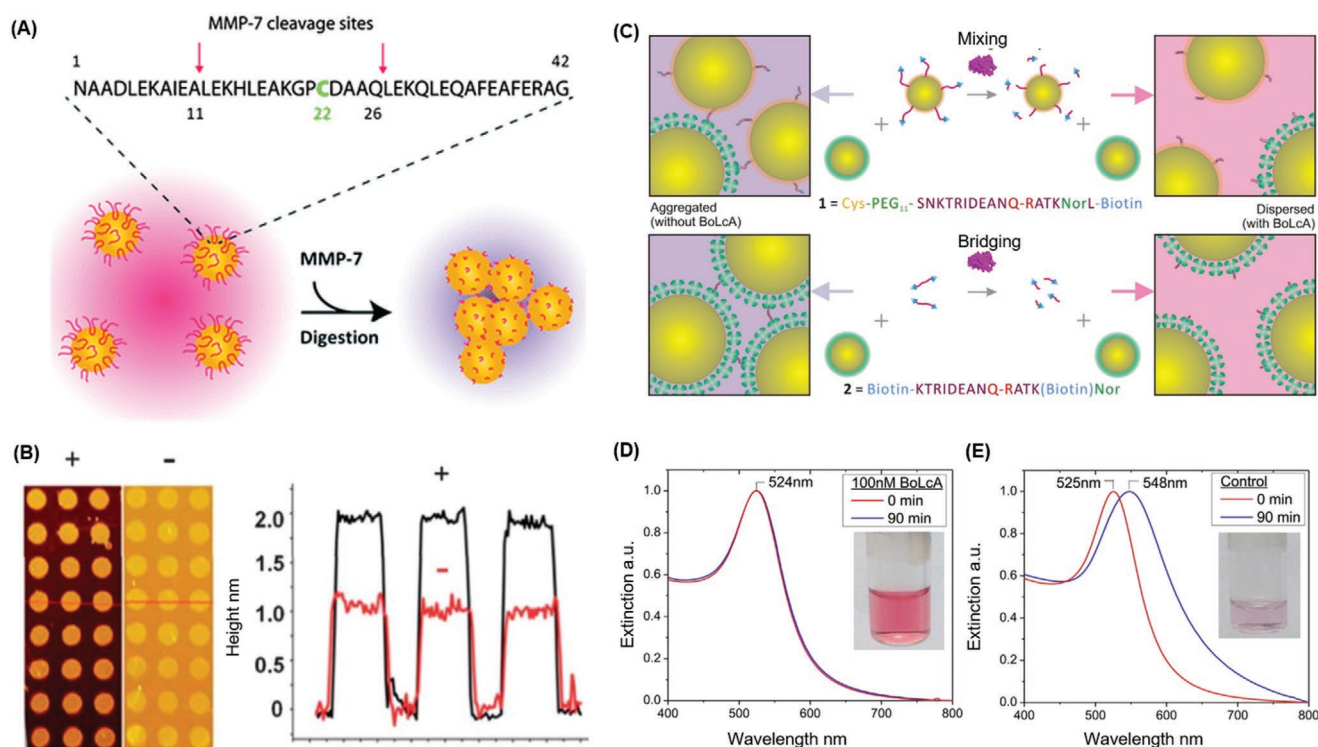


Figure 6. A) Schematic illustration of aggregation process induced by MMP-7 that cleaves substrate peptides on AuNPs. B) Ellipsometric contrast image of patterned peptide substrates on gold surfaces before (+, black) and after (-, red) digestion by MMP-7 protease with the corresponding height profile. Reproduced with permission.^[73] Copyright 2013, The Royal Society of Chemistry. C) Mixing and bridging assays for detection of BoLcA using two peptide designs (1 and 2) and biofunctionalized AuNPs. Normalized extinction spectra of the mixture solution of navi-AuNPs and 1-AuNPs which was preincubated D) with 100 nM BoLcA and E) without BoLcA (as control). Insets are photographs of the corresponding AuNP solutions showing the color change. Reproduced with permission.^[72] Copyright 2014, American Chemical Society.

Similar sensing concept has also been applied with Förster resonance energy transfer (FRET) for the achievement of higher sensitivity. In this kind of assays, the fluorescence probe typically modified at one end of peptides is generally quenched by the AuNPs upon the other end of peptides anchoring on the particle surface (Figure 7A). Once the linker peptide is cleaved by the protease, the dye is released from the vicinity of AuNP surface and regains its fluorescence. Following this strategy, Wang and his colleagues utilized designed peptide substrate and small mono-maleimide AuNP conjugates as the linker and quencher.^[71] With the help of fluorescence-labeled streptavidin, various concentrations of BoLcA and trypsin were probed in a time-dependent manner (Figure 7B,C). The LOD of BoLcA detection was estimated as low as 1 pM (Figure 7D). Multi-detection of various proteases was also realized by incorporating several recognition sites into one labeled peptide substrate so that the existence of any protease would result in reduced quenching effect by AuNPs.^[74] However, the specificity had to be compromised since it was not possible to distinguish the proteases from single signal response. This problem was finely addressed by introducing quantum dots-peptide-AuNP. Quantum dots (QDs) instead of dyes were quenched by AuNPs through the peptide linkers (Figure 7E).^[75,76] By conjugating different peptide substrates of the proteases to different QDs with specific emission wavelengths, the multiplexed assay was achieved. Individual protease was detected simultaneously according to their corresponding color outputs (Figure 7F).^[76]

More recently, several peptide substrate-AuNP based approaches have been reported for different proteases such as HIV 1 protease,^[77] thrombin,^[78] caspases,^[79–82] urokinase-type plasminogen activator,^[83] β -secretase,^[84,85] MMPs,^[86–90] collagenase,^[91] and for PSA.^[92,93] The strategies involve extended detection methods like electrochemistry, voltammetry, and localized surface plasmon resonance (LSPR) using various nano-complexes. For example, an amazingly low LOD (0.8 pM) has been achieved by introducing the peptide/single walled carbon nanotube/AuNP structure on electrode for detection of HIV 1 protease.^[77]

The protease reaction involving peptide-gold nanomaterials has recently been further developed to address the following problems such as diagnostic field tests, cellular and in vivo detection/imaging, and drug delivery. One novel work of live cell imaging was done by Alivisatos and his colleagues who employed label-free “plasmon ruler” for the detection of caspase-3 at single molecule level.^[15] The plasmon ruler was composed of a central avidin-AuNP crowned by peptide substrate functionalized AuNPs, which could be disassociated upon caspase-3 cleavage (Figure 8A,B). The particle assembly scattered light efficiently but it gradually faded out in the presence of caspase-3, which was recorded under simple light-scattering microscopy and further analyzed by spectrometry (Figure 8C,D). The intensity decreased after the activation of caspase-3 step-wisely indicating the occurrence of single cleavage event (Figure 8E). In live cell imaging, an additional cell penetration peptide threonine (Thr)-Ala-Thr (TAT) was conjugated on the crown particles and helped the cellular internalization. Figure 8F

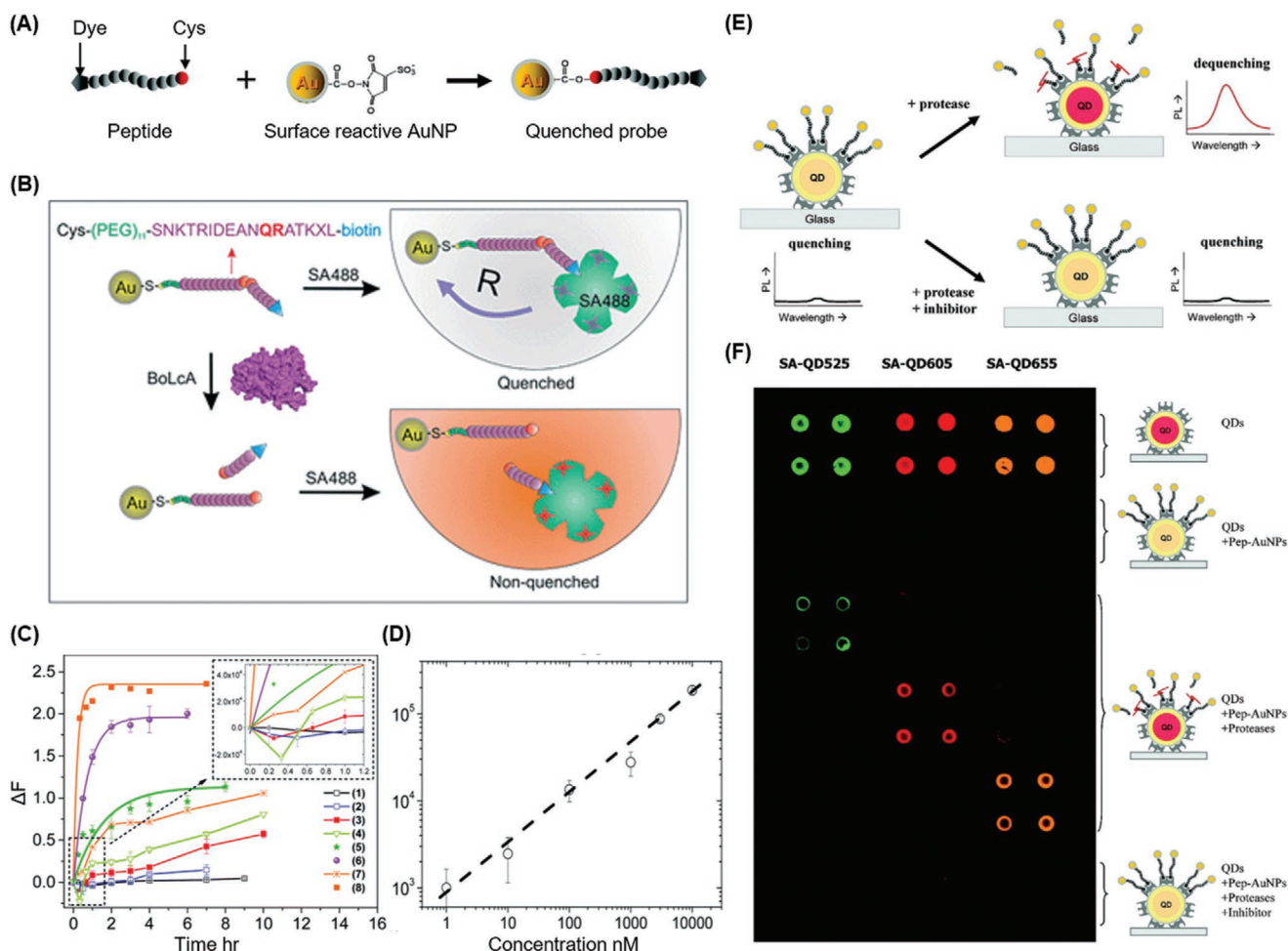


Figure 7. A) General scheme of quenched probe used in FRET consisted fluorescent dye labeled peptide substrate and surface reactive AuNPs. B) Schematic illustration of the energy transfer between the peptide-functionalized AuNP and streptavidin–Alexa488 (SA488) before (quenching) and after (recovery) catalytic cleavage by BoLcA. C) The time-dependent fluorescence intensity changes ΔF of SA488 on 1.4 nm AuNP–pep pretreated with different concentrations of BoLcA (1 μ M, 10 μ M, 100 μ M, 1 nM, 3 nM, and 10 nM) and trypsin (10 μ M and 1 nM). D) The calibration curve for the detection of BoLcA corresponding to the response at 2 h reaction time in (C). Reproduced with permission.^[71] Copyright 2014, The Royal Society of Chemistry. E) Schematic illustration of protease detection principle and inhibitor screening by using AuNP–peptide–QD conjugates on glass. F) Schematic illustration of multiplexed proteases assay by using various QDs conjugated to AuNPs with protease-specific peptide substrates, showing their corresponding colors on glass (green: MMP-7, red: caspase-3, orange: thrombin). Reproduced with permission.^[76] Copyright 2008, American Chemical Society.

showed the successful delivery of the particle assembly in HeLa cells and colon cancer cells (SW620) denoted by the bright spots. For imaging the caspase-3 activation process by using the plasmon ruler in the live SW620 cells, the particle-loaded cells started with introducing the apoptosis inducers which subsequently activated caspase-3, resulting in gradual dimming of bright spots in continuous imaging recording and confirmed by controls (Figure 8G). In relation to nanomedicine, a potential drug delivery system was suggested targeting cancer cells due to overexpression of proteases which deviated from healthy cells and facilitated the hydrolytic release of cargo drugs.^[94]

Phosphatases and Others: Other hydrolases than proteases are also of great interest for biosensors based on peptide substrates, such as phosphatase and deacetylase that play important physiological roles in the cells. Phosphatase hydrolyses a pre-phosphorylated peptide substrate at the phosphoric acid monoester by splitting it into free phosphate and hydroxyl group on serine, Thr, or tyrosine (Tyr), which functions oppo-

sitely to kinase but works cooperatively, especially in cell signaling.^[95] The signaling pathways regulated closely by them are involved in almost all types of cancers, and thus make them major clinical-therapeutic targets.^[96,97]

In the pioneering work by Tung et al., they demonstrated the detection of alkaline phosphatase (ALP) utilizing AuNP aggregation.^[98] The short phosphorylated peptide, Cys-Tyr(PO₃²⁻)-Arg, was prohibited to aggregate negatively charged AuNPs due to the phosphate group. After the cleavage by ALP at Tyr, the peptide bridged AuNPs by thiol of Cys and the positive charge of Arg resulting in the colorimetric change (Figure 9A,B). Based on the same colorimetric sensing platform, an inhibition assay of ALP also was performed by introducing an ALP inhibitor molecule, *p*-BO (Figure 9C). Another work for the detection of ALP was reported using a similar principle years later, but with a novel assay procedure.^[99] The color development during synthesis of AuNPs was utilized as an indicator of ALP with its substrate. In the presence of ALP, massively aggregated AuNPs

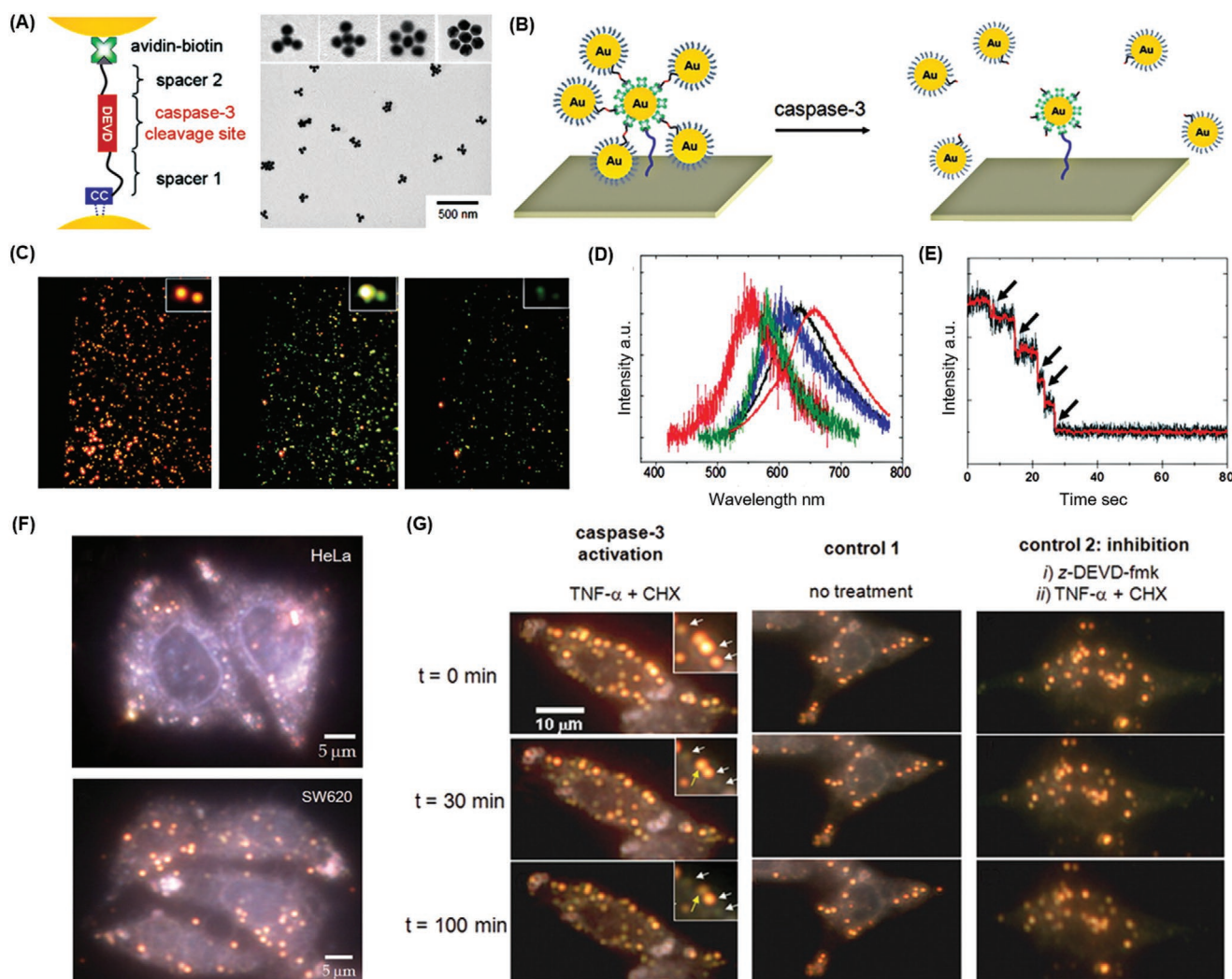


Figure 8. A) Schematic illustration of crown nanoparticle probes composed of a neutravidin-coated AuNP as the core and biotinylated peptide-AuNP as satellites. The designed peptide substrate containing a specific caspase-3 cleavage sequence (DEVD). The crown structure was observed by TEM images. B) Schematic illustration of caspase-3-mediated cleavage of crown nanoparticle probes. Caspase-3 cleavage caused the disassembly process of crown nanoparticle probes shown in C) scattering images: red to yellow to dim green spots, and in D) spectra: blue shift initially from 654 nm (red). E) Step-wise intensity drop indicating single satellite nanoparticle cleavage. F) Bright and red spots in microscopic images showed cellular delivery of crown nanoparticle probes into HeLa and SW620 with the help of cell penetration peptide (Thr-Ala-Thr). G) Caspase-3 activity in cells was observed as the red spots gradually turned into dim red/green ones upon addition of apoptosis inducers (TNF- α and CHX), while in cells either without the apoptosis inducers or with an additional caspase-3 inhibitor (z-DEVD-fmk), no signal change was observed. Reproduced with permission.^[15] Copyright 2009, National Academy of Sciences.

were synthesized due to positively charged dephosphorylated peptide instead of violet well-dispersed AuNPs (Figure 9D,E).

Lately, another hydrolase histone deacetylase (HDAC), which regulates the genetic transcription process, was detected based on an immunoassay using antibody-coated AuNPs and labeled acetylated peptide substrates.^[100] The antibody specifically targeted the acetyl group of peptide substrate leading to quenching, whereas in the presence of HDAC, antibody would no longer recognize or bind to the labeled peptide thus resulting in a recovery of fluorescence. The histone demethylase (LSD1) has a similar biological function as HDAC, though it does not belong to hydrolase but to oxidoreductase. The colorimetric detection of LSD1 was reported based on a dimethylated peptide substrate which also was biotinylated to enable binding to avidin.^[101] The dimethyl-antibody blocked the peptide substrate

from aggregating avidin-AuNPs unless LSD1 removed the dimethyl group and inhibited the antibody binding to peptides that eventually induced the massive aggregation (Figure 9F).

3.1.2. Phosphorylation Reactions

Transferases are involved in many regulatory processes from genetic expression to carbohydrate metabolism. One of the most well studied and important enzymes within the transferase family is protein kinase which coordinates the phosphorylation from a high-energy donor (i.e., ATP) to specific protein substrates/residues. As mentioned in the last section, they together with phosphatases mediate most of the signal transduction in and among the eukaryotic cells, to directly/indirectly

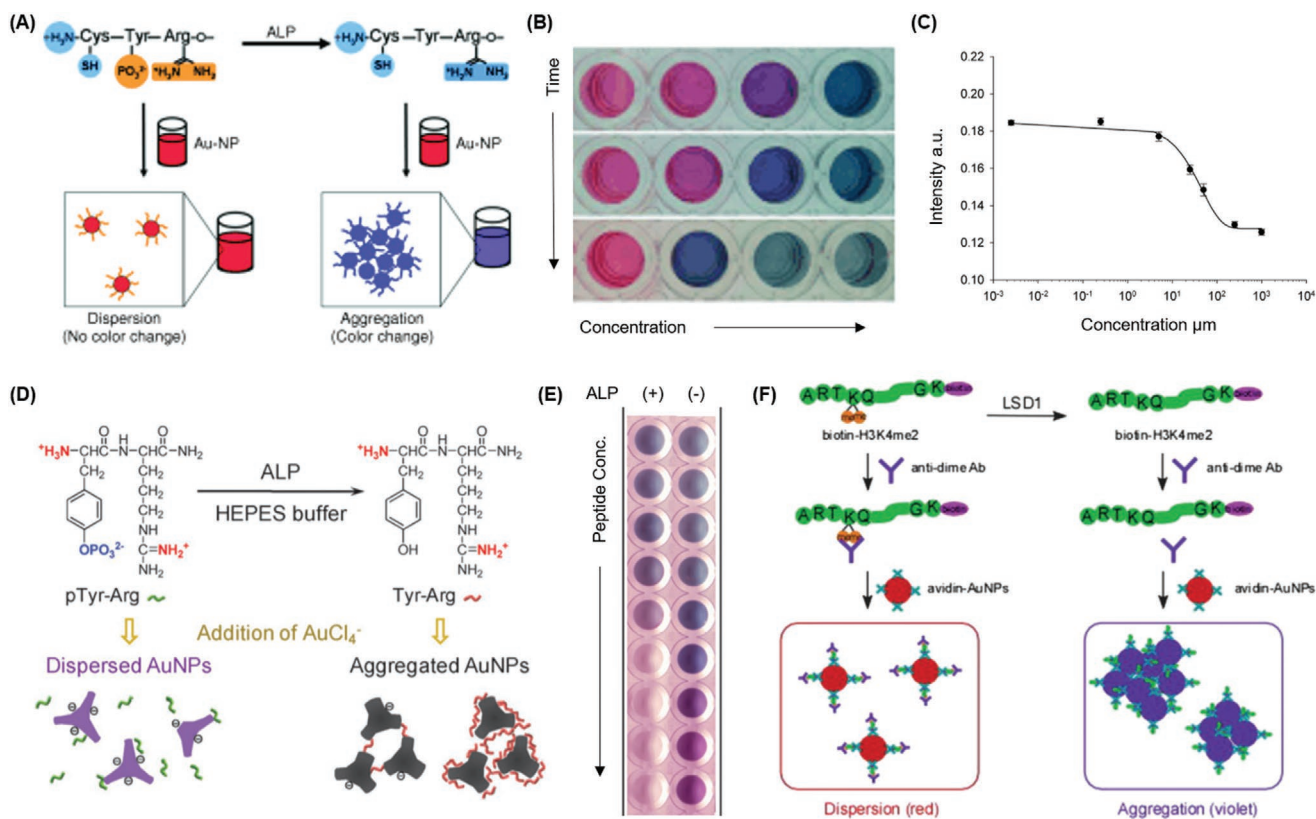


Figure 9. A) Schematic illustration of colorimetric ALP assay based on designed peptide substrates and AuNPs, where the negative charges of phosphotyrosine in the peptides prevented AuNP aggregation until ALP removed the phosphate group on the peptides, resulting in peptide-bridging AuNP aggregation followed by color changing. B) Colorimetric assay of ALP showing the color gradually change as time elapse at a dose-dependent rate. C) Absorbance intensity at 650 nm versus an ALP inhibitor (*p*-BO) concentrations showing the kinetic profile in the ALP inhibition assay based on the same colorimetric system. Reproduced with permission.^[98] Copyright 2007, Wiley-VCH. D) Schematic illustration of colorimetric ALP assay based on synthesis of AuNPs in the presence of phosphorylated dipeptide. The de-phosphorylation by ALP caused ill-synthesized aggregated AuNPs. E) Photographs showed the color differences of synthesized AuNPs with series of peptide concentrations in the presence (+) and absence (-) of ALP pre-treatments. Reproduced with permission.^[99] Copyright 2010, The Royal Society of Chemistry. F) Schematic illustration of colorimetric LSD1 assay based on designed biotinylated-dimethylated peptide substrates and avidin-coated AuNPs with the help of anti-dimethyl antibody. Reproduced with permission.^[101] Copyright 2012, The Royal Society of Chemistry.

control the cellular processes and intercellular system functions such as transcription, cell cycle progression, metabolism, physiological responses, homeostasis, and so forth.^[95,97,102] It is therefore of great interest to develop assays capable of monitoring the kinase activity based on peptide substrate and AuNPs.

The first demonstration was reported by Brust et al.^[14] In their assay, the phosphorylation donor molecule was γ -biotin-ATP instead of ATP, which successfully combined the phosphorylation process with biotinylation of peptide substrate on AuNPs in the presence of kinase. The biotinylated peptide-AuNPs aggregate accordingly upon the addition of avidin-coated AuNPs, whereas no aggregation was observed in the presence of inhibitor (**Figure 10A**). Right after this, Katayama and co-workers measured the activity of several kinases and the effect of inhibitor H-89 based on the negatively charged AuNP aggregation triggered by the positively charged peptide substrates,^[103] whereas after reaction with the protein kinase A (PKA), the peptide can no longer induce AuNP aggregation due to loss of positive charges (**Figure 10B,C**). The same approach was applied for a deeper understanding of the non-crosslinking aggregation behavior of AuNPs as well as developing a

high-throughput method for screening inhibitors and cancer diagnosis.^[104–107] For example, the elevated level of activated protein kinase C alpha associated with cancer cells was correlated to the color change of AuNPs, which was further applied to human breast cancer samples showing a potential way of cancer diagnosis.^[106] As a more direct approach, an immuno-aggregation of peptide-AuNP conjugates facilitated by anti-phosphate antibody-AuNPs was illustrated for the detection of Src-kinase with an LOD of sub-nM (**Figure 10D,E**).^[108]

Besides colorimetric assays, other optical methods have been intensively employed for the detection and inhibitor screening of kinases based on peptide-AuNPs. For instance of using scattering light, Wang et al. employed a peptide-coated microarray, biotin-ATP, and avidin-AuNPs for the detection of kinase activity with resonance scattering light (RLS).^[109–112] In the presence of kinase, the biotin-phosphate was added to the peptide substrates on the microarray which resulted in the binding of avidin-AuNPs to the peptides. The RLS signal of the AuNPs was further amplified by silver disposition to achieve high sensitivity for the detection of PKA and its inhibitor (**Figure 11A**). Furthermore, on chip phosphorylated peptides were applied

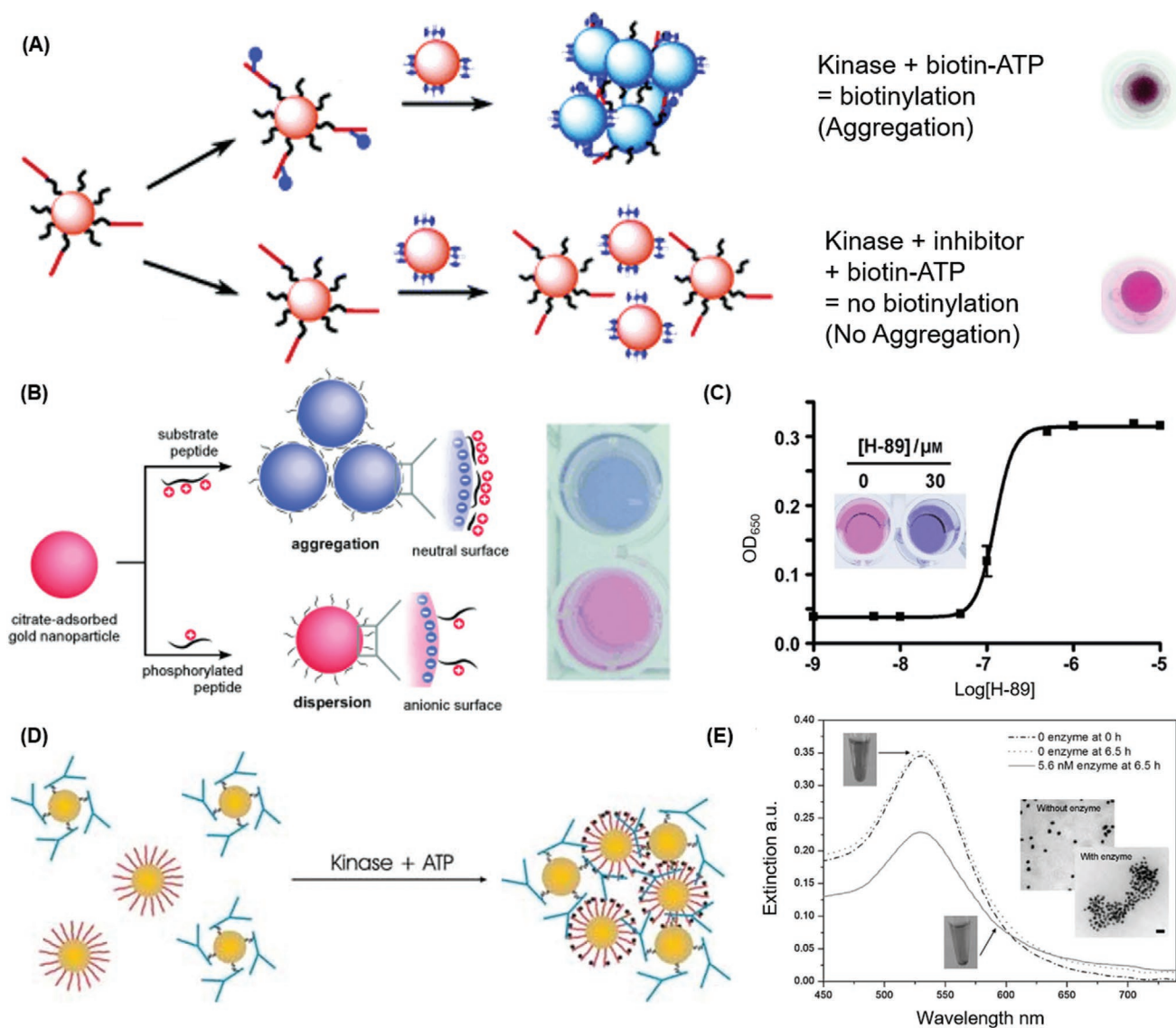


Figure 10. A) Schematic illustration of biotinylation paired with phosphorylation of substrate peptides modified on AuNPs by kinase resulting in subsequent aggregation (color changes) upon adding of avidin-coated AuNPs, whereas in the presence of kinase inhibitors no aggregation was observed (red color remains). Reproduced with permission.^[14] Copyright 2006, American Chemical Society. B) Colorimetric kinase activity assay based on AuNP aggregation: Positively charged peptide substrates induce AuNP aggregation (color change) without kinase, whereas after PKA kinase reaction the peptide can no longer induce AuNP aggregation due to positive charge loss. C) Inhibition assay of PKA activity by inhibitor H-89. Insets showing the color difference of AuNPs: red, no inhibitor; blue, 30 μM of H-89. Reproduced with permission.^[103] Copyright 2007, Wiley-VCH. D) Schematic illustration of colorimetric kinases assay based on designed peptide functionalized AuNPs and anti-phosphate antibody-AuNPs: peptide phosphorylation by kinases resulting in AuNP mixture aggregation. E) UV-vis spectra of the mixed AuNPs solution in the absence of kinases (broken line) and presence of v-Src-kinase (solid line). Insets: TEM images showing the corresponding AuNPs solutions. Reproduced with permission.^[108] Copyright 2010, Wiley-VCH.

for the detection and quantification of PKA based on surface plasmon resonance imaging (SPRi) techniques.^[113] The array of peptide probes immobilized on SPR sensor chips was phosphorylated in the presence of PKA, which was detected and quantified by SPRi based on the signal amplification with biotinylated zinc(II) complex, streptavidin, and anti-streptavidin antibody.

Fluorescent methods also have been developed. Jiang's group prepared high fluorescent gold nanoclusters with different peptide templates using NaBH₄ as the reduction agent and 3-mercaptopropionic acid as the auxiliary ligand.^[114] They employed this gold nanocluster-peptide as an enzyme-

responsive fluorescent nanocluster beacon that was highly sensitive and selective for label-free quantification of protein post-translational modification (PTM) enzymes such as PKA and HDAC-1. The modifications of peptide templates (i.e., phosphorylation by PKA or de-acetylation by HDAC-1) resulted in the quenching of fluorescent nanocluster beacon (Figure 11B). Quantitative detection of tested enzymes could be done by measuring the quenched fluorescent intensity (Figure 11C). With similar fluorescent strategy but opposite response, Qiu et al. had developed a green and simple one-step bio-mineralization method for synthesizing peptide-templated

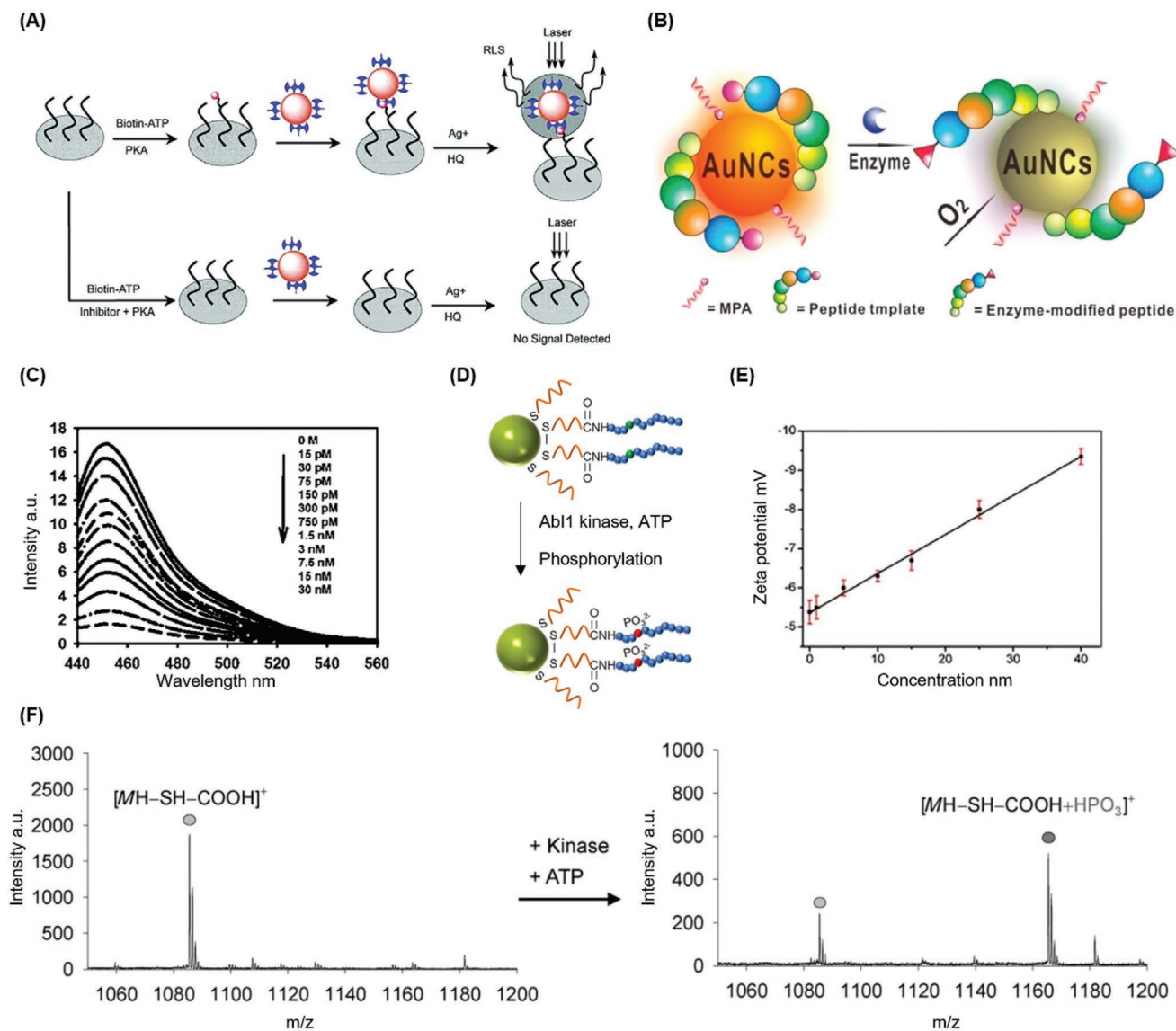


Figure 11. A) Schematic illustration of PKA and its inhibition assay based on RLS: biotinylation and phosphorylation of designed peptide substrates in the presence of PKA leading to attachment of avidin coated AuNPs followed by silver deposition for enhanced RLS signals. Reproduced with permission.^[112] Copyright 2013, American Chemical Society. B) Schematic illustration of fluorescent PTM enzymes assay based on the designed peptide-templated gold nanoclusters. PTM-modified peptide substrates quenched the fluorescent conjugated nanomaterials. C) Fluorescence emission spectra dropped gradually corresponding to increasing concentration of HDAC-1. Reproduced with permission.^[114] Copyright 2013, American Chemical Society. D) Schematic illustration of kinase activity assay based on surface charge detection by using designed peptides functionalized AuNPs. E) Calibration curve of surface zeta potential of AuNPs and Abl1 kinase concentrations. Reproduced with permission.^[121] Copyright 2018, American Chemical Society. F) Time-of-flight secondary-ion mass spectrometry showed a direct increase of molecular mass of peptide substrate which was equivalent to HPO₃ after the kinase reaction accompanied by the intensity decrease of the original signal. Reproduced with permission.^[122] Copyright 2007, Wiley-VCH.

nanoclusters as the fluorescence probe.^[115] In the presence of a carboxypeptidase, the peptide-nanoclusters always would be digested and disassembled, leading to loss of fluorescence, while the phosphorylation of peptide by PKA inhibited the digestion and thus retained the fluorescence. This technology was used for the detection of protein kinase and could be applied to screen inhibitors in human serum samples. Alternative chemiluminescent^[116–118] approaches for detecting the activity of kinases with extremely low LOD also have been reported, which are included in **Table 2**.

There are some other interesting works based on electrochemical,^[119,120] surface potential,^[121] and mass spectrometry.^[122] As an example, Yi et al. presented a method for homogeneous detection of protein kinase activity and screening of inhibitor by measuring surface charge changes with zeta potential analyzer on the peptide-modified AuNPs (Figure 11D).^[121] In this assay, the presence of Abl kinase and ATP increased the surface negative charges significantly due to phosphorylation of the peptide-modified AuNPs in a concentration-dependent manner (Figure 11E). Kim et al. reported a label-free assay of

Table 2. Works that involve peptide functioning as substrate of enzymatic reactions in biosensing.

Targets	Peptide sequences	Binding strategy	Methods	LODs (assay times)/ [dynamic ranges]	Highlights	Refs.
Proteases						
Thrombin	Ac-C(Ac)GF _D PRGC-Ac (F _D : d-phenylalanine)	Thiol-gold	Colorimetric	Less than 5 nM (90 min)/[low nanomolar range]	Cleavage of free peptides functioning as crosslinkers for bare AuNPs aggregation	[13]
Thrombin	GLACSGFPRGRW	Thiol-gold	Spectrofluorometric method	0.1 nM (40 min)/ [10 ⁰⁻² nM]	Cleaved tryptophan W residue from AuNP surface as the reporter for detection	[78]
Metalloproteinase-7 (MMP-7)	HHHHHHGPLGMRGLHHHHHH	Metal coordination	Colorimetric	10 nM (less than 1 h)/ [10 ⁰⁻¹ nM]	Metal ions coordinating functioning free peptides and carboxyl-protected AuNPs	[69]
MMP-7	NAADLEKAIEALEKHLEAKG- PCDAAQLEKQLEQAFERAG	Thiol-gold	Colorimetric	5 nM (4 min)/ [10 ¹⁻² nM]	Aggregation of AuNPs induced by reducing the negative charges on peptide	[73]
MMP-7	Tamra-GPLGMRGLHHHHHH	Metal coordination	Förster resonance energy transfer (FRET)	10 ng mL ⁻¹ (2 h)/ [10 ⁰⁻² ng mL ⁻¹]	Simple one-pot fluorogenic detection of MMP-7 activity	[87]
Thermolysin and nonbinding R1-antichymotrypsin prostate specific antigen	Fmoc-GFC-NH ₂ ; Fmoc-SSFYSGGGC-NH ₂	Thiol-gold	Colorimetric	90 zg mL ⁻¹ (2 h)/ [within 10 ²⁻¹⁴ zg mL ⁻¹]; 10 ag mL ⁻¹ (less than 30 min)	Redispersion of pre-aggregated AuNPs	[70]
Trypsin, chymotrypsin, proteinase K and thermolysin	FITC-PEG ₂ -ALNNGGGG- HAKRRLIFGGGC (multiple cleavage sites)	Thiol-gold	FRET	0.7 nM (4.7 nM in urine) trypsin, 0.4 nM chymotrypsin, 0.05 nM proteinase K, and 0.5 nM thermolysin (less than 10 min)/[10 ⁻¹ nM]	Multi-detection realized by one peptide substrate containing multiple cleavage sites in a “add-mix-measure” form	[74]
MMP-7, caspase-3, and thrombin	For MMP-7: CRPLALWRSK-biotin; For caspase-3: biotin-GRRGDEVDGRRRC-NH ₂ ; For thrombin: biotin-GKGGVLPRGSGC-NH ₂	Thiol-gold	FRET	10 ng mL ⁻¹ MMP-7, 20 ng mL ⁻¹ caspase-3 and 1 U mL ⁻¹ thrombin (2 h)/[10 ⁻⁴ ng mL ⁻¹ MMP-7, 10 ⁻³ ng mL ⁻¹ caspase-3, 10 ⁰⁻² U mL ⁻¹ thrombin]	Multiplexed assay on chip with different colored quantum dot-peptide-AuNP conjugates	[76]
Botox A light chain (BoLcA)	Pep1: C-PEG ₁₁ -SNKTRIDEANQRATKXL-biotin; Pep2: biotin-KTRIDEANQRATK(biotin) X (X:norleucine)	Thiol-gold; Biotin- streptavidin	Colorimetric	0.1 nM (4 h)/ [10 ⁻¹⁻¹ nM]	Designed peptide substrates for biomimicking SNAP-25 protein	[72]
BoLcA	C-PEG ₁₁ -SNKTRIDEANQRATKXL-biotin (X:norleucine)	Thiol-gold	FRET	1 pM (2–3 h)/ [10 ⁰⁻⁴ pM]	Fluorophore quenched by various sized AuNPs and biomimicking peptide substrate	[71]
Prostate-specific antigen (PSA)	CCCCCGLXAAGGHSSKLQK-FITC (X: α-isobutyric acid)	Thiol-gold	FRET	Less than 10 pM in both PBS and human serum (1 h)/[10 ⁻⁵ pM]	Suitable detection limit and dynamic range for clinical considerations	[92]
Caspase-3	FITC-DEVDC	Thiol-gold	FRET	N.A.	FITC-DEVDC-nanogel-GNP nano-probe for real-time monitoring and early response to cancer therapy by sensing activated caspase-3 in apoptosis cells	[79]
Caspase-3	Ac-GDEVDCCR-NH ₂	Thiol-gold	Colorimetric	5 ng mL ⁻¹ (30 min)/ [10 ⁰⁻² ng mL ⁻¹]	Colorimetric detection of apoptosis based on caspase-3 activity through peptide substrates	[80]
Caspase-3	CALNNDEVGDK(biotin)G	Thiol-gold	Chemiluminescence resonance energy transfer	N.A.	AuNP-peptide-biotin-streptavidin-HRP complexes as the main function unit for detection of caspase-3 activity, referring to cell apoptosis status	[81]

Table 2. Continued.

Targets	Peptide sequences	Binding strategy	Methods	LODs (assay times)/ [dynamic ranges]	Highlights	Refs.
Caspase-3	Biotin-GDGDEVDGC	Thiol-gold	Square wave voltammetry	5 fM [10^{-7} fM]	Peptide-AuNPs functionalized silica-based mesoporous materials	[82]
Urokinase-type plasminogen activator	thiol-(CH ₂) ₂ -GGRGGG-Cypate	Thiol-gold	FRET	N.A.	Peptide-AuNPs conjugates as a tool for conditional fluorescent study	[83]
β -secretase (BACE1)	CLXGGEVNLD AEFGLHHHHHHH (X: α -isobutyric acid)	Thiol-gold	FRET	0.15 μ M (1 h)/ [10^{-1-0} μ M]	Automated cell-based assay using fluorogenic QD-AuNP probes for screening BACE1 inhibitors	[84]
Matriptases	FITC-GRQSRAGC-NH ₂	Thiol-gold	FRET	N.A.	Detection of over-expression of matriptase on tumor cells both in vitro and in vivo	[89]
Membrane type-1 matrix metalloproteinase	FITC-GPLPLRSWGLK	Catechol-gold	Nanosurface energy transfer	N.A.	Peptide-AuNPs enabling the activity detection of target on invasive cancer cells	[90]
Membrane type-1 matrix metalloproteinase	Unrevealed	N.A.	Localized surface plasmon resonance (LSPR)	Less than 1 nM (less than 1 h)/ [10^{0-2} nM]	On-substrate LSPR detection for target activity from buffer and whole cell lysate	[90]
PSA	HSSKLQK	Thiol-gold	Electrochemical	27 pg mL ⁻¹ [10^{-1-0} ng mL ⁻¹]	The amount of peptide-AuNPs attached on the microplate decreased due to the peptide cleavage by PSA	[93]
PSA	CHSSKLQK	Thiol-gold	FRET	0.3 pg mL ⁻¹ [10^{1-3} pg mL ⁻¹]	Peptides modified on the Fe ₃ O ₄ @SiO ₂ -Au nanoparticles were cleaved by PSA, leading to the fluorescence recovery	[124]
Collagenase	P1 containing a terminal Cys.	Thiol-gold	QCM	0.96 ng mL ⁻¹	Peptide-AuNPs immobilized on QCM chips were cleaved at the presence of collagenase	[91]
Dipeptidyl peptidase-IV (DDP-IV)	RPRPPPPC	Thiol-gold	Colorimetric, electrochemical	70 μ U mL ⁻¹ , 0.55 μ U mL ⁻¹	Determination of DDP-IV activity and screening of its inhibitor using AuNP as the probe	[125]
Phosphatases						
Alkaline phosphatase (ALP)	CXR (X: phosphotyrosine)	Thiol-gold	Colorimetric	Less than 0.3 μ M (4 min)/[10^{-1-1} μ M]	Removal of negatively charged phosphate group of peptide substrate which induces AuNPs aggregation by peptide crosslinking	[98]
ALP	XR (X: phosphotyrosine)	Electrostatic	Colorimetric	0.01 U mL ⁻¹ (30 min)/ [10^{-3} to 10^{-1} U mL ⁻¹]	Outcome of AuNP synthesis (by HEPES buffer) determined by peptide substrate de-phosphorylation status thus sensing the presence of ALP	[99]
Deacetylase						
Histone deacetylase sirtuin 2	SGRGKGGK GLGKGGAK(Ac) RHRKK-FAM (FAM: carboxyfluorescein)	Electrostatic and hydrophobic	FRET	11.9 nM (2 h)/[10^{-3} nM]	Immunoassay for binding of acetyl group on peptide substrate.	[100]
Demethylase						
Lysine-specific demethylase 1	ARTK(dimethyl) QTARKSTGGKAPRKQLAGGK-biotin	Biotin-avidin	Colorimetric	13 pM (1 h)/ [10^{1-5} pM]	Immunoassay for binding of methyl group on peptide substrate so that sterically blocking AuNPs from aggregation	[101]

Table 2. Continued.

Targets	Peptide sequences	Binding strategy	Methods	LODs (assay times)/ [dynamic ranges]	Highlights	Refs.
Kinases						
Protein kinase A (PKA)	CALNNAALRRASLG	Thiol-gold	Colorimetric	N.A.	Simultaneous phosphorylation and biotinylation of peptide inducing aggregation of avidin coated AuNPs for inhibitors screening	[14]
Calmodulin-dependent kinase II	CALNNAAKKLNRTLSVA	Thiol-gold	Colorimetric			
Several kinases	For PKA: CXXALRRASLGW-NH ₂ ; For PKC α : CXXFKKQGSFAKKK-NH ₂ ; For MAPKAPK-2: CGGKKLNRLSVAGW-NH ₂ ; For c-Src: GGIYGEFDKKKK-NH ₂ (X: 8-amino-3,6-dioxaoctanoic acid)	Thiol-gold; Electrostatic	Colorimetric	Less than 5.9 U mL ⁻¹ PKA; less than 0.05 μ g mL ⁻¹ PKC α ; less than 0.25 μ g mL ⁻¹ MAPKAPK-2; less than 100 U mL ⁻¹ c-Src (1 h)	Colorimetric measurement of kinase activities for understanding non-crosslinking aggregation of AuNPs, screening kinases inhibitors and cancer diagnosis	[103,104, 106,107]
PKA	LRRASLG CGGALRRASLGRRASPP	Thiol-gold	Resonance light scattering and SERS	N.A. (2 h)	Peptide substrate coated microarray for detecting PKA activity from cell lysate and screening inhibitors of PKA facilitated by AuNPs attachment and silver deposition enhancement	[109–112]
PKA	LRRASLG	Thiol-gold	Electrogenerated chemiluminescent assay	0.07 U mL ⁻¹ (1.5 h)/ [10 ⁻¹⁻² U mL ⁻¹]	Thiophosphorylated peptide bound AuNPs amplifying the signal significantly	[116]
PKA	CLRRASLG	Thiol-gold	Electrogenerated chemiluminescent assay	0.09 U mL ⁻¹ (>2 h)/ [10 ⁻¹⁻¹ U mL ⁻¹]	Multiple signal amplification steps by xanthine oxidase-DNA-AuNPs conjugates	[117]
PKA	CCLRRASLG	Thiol-gold	Fluorescence	0.0004 U mL ⁻¹ (45 min)/ [10 ⁻³⁻¹ U mL ⁻¹]	Fluorescent peptide-gold nano-clusters for detection of real-time reaction of PKA	[114]
PKA	CCYLRRASLG	Thiol-gold	Fluorescence	0.004 U mL ⁻¹ [10 ⁻²⁻¹ U mL ⁻¹]	Carboxypeptidase Y facilitating the fluorescent turn-on assay in the presence of PKA, in which peptide substrates playing a central role	[115]
Casein kinase II and PKA	For casein kinase II: CRRRADDSDDDDD For PKA: CLRRASLG	Thiol-gold	Electrogenerated chemiluminescent assay	0.008 U mL ⁻¹ casein kinase II; 0.005 U mL ⁻¹ PKA (>2 h)/ [10 ⁻²⁻⁰ U mL ⁻¹]	Thiophosphorylation of peptide substrates enabling coupling of tris(2,2'-bipyridine) dichlororuthenium(II)-functionalized AuNPs and subsequent response	[118]
p60 ^{c-Src} kinase and PKA	For p60 ^{c-Src} kinase: KKKGPWLEEEEEAYGLDF; For PKA: LRRASLG	Biotin-streptavidin	Electrochemical assays	5 U mL ⁻¹ p60 ^{c-Src} kinase; 10 U mL ⁻¹ PKA (1.5 h)/ [10 ⁻¹⁻² U/mL]	Electrochemical method for detection and inhibitor screening of kinases through attachment of AuNPs induced by phosphorylation of peptides	[119]
Protein tyrosine kinase Abl-T315I	Biotin-EGIYDVP	Thiol-gold	Electrochemical assays	10 ng mL ⁻¹ (2.5 h)/ [10 ⁻¹⁻² ng mL ⁻¹]	Thiophosphorylation of peptide substrate enabling the attachment of bare AuNPs and subsequent measurements	[120]
Abl	EAIYAAPFAKKK	Thiol-gold	Zeta potential analyzer	1 nM	Surface charge increases upon the presence of Abl kinase and ATP due to phosphorylation of peptide-modified AuNPs	[121]
v-Src	Ac-IYGEFKKCC	Thiol-gold	Colorimetric	Low nM (4.5 h)/ [10 ⁰⁻¹ nM]	Immunoaggregation of peptide-AuNP conjugates facilitated by antibody-AuNPs	[108]

protein kinase on peptide-AuNPs by using secondary-ion mass spectrometric imaging.^[122] In this assay, the peptide substrate for Abl kinase with surface orientation, two cysteine-terminated peptides with different lengths (Ac-IYAAAPKK(G)₄C; IYAAAPKKC), were conjugated to AuNPs. The Abl kinase reaction with the peptide resulted in an additional positive ion signal shifted by a mass equivalent to that of HPO₃ (80 Da), thereby causing a decrease in the original un-phosphorylated signal intensity (Figure 11F). Based on the signal intensity ratio measurement, they found the longer peptide gives higher phosphorylation efficiency (70%) than the shorter one (29%) due to the different accessibility of the enzyme to the peptides.

One excellent review has been published years earlier regarding to AuNP-based enzymatic assays by Hutter and Maysinger, mainly focusing on various assay methods.^[123] Instead, works reviewed in this section are categorized by different functions of designed peptides, thereby putting more emphasis on the interactions between target enzymes and their peptide substrates. A list of works is summarized in Table 2, including those works not mentioned in detail above due to the limited space.

3.2. Peptide Binder for Biosensing and Cell Targeting

Peptide binders are promising candidates for replacing antibodies for molecular recognition. They can be rationally designed or randomly selected from a library. As the understanding of the biochemical interactions beneath biological processes steadily increases, it is becoming relatively easier to obtain peptide binders for various bio-relevant target molecules.^[126] These synthetic peptides with certain binding motifs, selected either by direct rational design or random phage display, have been used to target a wide spectrum of analytes, including ions,^[127–129] small molecules,^[130–134] large biomolecules,^[135–140] and whole cells.^[141,142]

3.2.1. For Biosensing

Metal Ions and Small Molecules: In the human body, especially in the fluids, metal ions like sodium, potassium, calcium, magnesium, and others take part in many important chemical processes, together with biological molecules such as nucleic acids, proteins, peptides, and enzymes. For example, DNA replication is carried out using enzymes such as DNA polymerase, which essentially requires magnesium to function properly.^[143] Metals can serve as cofactors to assist in binding and localization of substrate with respect to functional groups of biomolecules in the active site.^[144]

The interaction between metal ions with specific peptides may trigger their folding or conformational changes, thus providing an avenue for ion analysis and diagnosis. For instance, Aili et al. developed a novel competitive assay where Zn²⁺-triggered folding of peptides immobilized on AuNPs was prevented by specific binding of human carbonic anhydrase II (HCAII) to a ligand present on the same peptide motif (Figure 12A).^[145,146] The peptides of JR2EC and KE2C were designed based on a 42-amino-acid helix-loop-helix polypeptide that dimerized in

solution and folds into an antiparallel four-helix bundle.^[42] Folding is primarily driven by the formation of a hydrophobic core made up of the hydrophobic faces of the amphiphilic helices. Homo-dimerization and folding (between JR2EC peptides immobilized on different AuNPs) occurred at pH < 6 or at pH 7 in the presence of Zn²⁺, which triggered the aggregation of the peptide-functionalized AuNPs (Figure 12B). In order to allow for specific binding of HCAII, the peptide KE2C was site specifically modified with a benzenesulphonamide derivative at the lysine in position 34 using an orthogonal protection-group strategy to yield JKE2C-C6. Benzenesulphonamide (H₂NO₂SC₆H₅) is a commonly used inhibitor of HCAII with the dissociation constant (*K_d*) of their interaction 1.5 μM. Therefore, the binding of HCAII to the peptide KE2C-C6 blocked the aggregation of peptide (JR2EC and JKE2C-C6)-modified AuNPs (Figure 12C). This method was also proposed as a generic sensing platform for the detection of HCAII with sensitivity down to 10 nM. The versatility of the technique was demonstrated using another peptide (CRGTGSYNRSSFESSGLV) derived from the tobacco mosaic virus coat protein which was co-immobilized with JR2EC on AuNPs to allow for the detection of recombinant antibody fragment (Fab57P) with detection limit down to 25 nM.

Similarly, Li et al. reported an ultrasensitive assay for the detection of silver ion based on peptide-modified AuNPs. The peptide (RFRRGGDD) was folded in the presence of Ag⁺, which resulted in the aggregation of AuNPs (Figure 12D).^[147] Instead of the peptide folding triggered by metal ions, the detection of ions also can be achieved through the binding of metal ions to the peptide ligand resulting in the aggregation of nanoparticles via bridging of neighboring nanoparticles or by affecting the charge distribution of the peptide coatings. Typically, charged, aromatic, and hydroxyl-containing amino acids are known to interact with metal ions via noncovalent interactions, and short polyacidic stretches have been shown to bind to metal ions.^[148–151] Therefore, the modifications in the peptide sequences could affect the metal speciation and coordination geometry. Slocik et al. designed a Flg-A3 peptide ligand (DYKDDDDKPAYSS-GPAPPMPF), which is overall negatively charged (pI = 3.9) and is modified on the AuNPs for metal ion detection.^[152] The amino terminus of the peptide (DYKDDDDK) contains charged and aromatic residues that are known to be involved in the complexation of metal ions. The other peptide domains (AYSS-GPAPPMPF) are designed to bind to the gold surface. The addition of series metal ions such as Co²⁺, Hg²⁺, Pb²⁺, Pd⁴⁺, and Pt²⁺ to the peptide-AuNPs solution resulted in a rapid color change within 1 min (Figure 12E). Importantly, the colorimetric response and absorbance spectroscopy were distinct and reproducible for a given metal ion species (Figure 12F). This peptide-AuNP showed high sensitivity for the detection of metal ions as Hg²⁺ (26 nM) based on absorbance spectra measurement.

For the small molecular detection, such as 2,4,6-trinitrotoluene (TNT), a peptide with specific affinity was developed,^[153–155] and applied in electrochemiluminescent (ECL) assays. The specific designed peptide-AuNPs formed a complex with the ruthenium (II)-modified graphene oxide (GO), which quenched the ECL emission of Ru complex due to the energy transfer from luminophore to the AuNPs. In the presence of TNT, the peptide-AuNPs were released from the

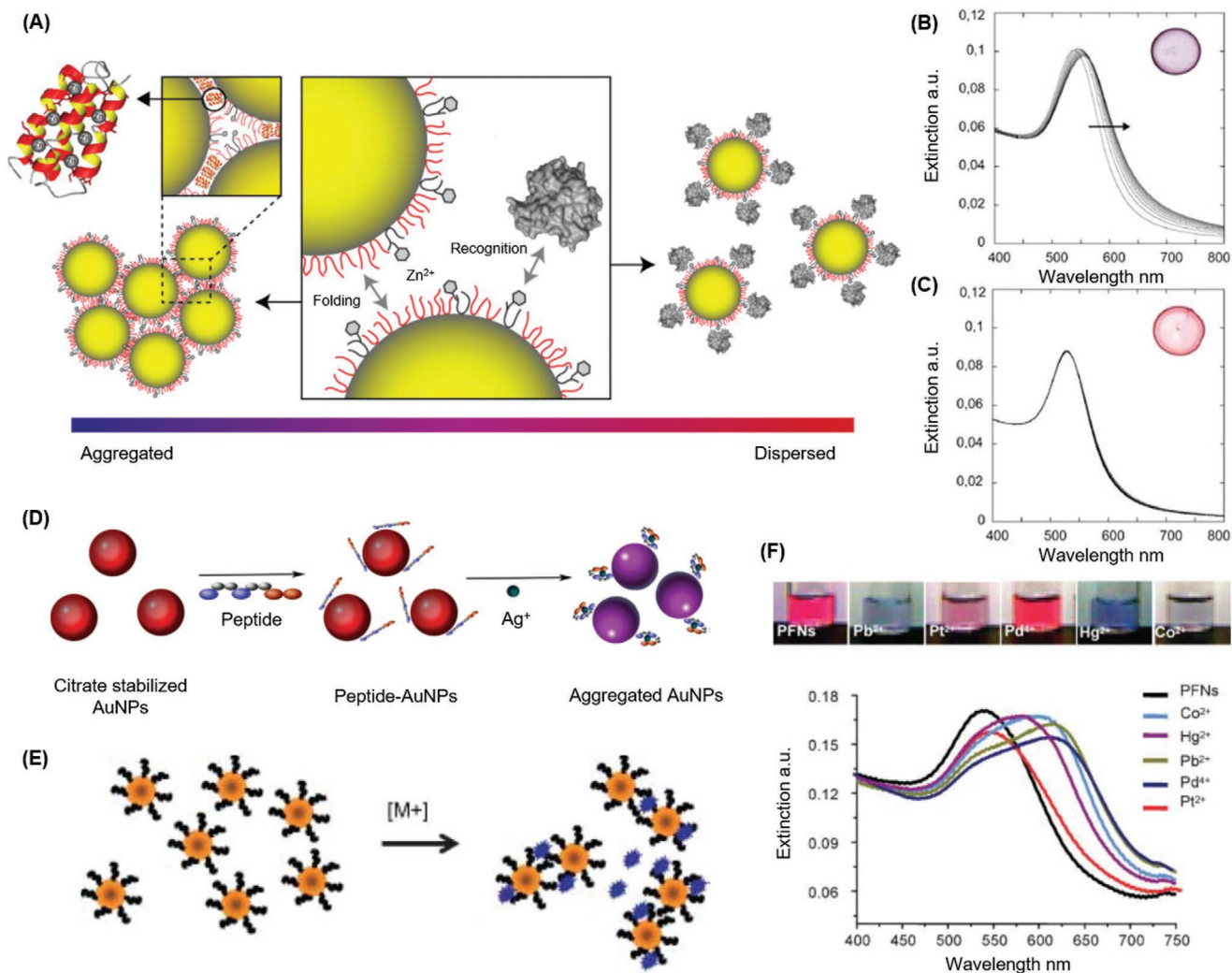


Figure 12. A) Schematic illustration of detection principle for protein analytes based on designed peptide binder functionalized AuNPs. The folding of peptide induced by Zn^{2+} ions subsequently caused aggregation of AuNPs, whereas the binding of protein analytes such as HCAII precluded the folding of peptide and the following aggregation. UV-vis spectra recorded with 2-min intervals for 20 min after addition of 10 mM Zn^{2+} ions in the absence (B) and in the presence (C) of HCAII proteins. Insets showing the corresponding colors of the dried AuNPs solutions. Reproduced with permission.^[145] Copyright 2009, Wiley-VCH. D) Schematic illustration of colorimetric detection of Ag^+ based on peptide binder and AuNPs. The folding of peptide binders upon addition of Ag^+ induced aggregation of AuNPs. Reproduced with permission.^[147] Copyright 2016, Elsevier B.V. E) Schematic illustration of colorimetric detection of metal ions based on peptide functionalized AuNPs by complexation. F) Colorimetric responses of peptide functionalized AuNPs to various metal ions and their corresponding spectra. Reproduced with permission.^[152] Copyright 2008, Wiley-VCH.

Ru-GO surface due to the peptide-TNT interaction, leading to ECL signal restoration.^[134] Goldman et al. selected phage-displayed peptides that bind to a TNT derivative, 2,4,6-trinitrobenzene in environmentally relevant artificial seawater, and integrated the selected phage for competitive detection of TNT. The best-binding phage shared the consensus sequence His, Arg, and Trp at position 2, 3, and 9 of the amino terminals of the fused 12-mer peptide.^[156] Kuang et al. rationally designed a peptide binder that is capable of spontaneously attaching to SWNT and TNT, and applied the peptides for SWNT field effect transistor detection of TNT.^[46] Other peptides were also designed for the specific detection of acetic acid and ammonia vapors based on peptide/nanowire sensors.^[47]

Proteins: Binding interactions among proteins/peptides are plentiful and fundamental in biological processes, not only because all aforementioned enzymatic reactions in Section 3.1 involve first binding followed by catalysis, but also because there are many other non-enzymatic binding events occurring to support life forms. Therefore, they constitute an attractive source of inspiration for the design of peptide binders for applications in drug discovery and biomolecular detection. Recently, Liu et al. reported a direct binding induced AuNP aggregation assay for human cardiac troponin I (cTnI) protein.^[157] The specific peptide binder (FYSHSFHENWPS) was adopted from previous study^[158] and modified onto AuNP surface mixed with spacer peptide. Immediately after the addition of target protein, peptide-functionalized AuNP aggregated which resulted in a

concomitant UV-visible spectral peak-shift and color change (Figure 13A). In this case, the peptide ligand could bind to different binding sites on cTnI, which triggered the aggregation of AuNPs. In addition, they investigated different sizes of AuNPs and found that peak-shift increased with decreasing the total surface area of AuNPs (Figure 13B). Another colorimetric assay for the detection of vascular endothelial growth factor receptor 1 (Flt-1) based on peptide-decorated AuNPs was recently developed.^[159] The peptide (WHSDMEWYLLG-GGGGC) was designed with Flt-1 binding motif (WHSDMEWYLLG) at the N-terminus, hydrophobic spacing region (GGGG) in the middle to reduce the steric hindrance between protein molecule and gold surface, and a cysteine residue to attach on the gold surface. In this strategy, cucurbit[8]uril molecule (CB_[8]) was applied to trigger the aggregation of the peptide-AuNPs because two aromatic residues from the peptide can be selectively accommodated in the CB_[8] cavity. However, when the

target protein Flt-1 is preincubated with the AuNPs and is then exposed to the CB_[8], no aggregation occurred because the peptide binding sites were occupied by Flt-1 which competed the interaction between the peptides and CB_[8] (Figure 13C). Interestingly, instead of 2 peptides reacting with one target protein, as mentioned previous for cTnI, this peptide reacted with Flt-1 at 1 to 1 ratio. Therefore, rather than aggregation triggered by the target (cTnI), the presence of Flt-1 hindered the aggregation of AuNPs.

Alternatively, a colorimetric immunoassay had been developed by Stevens' group who utilized peptidyl epitope tagged AuNPs for detecting the corresponding antiviral antibodies. A series of peptide epitopes were designed based on the *Haemophilus influenzae* hemagglutinin epitope YPYDVPDYA (HA), herpes simplex virus glycoprotein D epitope TQPELAPEDPED (HSV), and c-Myc protein epitope EEQKLISEEDLL (Myc), which were modified with linker amino acids terminated

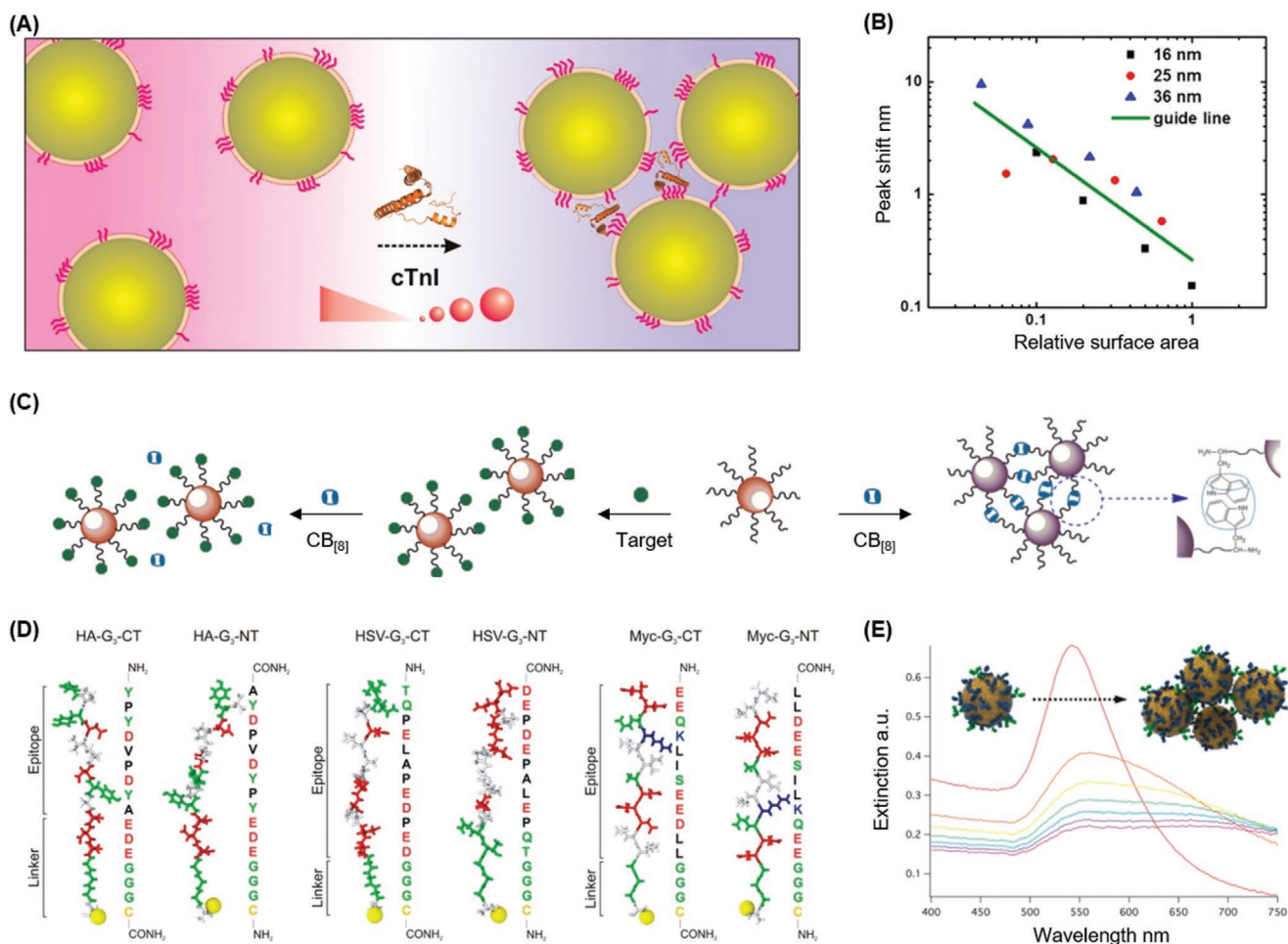


Figure 13. A) Schematic illustration of detecting cTnI by using peptide binders functionalized AuNPs in different sizes and concentrations. Simple addition of target cTnI induced rapid aggregation in a concentration-dependent manner. B) Peak (centroid) shifts plotted versus different relative surface areas of AuNPs (four dilution factors in each size: 16 nm, black square; 25 nm, red circle; and 36 nm, blue triangle) in response to 100 ng mL⁻¹ cTnI. Reproduced with permission.^[157] Copyright 2016, American Chemical Society. C) Schematic illustration of colorimetric detection Flt-1 in the presence of CB_[8] molecules based on peptide functionalized AuNPs. Reproduced with permission.^[159] Copyright 2015, Elsevier B.V. D) Linear structures of designed peptides containing target virus epitopes, linkers (GGG) and a cysteine residue. E) UV-vis spectra recorded with 10-min intervals after addition of 200 nM monoclonal antibodies in the corresponding peptidyl epitopes coated AuNPs solution, indicating the massive aggregation. Reproduced with permission.^[160] Copyright 2014, American Chemical Society.

with cystine to yield a fully dispersed suspension of AuNPs (Figure 13D).^[160] These functionalized AuNPs aggregated in the presence of corresponding antiviral antibodies as demonstrated with the changes of the absorbance spectra (Figure 13E). This immunoassay achieved low-nM range LOD of antibodies for potential applications in point-of-care diagnostics. A similar competitive fluorescence assay for multiple targets was demonstrated involving antibody–peptide epitope conjugating pairs and AuNPs as the quencher.^[161] The dye-labeled peptide antigens were reacted with the antibody-conjugated AuNPs that induced the fluorescence quenching. While in the presence of target molecules, the dye-labeled peptides were blocked from binding to the antibodies resulting in free peptides in the solution with high fluorescence intensity. These methods were applied for multicolor detection of three different targets incorporated with their relevant antibodies and three peptide antigens labeled with different fluorescent dyes.

Others biosensing assays based on the peptide binder include the inhibition assay. For instance, an human chorionic gonadotropin (hCG)-binding peptide that can trigger the aggregation of AuNPs in solution was modified on an electrode surface and resulted in the assembly of AuNPs on the electrode surface. The presence of hCG onto the electrode surface through the probe–target interaction made the peptide incapable of triggering the formation of the AuNP aggregates on electrode surface, thus leading to an increased charge transfer resistance. This electrochemical impedance technique allowed for the detection of hCG with an LOD of 0.6 mIU mL⁻¹.^[162] A similar method was carried out based on a kinase peptide binder for the detection of kinase with an LOD of 20 mU mL⁻¹.^[163]

Extracellular Vesicles: Intercompartmental transfer via extracellular vesicles (EVs) has been discovered as a mechanism for intercellular communication that is of vital importance in multi-cellular organisms, allowing cells to exchange various cargos such as proteins and nucleic acids.^[164–167] Generally, EVs can be divided into exosomes and microvesicles originating from endosomal and plasma membranes, respectively, with typical sizes ranging from 50 up to 500 nm.^[164] EVs are involved in many physiological and pathological processes, which prove their significance for clinical applications.^[164,166]

Since exosomes, as one major category of EVs, are present in many body fluids, carrying unique sets of functional biological molecules depending on their origin and status, they thus have been used as novel biomarkers for clinical diagnosis, especially in cancer diagnosis.^[168–174] With the aforementioned properties of peptide and gold conjugates, novel assays involving such hybrid nanomaterials will be focused below. Recently, Packirisamy's group utilized a synthetic peptide called venteremin for specific targeting of tumor-derived exosomes via surface over-expressed heat shock proteins.^[175] LSPR responses of gold nanoislands provided a novel sensing platform for cancer diagnosis.^[176–178] Using the same strategy of LSPR, Im et al. reported a nanoplasmonic sensor (nPLEX) for detection of exosomes isolated from cancer cell lines.^[179] The sensing chip was functionalized with PEG and specific antibodies for the capture of exosomes (Figure 14A). The sensitivity was amazingly higher than ELISA with the potential for further improvement by applying secondary labeling of AuNPs (Figure 14B). More importantly, molecular profiling of exosomes also was

done which enabled the investigators to distinguish ovarian cancer patients from noncancer ones. Other than LSPR, surface-enhanced Raman scattering (SERS) was also used for selectively capturing exosomes secreted by cancer cells based on specific peptides and plasmonic nanoparticles.^[180]

Bacteria and Virus: Bacterial infections remain one of the leading causes of death in developing nations.^[181] The current detection methods rely on the antibodies as molecular recognition elements due to their highly specific targeting of antigenic sites. However, the stability of antibodies is limited for the detection of species in harsh environments. Therefore, detection of bacteria with specific designed peptide ligands were intensively studied, especially antimicrobial peptides.^[182–184] For instance, Mannoor et al. employed an antimicrobial peptide magainin I (GIGKFLHSAGKFGKAFVGEIMKS) as the recognition element to selectively bind the bacterial *Escherichia coli* O157:H7 (Figure 14C). After immobilization of the peptide on the gold microelectrode array, the selective binding of bacteria was monitored by impedance spectroscopy with the sensitivity down to 1 bacterium per μL , a clinically relevant limit (Figure 14D).^[185] In addition, Azmi et al. employed a synthetic peptide array library to screen short peptide fragments for high and specific binding to *Listeria monocytogenes*, one of the most common food pathogens.^[186,187] The peptide fragments were derived from three potent anti-listerial peptides that belong to class IIa bacteriocins. The results showed that the fragment Leu-10 (GEAFSAGVHRLANG) possessed the highest binding affinity to several pathogenic Gam-positive bacteria. Further study using peptide-modified gold microcantilevers showed that the 14-residue peptide fragment offered the same sensitivity for detection of *Listeria* as the 37-residue peptide, suggesting that Leu-10 may possess a similar conformation and binding mechanism as that of full-length bacteriocins to the target bacteria.

Biosensor assays for the detection of virus also have been developed based on synthetic peptide binders.^[188–190] For instance, Hwang et al. described a short linear peptide binder obtained through phage display specific for recombinant noroviral capsid protein with binding affinity of nanomolar range.^[190] Later, they immobilized this peptide (QHKMHK-PHKNTKGGGSC) on gold surface for electrochemical detection of human norovirus with detection limit down to 78 copies per mL (Figure 14E).^[189]

Besides all the examples discussed above, many other specific peptides^[191] that function as peptide binders have been studied and utilized for various bioassay development against multiple targets such as TNT,^[192] beta-amyloid oligomers,^[193] as well as renin.^[194] Table 3 lists presentative assays based on utilizing peptide as binders in conjunction with peptide–gold conjugates.

3.2.2. For Cell Targeting and Subsequent Applications

Peptide ligands labeled with AuNPs have been intensively used for cell targeting, subsequent imaging, cellular internalization, or therapy due to their relatively low toxicity and high permeability. The underlying design principles are very similar to those employed in biosensing: peptide as a specific ligand for

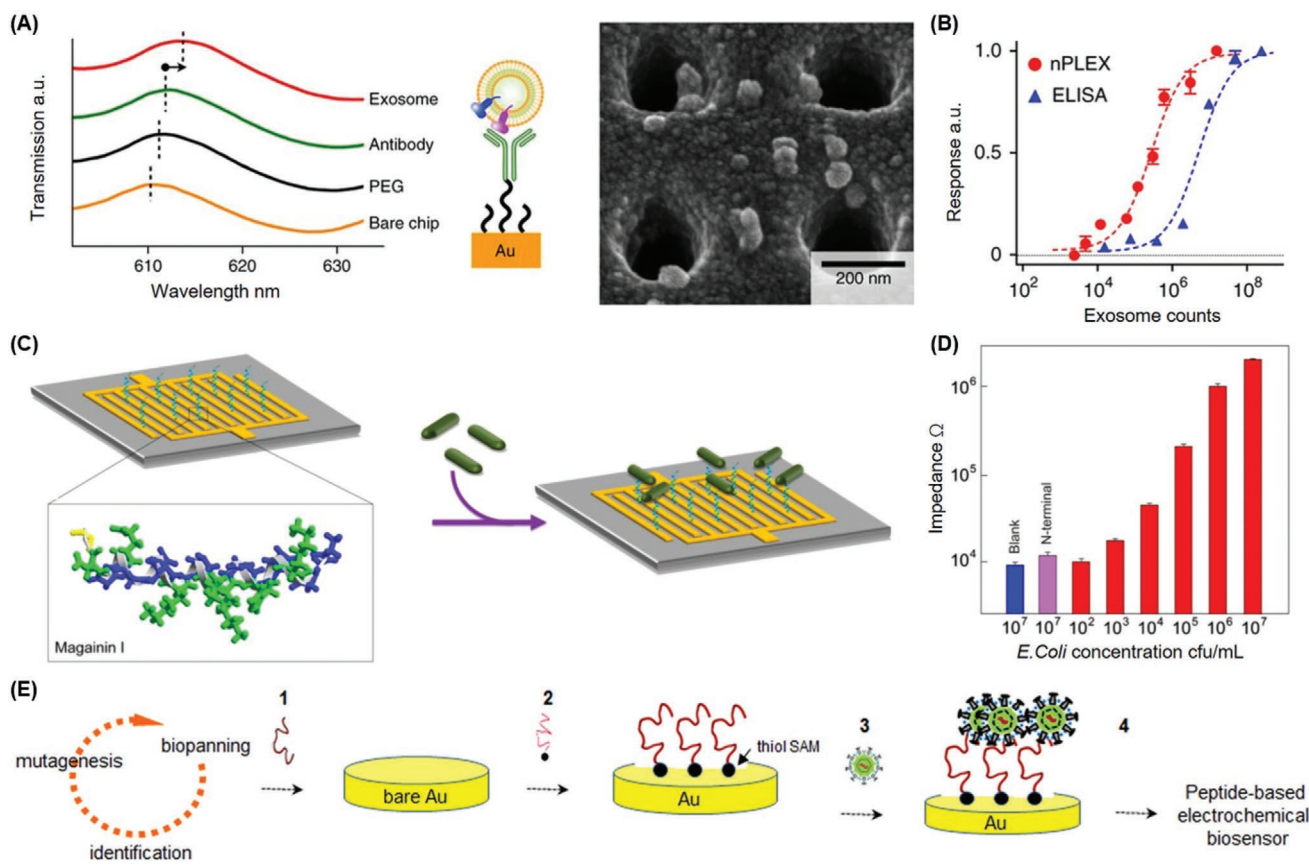


Figure 14. A) Representative LSPR spectra of bare gold (orange), after immobilizations of PEG layer (black) and antibody (green), and final detection of exosomes (red) with a simple schematic illustration aside. SEM image showed the binding of exosomes on gold nanoholes. B) Sensitivity comparison of nPLEX and ELISA, in which nPLEX showed a better result than ELISA by titrating various concentrations of exosomes. Reproduced with permission.^[179] Copyright 2014, Nature Publishing Group. C) Schematic illustration of electrical detection of bacteria based on antimicrobial peptides, magainin I with its structure (colored α -helix), including immobilization on gold microelectrode array and binding of target bacteria. D) Impedance measurements at 10 Hz versus various concentrations of *E. coli* with an estimated LOD of 10³ cfu mL⁻¹ (\approx 1 bacterium per μ L). Reproduced with permission.^[185] Copyright 2010, National Academy of Sciences. E) Schematic work flow of peptide-binder based electrochemical detection of norovirus including peptide selection by phage display technique (1), design and synthesis of peptide binder (1–2), immobilization (2–3), and test (3–4). Reproduced with permission.^[189] Copyright 2017, Elsevier B.V.

binding to targets/receptors on (sub)cellular membranes. One of the pioneering works was published by Maus et al., who reported a way to conjugate conantokin-G peptide (ConG) to PEG-passivated AuNPs for selective binding to N-methyl-D-aspartate (NMDA) receptors recombinantly expressed on transfected HEK 293 cell surface (Figure 15A,B).^[17] The results also showed 10³ times increase in binding affinity for the AuNP-coupled peptide compared to the free peptide in solution due to the multivalency of these AuNPs,^[200] indicating that even in the case of relatively weak ligand–receptor interaction, high-affinity AuNP probes can be developed (Figure 15C). In addition, the peptide-functionalized AuNPs attached to the cell surface may also indicate the amount of target protein on the cell surface. Some specific membrane proteins, for instance in cancer cells, are over expressed and can be potentially evaluated based on the amount of peptide-functionalized AuNPs attached on the cells. Gao et al. reported peptide-conjugated gold nanoprobe for intrinsic nanozyme-linked immunosorbent assay of integrin expression level on human erythroleukemia (HEL) cells as well as visualizing spatial positions of

integrins by two-photon photoluminescence (Figure 15D).^[201] Integrin is a cell membrane receptor whose expression level is closely related to platelet aggregation and cancer pathogenesis, including prostate cancer and HEL cells. In this work, they utilized the AuNPs' enzyme-like catalysis property to amplify the colorimetric signal and quantified the expression level of integrin on HEL cells without cell lysis and protein extraction process. In addition, the unique nonlinear optical property of AuNPs allow the investigators to use two-photon photoluminescence for directly visualizing spatial position of the protein on cell membrane (Figure 15E). The absorbance intensity and the element Au content against the cell number shows a linearly increasing manner, indicating feasibility for the evaluation of integrin expression levels on cells (Figure 15F).

Tumor cells are considered the most concerned targets in cancer diagnosis and therapy.^[19,20,202–204] Targeting of tumor cells via molecular interactions between the membrane protein/receptors on the cells and specific molecules such as antibodies, aptamers, and peptides have been frequently applied. For instance, in vivo tumor cell targeting and imaging

Table 3. Works that involve peptide functioning as binder in biosensing.

Targets	Peptide sequences	Binding strategy	Methods	LODs (assay times)/ [dynamic ranges]	Highlights	Ref.
Metal ions and small molecules						
Ag ⁺	RFRRGDD	Amine-gold	Colorimetric	7.4 nM [10 ⁻³ nM]	Peptide folding upon the presence of silver ion and resulted aggregation of AuNPs	[147]
Co ²⁺ , Hg ²⁺ , Pb ²⁺ , Pd ⁴⁺ , and Pt ²⁺	DYKDDDDKPAYSSGPAPMPF	Thiol-gold	Colorimetric	190 nM Co ²⁺ , 26 nM Hg ²⁺ /[10 ⁰ -10 ² nM], 242 nM Pb ²⁺ , 31 nM Pd ⁴⁺ , and 23 nM Pt ²⁺ (1 min)	Metal ions crosslinking peptides via noncovalent binding and inducing the aggregation of AuNPs	[152]
Arsenic(III)	TQSYKHGC	Thiol-gold	Colorimetric	54 nM	Peptide-AuNPs aggregated at the presence of As(III)	[195]
2,4,6-trinitrotoluene (TNT)	WHWQRPLMPVSIK	Thiol-gold	Electrochemiluminescent	3.6 pg mL ⁻¹ [10 ⁻²⁻² ng mL ⁻¹]	Peptide as the binder for TNT which induced the release of peptide-AuNPs from graphene oxides surface	[134]
TNT	WHWQRPLMPVSIK-cysteamine	Thiol-gold	Impedimetric assay	0.15 μM (70 min)/ [10 ⁻¹ μM]	Peptide aptamers enabling electrochemical methods	[192]
Acetic acid	RVNEWVID	N.A.	Field-effect transistor (FET)	100 ppm	Peptide binder modified on FET sensor chips for direct detection of gas	[47]
Ammonia	DLESFLD	N.A.	FET	100 ppm	Peptide aptamers enabling electrochemical methods	[47]
Proteins and large molecules						
Human carbonic anhydrase II	Ac-NAADLEAAIRHLAEKLAARG-PCDAAQLAEQLAKXFEAFARAG (X: benzenesulphonamide modified lysine)	Thiol-gold	Colorimetric	10 nM (30 min)/ [10 ⁻² nM]	Bound of analytes to peptide binder inhibiting immediate aggregation of AuNPs due to addition of zinc ions	[145]
Recombinant antibody fragment (Fab57P)	CRGTGSYNRSSFESSGLV-NH ₂	Thiol-gold	Colorimetric	25 nM (30 min)		
Cardiac Troponin I (cTnI)	CALNN-PEG ₄ -FYSHSFHENWPS	Thiol-gold	Colorimetric	0.2 ng mL ⁻¹ in diluted serum (10 min)/ [10 ⁰⁻³ ng mL ⁻¹]	Achieving low detection limit of troponin I in diluted serum by using peptide functionalized AuNP	[157]
cTnI	CFYSHSFHENWPS	Thiol-gold	Electrochemiluminescent	0.5 pg mL ⁻¹ [3-70 pg mL ⁻¹]	A sandwich assay based on peptide-AuNPs was employed on a gold electrode	[196]
Antiviral antibodies	For anti-HA antibody: CGGEDEYYPDYPDA-NH ₂ ; CGGEDEAYDPVDYPY-NH ₂ For anti-HSV antibody: CCGTQPELAPEDPED-NH ₂ ; CCGDEPDEPALEPQT-NH ₂	Thiol-gold	Colorimetric	Low nM (30 min)/ [10 ⁰⁻² nM]	Antiviral antibody detection using peptide epitopes and further investigation on mechanism of AuNP aggregation	[160]
Leucine-enkephalin (LE); prion protein (PP); cTnI	For LE: FITC-YGGFL; For PP: Cy3-RESQAYYQRGASVIL; For cTnI: Cy5-MADGSSDAAREPRPAC	Antigen-antibody	FRET	5 pg mL ⁻¹ for LE, 8 pg mL ⁻¹ for PP, and 14 pg mL ⁻¹ for cTnI; less than 100 pg mL ⁻¹ for all targets in diluted human serum (30 min)/ [10 ⁻⁴ pg mL ⁻¹]	Differently labeled peptides mimicking targets for competing multi-targets assay	[161]
HIV-1 protease	pepstatin: XVVX'AX' (X: Isovaleryl; X': statine)	Thiol-gold	Electrochemical impedance spectroscopy (EIS)	Less than 10 pM (60 min)	Peptide/single walled carbon nanotube/AuNP structure: for detecting and inhibitor screening	[77]

Table 3. Continued.

Targets	Peptide sequences	Binding strategy	Methods	LODs (assay times)/ [dynamic ranges]	Highlights	Ref.
Beta-amyloid oligomers (A β O)	THSQWNKPSKPKTNMK	Electrostatic	Colorimetric and fluorescence	0.2 nM (10 min)/ [10 ⁰⁻² nM]	Soluble peptide aptamer receptors for detecting presence of beta-amyloid oligomers, resulting in failure of triggering AuNP aggregation and subsequent fluorescence recovery of quantum dots	[193]
A β O	CTHSQWNKPSKPKTNMK	Thiol-gold	EIS	45 μ M	Presence of A β O inhibited the formation of AuNP aggregates on the electrode surface	[162]
Renin	IQRKRQGP	N.A.	Electrochemical assay	0.3 μ g mL ⁻¹ (15 min)/ [10 ⁻¹⁻² μ g mL ⁻¹]	Peptide aptamer screening for specific renin binders through cDNA display technology, followed by competitive electrochemical assays for renin detection facilitated by peptide-AuNPs	[194]
Human chorionic gonadotropin (hCG)	CPPLRINRHILTR	Thiol-gold	EIS	0.6 mIU mL ⁻¹	Presence of hCG inhibited the formation of peptide-AuNPs aggregation on the electrode surface	[162]
hCG	PPLRINRHILTR	N.A.	SPR	0.065 nM	Direct detection of hCG with the peptide modified SPR chip.	[197]
PKA	TTYADFIASGRTGRRNAIHD	Electrostatic	Colorimetric and Electrochemical assay	2 U mL ⁻¹ (15 min)/ [10 ⁰⁻¹⁰ U mL ⁻¹] of colorimetric assay 0.02 U mL ⁻¹ (30 min)/ [10 ⁻²⁻¹⁰ U mL ⁻¹] of electrochemical assay	Peptide induced AuNP aggregation was prevented by peptide once binding to PKA; peptide binding of PKA inhibited further binding of AuNPs onto the electrode surface	[163]
Cholera toxin	VQCRLGPPWCAK	Thiol-gold	LSPR/surface-enhanced Raman scattering (SERS)	1.89 ng mL ⁻¹ by LSPR; 3.51 μ g mL ⁻¹ by SERS	Peptide modified on the sensor chip for the binding of cholera toxin	[198]
Lipopolysaccharides (LPS)	KKNYSSSISSIHIC	Thiol-gold	SPR	32.5 ng mL ⁻¹	Peptide as the LPS receptor was immobilized on gold chips for the SPR sensors	[140]
Extracellular vesicles						
Breast cancer cell derived exosomes MCF7	Venceremin (patented peptide)	Biotin-streptavidin	LSPR	Less than 2.66 \times 10 ⁸ particles per mL [10 ⁸⁻¹⁰ particles per mL]	Exosomes captured by peptide binder which was immobilized on gold nanoislands (LSPR response)	[177,178]
SKOV-3 ovarian tumor cells derived exosomes	LXY30: cyclic C _d D _d GX ₁ GX ₂ NC _d R X ₁ : 3,5-difluorophenylalanine X ₂ : hydroxyproline	Thiol-gold	SPR	Less than 3.4 \times 10 ⁹ particles per mL	Self-assembled on-chip capture of tumor derived exosomes by modified peptide	[173,199]
SKOV-3 ovarian tumor cells derived exosomes	LXY30: cyclic C _d D _d GX ₁ GX ₂ NC _d R X ₁ : 3,5-difluorophenylalanine X ₂ : hydroxyproline	Thiol-gold	SERS	—	Peptide-exosome-particles complex used for SERS detection	[180]
Bacteria and virus						
<i>E. coli</i> O157:H7	magainin I: CGIGKFLHSAGKFGKAFVGEIMKS	Thiol-gold	EIS	10 ³ cfu mL ⁻¹ (15 min)/ [10 ³⁻⁷ cfu mL ⁻¹]	Electrical detection of bacteria based on antimicrobial peptide and further enabled real-time detection on microfluidic chips	[185]
<i>Listeria monocytogenes</i>	Leu10: GEAFSAGVHRLANG	Thiol-gold	Microcantilever	Less than 10 ⁵ cfu mL ⁻¹ (20 min)	Screened peptide from a peptide library used in detection of several pathogenic Gram-positive bacteria	[187]
Norovirus	QHKMKHPKHNKGGGSC	Thiol-gold	EIS	7.8 copies per mL	Norovirus peptide binder immobilized on the electrode for the detection of human norovirus	[189]

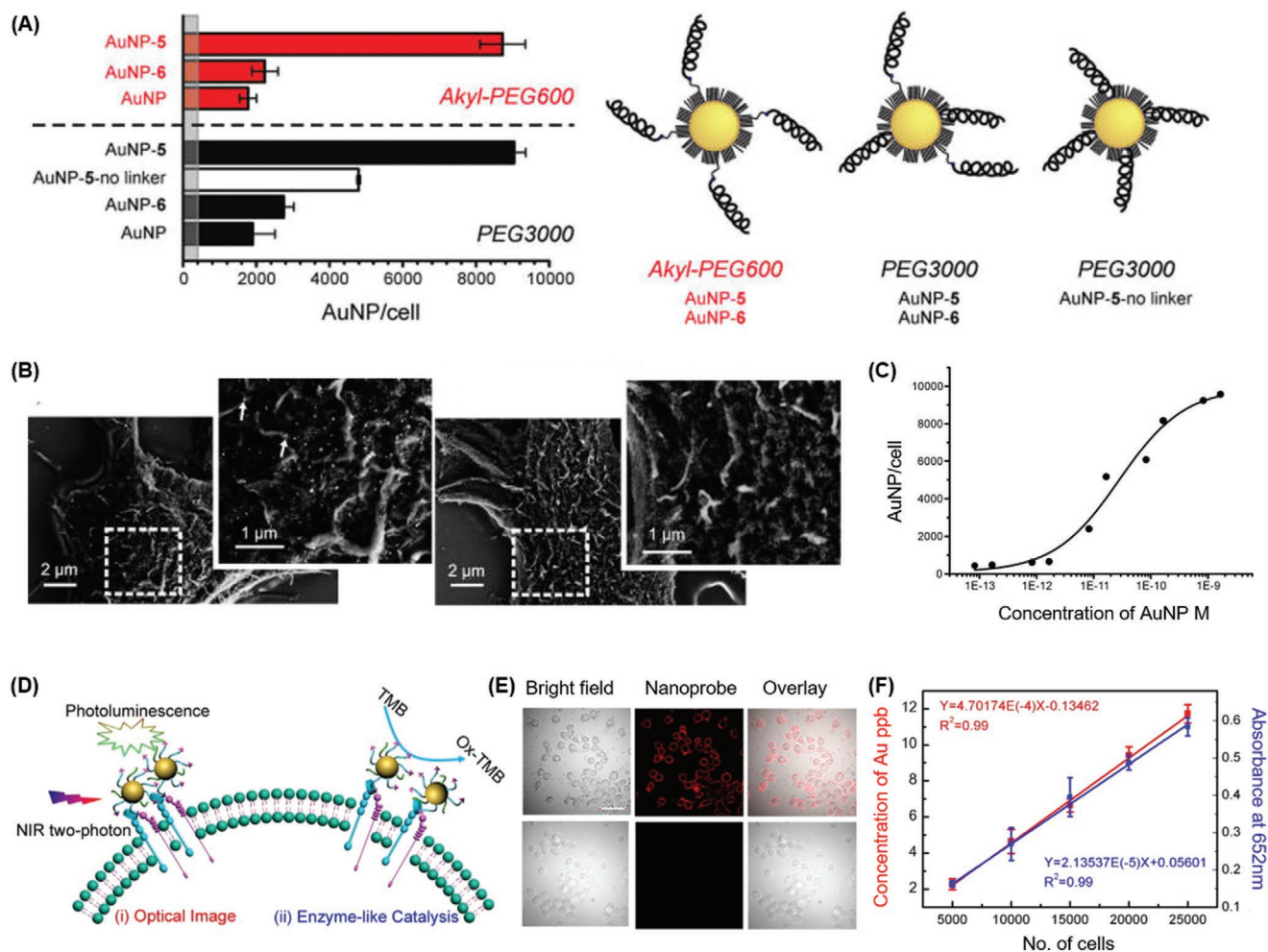


Figure 15. A) Bar chart showed the selective binding of peptide 5 (ConG sequence: GEXXLQXNQXLIRXKSNC, X: γ -carboxyglutamate, terminal C for immobilization) functionalized AuNPs (AuNP-5) onto HEK 293 cells with surface NMDA receptors. Peptide 6 was mock-peptide. Schematic drawings of peptides-AuNP were shown on the right suggesting the full accessibility in Alkyl-PEG600 passivation system. B) SEM images of the selective binding of AuNP-5 to the transfected cells (left, many bright dots) compared to AuNP-6 treated cells (right, hardly found). C) Binding curve of AuNP-5 to the transfected cells, indicating a thousand times increased binding affinity by calculation compared to free ConG due to multivalency. Reproduced with permission.^[17] Copyright 2010, American Chemical Society. D) Schematic illustration of peptide functionalized AuNPs selectively targeting cellular integrin GPIIb/IIIa for imaging (i) and quantitatively colorimetric sensing (ii). E) Bright field (first column) and two-photon photoluminescence (second column) images of cultured cells exposed to 120 nm peptide-AuNPs only (first row) and to disperse medium as negative control (second row), indicating the specificity of such nanoprobes. F) Linear fitting curves associated cell numbers with AuNPs concentrations (red) and colorimetric signals (blue), enabling to calculate the amount of integrin GPIIb/IIIa on each cell surface. Reproduced with permission.^[20] Copyright 2015, American Chemical Society.

using peptide–AuNP conjugates were realized by Bhatia’s group using “click” chemistry.^[205] The cyclic peptide Lyp-1 (CGNKRTRGC) targeting to p32-expressing tumor cells was synthesized to incorporate with pendent alkyne (i.e., propargylglycine or 6-heptynoic acid) and a 5,6-carboxytetramethylrhodamine fluorophore (Figure 16A). The “click” reaction took place between the pendent alkyne on the peptide and the azido-PEG-AuNPs under copper catalysis for immobilization of peptide on AuNPs (Figure 16B), and specific targeting of cancer cells with increased near-infrared fluorescence (Figure 16C). Further study of the Lyp-1-AuNPs injected intravenously into mice bearing human cancer xenografts showed the significant accumulation of Lyp-1-AuNPs in regions of high p32 expression. Later bombesin-AuNPs was demonstrated to have high

affinity toward gastrin-releasing peptide receptors in vivo which were usually overexpressed in prostate, breast, and lung carcinoma.^[16,206] Additionally, cyclic RGD peptide labeled AuNPs also displayed targeting capability to tumor cells via integrin $\alpha_v\beta_3$, which plays an important role in human tumor metastasis and tumor-induced angiogenesis and has a high affinity to ligands containing the RGD sequence.^[207,208] Qian et al. modified AuNPs with a single-chain variable fragment peptide (25 kDa) for in vitro and in vivo tumor targeting with SERS techniques.^[209] This peptide ligands/fragments recognize the epidermal growth factor receptor that is overexpressed in many types of human malignant tumor cells. The results demonstrated highly specific recognition and SERS detection of both human cancer cells and xenograft tumors in mice. With the

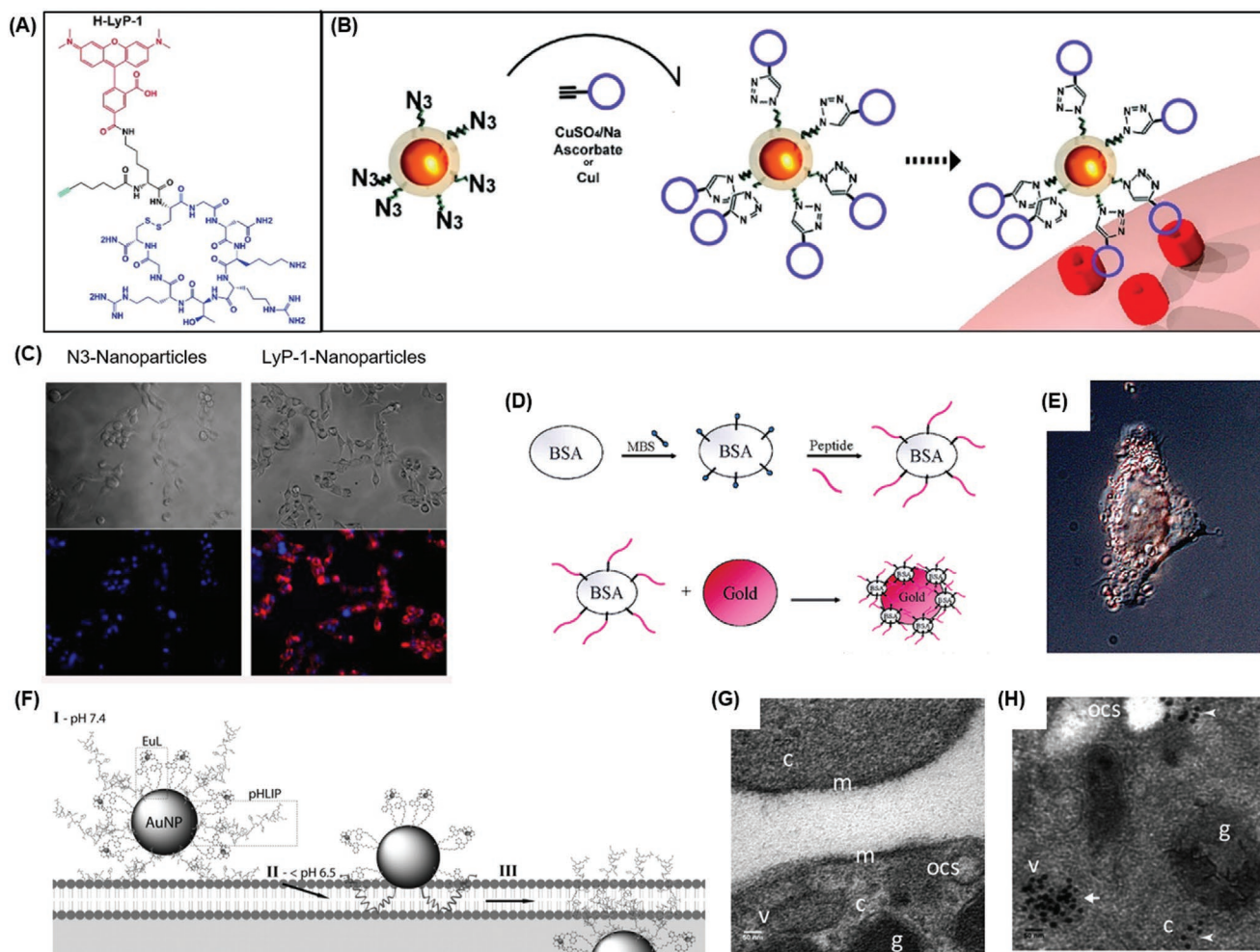


Figure 16. A) Chemical structure of native LyP-1 peptide which targeted p32-expressing MDA-MB-435 cells. B) Schematic illustration of the functionalization of LyP-1 peptide (purple circle) onto azido-PEG coated AuNPs via click chemistry and targeting the receptor (red) expressing cancer cells in vitro and in vivo. C) Fluorescence images of LyP-1-AuNPs (right) targeting cancer cells showed increased near-infrared fluorescence (red), while no detectable signal was observed for azido-PEG-AuNPs as control (left). Reproduced with permission.^[205] Copyright 2008, American Chemical Society. D) Schematic illustration of functionalization of AuNPs with specific nuclear-targeting peptide-bearing BSA proteins. According to more than 200 cells, it showed an estimated 80% targeting rate of nucleus. Representative overlapped image (E) of the cultured HepG2 cell was taken after 2-h incubation with the peptide-AuNPs. Reproduced with permission.^[210,211] Copyright 2003 and 2004, American Chemical Society. F) Schematic illustration of the pH-dependent pHLIP-EuL-AuNPs translocation into cells. The proposed mechanism was mainly due to the conformational change of pHLIP from random coil to helix at a lower pH. G) TEM images of human platelets untreated and H) treated with pHLIP-EuL-AuNPs. The latter showed nanoparticles penetrating into various platelet structures such as vesicles (v), open canalicular system (ocs), and cytoplasm (c). Reproduced with permission.^[215] Copyright 2012, National Academy of Sciences.

SERS technique, the method was able to achieve >200 times brighter with the AuNPs than near-infrared-emitting quantum dots, and allowed spectroscopic detection of small tumors of 0.03 cm³ at a penetration depth of 1–2 cm. In combination with genetic, photo-thermo, and chemo-therapies, Artzi and her colleagues employed peptide–AuNP (rod and sphere) embedded hydrogel to treat colorectal cancer in mice and successfully eliminated the tumor recurrence. Peptides involved in this work ensured the accurate delivery of nanoparticles to the tumor cells.^[20]

Cellular internalization of peptide–AuNP conjugates required penetration of the cell membrane usually via receptor-mediated endocytosis (RME), followed by escape of endosomal vesicles and subcellular targeting. Some early work done by Franzen's

and Feldheim's groups focused on nuclear targeting by multi-functional peptide–AuNPs (i.e., containing both RME peptide to enter the cell and nuclear localization signal [NLS] peptide to interact with the nuclear pore complex) illustrating a potential delivery vehicle for genetic therapy (Figure 16D,E).^[210–213] These peptides are from adenoviral RME (CKKKKKKSEDEYPYVPN) and NLS sequence (CGGFSTSLRARKA). The study on the targeting in HepG2 cells showed that the nanoparticles carrying both peptides displayed a greater propensity for nuclear targeting than any other single peptide, including the single full-length peptide containing both sequences. The other single peptide modified AuNPs either did not enter the cell (NLS peptide), or entered the cell but remained trapped in endosomes and did not reach the nucleus (RME peptide).

Replacement of the subcellular sorting peptides on AuNPs further enabled targeting the lysosome which enriched the strategy of treating lysosomal storage diseases.^[214] However, the internalization was not exclusively mediated by RME, as reported recently by Davies et al. who showed a pH-controlled delivery of AuNPs into platelets.^[215] It was proposed that the main functional component, the low pH insertion peptide, could adopt certain conformation and interact with lipid bilayer of platelets once $\text{pH} < 6.5$, followed by translocation into the cell (Figure 16F). Functionalized nanoparticles were observed penetrating into various platelet structures by SEM images with negative control (Figure 16G,H). Regardless of the various signal peptides, there are many other factors such as surface charges and particle sizes which would affect the internalization process and closely relate to toxicity as well.^[18,216,217]

It is well known that it is difficult to target the brain because of the presence of BBB which limits the development of treatment for many brain-related disorders like Alzheimer's disease^[218] and glioblastoma.^[219,220] This obstacle has to be overcome, requiring the so-called transcytosis. Surprisingly, using specific peptide conjugated AuNPs containing sequences that interacts with the transferrin receptor on the microvascular endothelial cell of BBB could significantly enhance the permeability, thus enabling drug delivery (Figure 17A).^[221] For example, the high permeability of THR-CLPFFD-AuNPs was proven by measuring the gold mass in the dry rat brain tissues and comparing it with various controls (Figure 17B).

On the other hand, if there is tumor developing in the brain, the BBB will be compromised because of the vascular leakiness as tumor cells develop, which offers an opportunity for functionalized AuNPs to cross the BBB and accumulate in tumors via the "enhanced permeability and retention effect" (EPR effect).^[222,223] Lesniak's group has employed a trans-activator of transcription peptide-modified AuNP (TAT-AuNP) with a 5 nm core size which was able to pass through the BBB efficiently by EPR effect for delivery of the anticancer drug doxorubicin (Dox) or Gd^{3+} contrast agents to brain tumor tissues for imaging (Figure 17C).^[19] The clear localization of AuNPs in mouse brain tumor cells was observed by microscopic image after staining (Figure 17D). Furthermore, the difference of survival rate for tumor-bearing mice with or without Dox-TAT-AuNP treatment indicated the successful delivery of Dox across BBB (Figure 17E). Meanwhile the Gd^{3+} contrast agent in Gd^{3+} -TAT-AuNPs was also delivered into tumor tissues and enhanced the MRI results (Figure 17F), which was double confirmed by histological studies (Figure 17G,H).

Alternatively, Gao et al. employed a pair of AuNPs which were decorated with azide and alkyne, respectively, prior to coating with PEG and BBB-permeable angioprep2 peptides (Figure 17J).^[219] After intravenous injection of the mixture of the two probes, they entered brain tumor by crossing the BBB via receptor-mediated transcytosis. These AuNPs were fully dispersed in a neutral environment, but aggregated and trapped after entering the tumors with acidic environment allowing removal of the PEG shielding layer and exposure of the azide and alkyne functionalities where the click cycloaddition occurs (Figure 17J,L). These probes guided both MRI and surface-enhanced resonance Raman spectroscopy imaging, which were further supported by histological studies (Figure 17K,M). Interestingly, microscopy studies verify the

precisely demarcated tumor margin marked by the assembled nanoprobe, which are considered as promising contrast agents in improving brain-tumor surgical outcome with high specificity, safety, and universality. All related works discussed in this section are summarized in Table 4.

4. Other Applications of Peptide–Gold Hybrid Nanomaterials

4.1. Antimicrobial Activities

The increase in antibiotic resistance has become a serious global health issue threatening the achievements of modern medicine.^[225] Antimicrobial peptides (AMPs), representing ancient host defence effector molecules, can combat drug-resistant bacteria mainly because their distinctive amino sequence can insert into and subsequently disintegrate bacterial cell surfaces.^[226–228] These peptides typically contain positively charged cationic domains which interact with negatively charged lipoteichoic acid and phospholipids on the membrane of microorganisms. While for the normal mammalian cells, the negatively charged lipids face to the cytoplasm, which explains the poor binding of cationic peptides to mammalian cells and the selective binding to bacteria.^[229] In addition, antimicrobial nanomaterials such as silver, copper oxide, zinc oxide, titanium dioxide, and gold nanoparticles have emerged as potential alternatives for the treatment of drug-resistant bacterial infections.^[230–236] The nanomaterials with small sizes provide large contact area with bacteria and lead to the destruction of the permeability and respiration functions of bacterial membranes.^[237] Among them, AuNPs are considered to be comparatively safer than other metallic nanoparticles because of the inert and non-toxic nature of gold. Moreover, the surface modification of AuNPs with cationic and hydrophobic groups has demonstrated effective resistance both to Gram-negative and Gram-positive uropathogens, including multi-drug resistant pathogens.^[22] Therefore, immobilization of AMPs to AuNPs present a promising solution with enhanced antimicrobial activity compared to each component.^[238,239] The AuNPs may also facilitate the interaction against lipopolysaccharide and proteins in the outer membrane of bacteria and get deposited on the membrane with relatively higher concentration of the peptides at the site of action,^[240–243] thus improving the permeability of the membrane through either porin channel^[244] or diffusion through the phospholipid bilayer.^[245] Some excellent works regarding peptide–AuNP conjugates discussed for antimicrobial applications have been reported in a recent review.^[246]

One of the earliest works on peptide-modified AuNPs for antibacterial was reported by Xu and co-workers who conjugated AuNPs with vancomycin (Van), a polypeptide antibiotic, via Au–S bonds (Figure 18A).^[247] The Au@Van nanoparticles showed an enhanced antibacterial activity against vancomycin-resistant enterococci (VRE) with minimum inhibitory concentration (MIC) of $2\text{--}4 \mu\text{g mL}^{-1}$ vancomycin on AuNPs, which was much lower than that for free vancomycin ($64 \mu\text{g mL}^{-1}$). Alternatively, Chen and colleagues prepared vancomycin-modified AuNPs via Au–O bonds through the direct reduction of gold ions by vancomycin in alkaline conditions ($\text{pH} = 12$) (Figure 18B).^[248] The MICs of the vancomycin-capped AuNPs

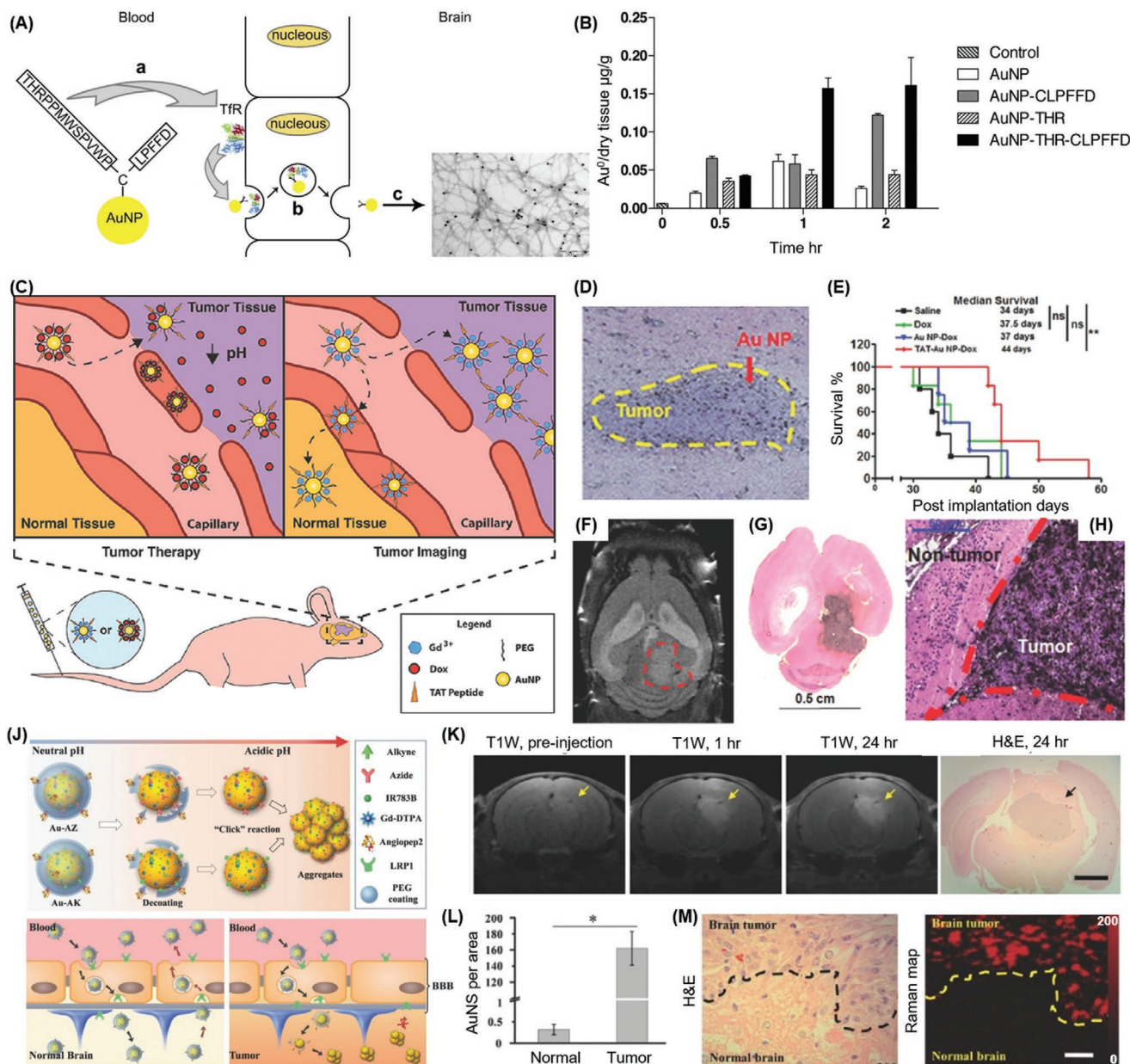


Figure 17. A) Schematic illustration of the design of peptide and the translocation of peptide-AuNPs from blood to brain via endocytic vesicles. The peptide contains THR sequence which recognizes the transferrin receptor, and LPFFD sequence which targets to $\alpha\beta$ aggregates in brain. B) The different gold contents in rat brain showed the highest amount of THR-CLPFFD-AuNPs was delivered across the blood–brain barrier compared to other controls. Reproduced with permission.^[221] Copyright 2012, Elsevier B.V. C) Schematic illustration of the delivery of TAT-AuNPs into brain tumors for therapeutic and diagnostic purposes. A therapeutic drug (Dox) was attached to TAT-AuNPs through a pH-sensitive linker (upper left); An MRI contrast agent (Gd^{3+}) was chelated on TAT-AuNPs and eventually accumulated in tumor cells (upper right). D) Microscopic image of mouse brain tissue stained by H&E (for tissue structures) and silver enhancement (for AuNPs) after Dox-TAT-AuNPs injection, showing the localization of nanoparticles on the tumor. E) Kaplan–Meier survival curves of intracranial tumor bearing mice after i.v. injected with Dox-TAT-AuNPs (red) comparing to other controls at the same dose of Dox. F) T_2 -weighted MRI horizontal section of an intracranial tumor bearing mouse after 24 h of Gd^{3+} -TAT-AuNPs injection (red dashed circle: tumor tissue). G, H) Histological studies of the intracranial tumor-bearing mouse with the same treatment. The brain tissue was stained by H&E and silver enhancement (black dots: enhanced AuNPs). Reproduced with permission.^[19] Copyright 2014, Wiley-VCH. J) Schematic illustration of the BBB-permeable angiopep2-peptides functionalized AuNPs that were acid-responsive. After de-coating of PEG layer triggered by physiological acidity, two kinds of nanoparticles (azido- and alkynyl-) aggregated via click chemistry, and eventually accumulated in brain tumor tissue. K) Brain T_1 -weighted MRI of a glioma xenograft bearing mouse before, at 1 h, and at 24 h after injection of the mixed functional AuNPs, showing the enhancement of signal due to the accumulation of nanoparticles in the glioma margin (yellow arrow). Histological studies of the same brain tissue after H&E staining that verified the margin. L) Average density of the functional AuNPs at the tumor and normal brain tissue area, showing the greatly increased amount of nanoparticles accumulated in tumor. M) Histological and Raman spectroscopic images of glioma brain tissue at 24 h after injection of the mixed functional AuNPs: area above dashed line. Reproduced with permission.^[219] Copyright 2017, Wiley-VCH.

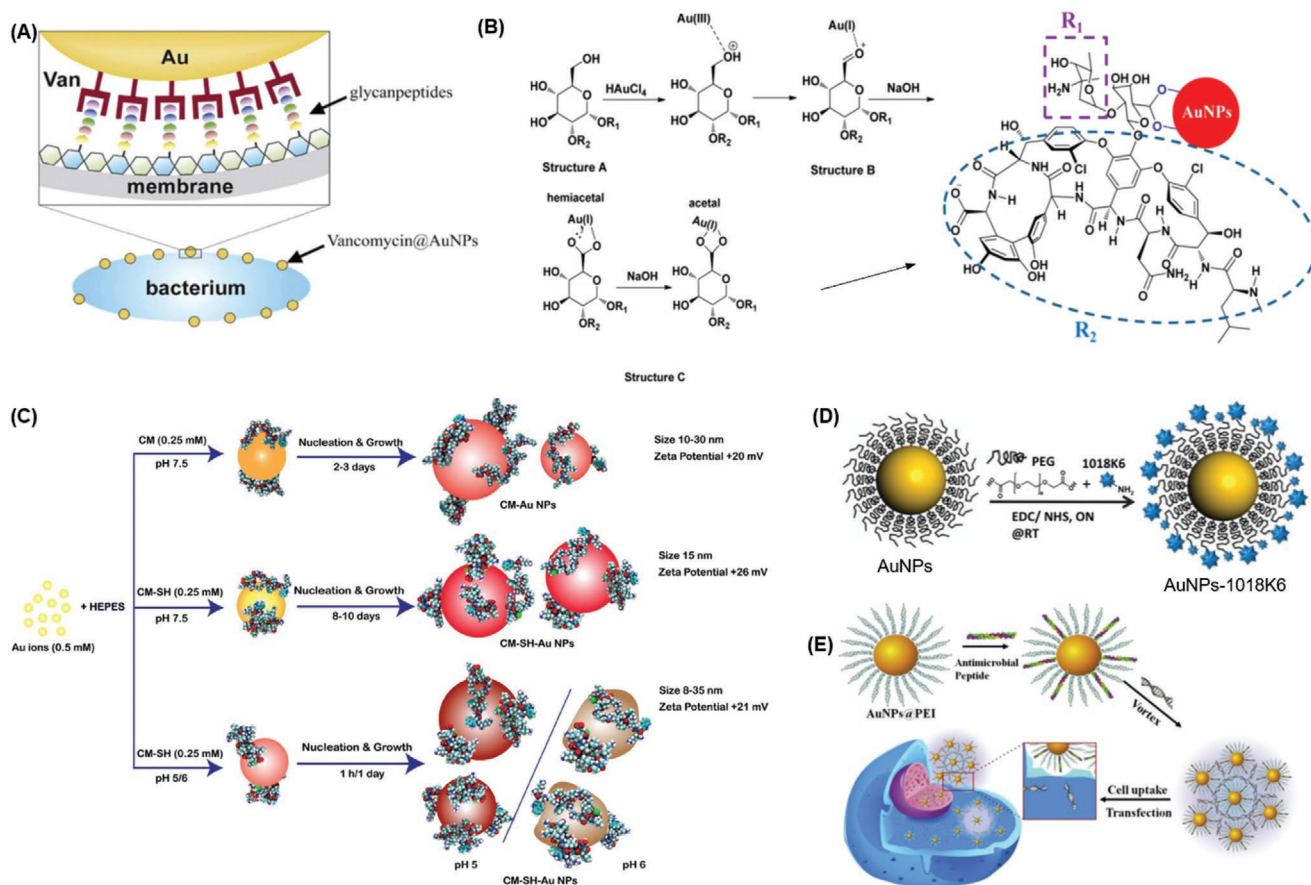


Figure 18. A) Illustration of the multivalent interaction between a vancomycin-conjugated AuNP and a VRE strain. Reproduced with permission.^[247] Copyright 2003, American Chemical Society. B) The reaction mechanism of vancomycin-directed synthesis of AuNPs. Reproduced with permission.^[248] Copyright 2015, American Chemical Society. C) The synthesis of AuNPs in the presence of CM-SH and CM peptide, under different experimental conditions. Reproduced with permission.^[249] Copyright 2016, Elsevier B.V. D) Conjugation of 1018K6 peptide to polymer-AuNPs via carbodiimide chemistry. Reproduced with permission.^[255] Copyright 2018, American Chemical Society. E) Schematic illustration of the preparation of antimicrobial peptide conjugated cationic AuNPs and their interaction with pDNAs and cells. Reproduced with permission.^[256] Copyright 2016, Elsevier B.V.

were significantly lower than the free vancomycin and showed excellent inhibition for the growth of vancomycin-resistant strains, including VRE1 (*Enterococcus faecalis*), VRE4 (*E. faecium*), methicillin-resistant *Staphylococcus aureus* (MRSA), and pandrug-resistant *Acinetobacter baumannii*. Similarly, Rai et al. also demonstrated a one-pot synthesis of AuNPs in the presence of *Cecropin melittin* peptide (KWKLFKKIGAVLKVLC, CM-SH), which formed a gold core and a hydrophilic cationic peptide shell (Figure 18C).^[249] This CM-SH-AuNP showed a higher antimicrobial activity accompanied with a higher stability in both serum and an animal model of systemic infection, compared to soluble CM-SH. This was attributed to the improved bacterial membrane permeability of the CM-SH-AuNPs compared to free CM-SH. They also pointed out that simple conjugation of CM-SH onto AuNPs by ligand exchange was, however, not stable after 1 h.

AuNPs with smaller sizes and different surface chemistries were also reported for antimicrobial applications. For instance, gold nanodots with a diameter of 2.5 nm were coated by surfactin (SFT),^[250] a cyclic lipopeptide with a sequence of ELLVDLL linked by a lactone bond to a C11-15 β -hydroxy fatty acid,

providing antimicrobial and antiviral properties.^[251] The peptide penetrated cellular membranes mainly because of its cation-carrier, pore-forming, and detergent-like properties.^[252,253] Compared to free SFT, the hybrid nanomaterials exhibited superior biocompatibility and significantly higher antimicrobial activity (>80-fold lower MIC) to both non-multi-drug-resistant bacteria and multi-drug-resistant bacteria, due to their synergistic effect on the disruption of the bacterial membrane.^[250] Moreover, in vivo wound healing studies in rats suggested faster healing and better epithelialization when hybrid nanomaterials were used as a dressing material.^[250] Wang and co-authors prepared antibacterial hybrid by covalent bond between gold nanoclusters (AuNCs) and daptomycin (Dap), a cyclic antimicrobial lipopeptide. Compared with the physically mixed AuNC and daptomycin, the synthesized Dap-AuNCs hybrid showed higher antibacterial activity against MRSA. The nanomaterials also showed significant fluorescence enhancement resulting from the aggregation-induced emission caused by Dap-AuNCs hybrid. In addition, the hybrid nanomaterials might also induce strong DNA destruction of bacteria due to localized high concentration of ROS generated by the localization of AuNCs.^[254]

Palmieri et al. conjugated 1018K6 peptide (VRLIVKVRIWRR) to hybrid polymer coated AuNPs via carbodiimide chemistry (Figure 18D).^[255] The 1018K6 peptide were designed by Palmieri with specific antibacterial activity against *L. monocytogenes*, one of the most common food pathogens.^[186] The resulting nanomaterials showed an enhanced antibacterial activity with MICs at submicromolar (<100 nM) concentrations of peptide, which killed almost 100% of pathogen bacteria, such as *Listeria* and *Salmonella* genera. Such low concentration of this small peptide, bioconjugated to AuNPs, paved the way for its large-scale production and usage at sustainable costs.^[255]

Peptide–AuNPs can act as potential candidates for both antimicrobial and drug delivery. Peng et al. modified AuNPs with AMP as non-viral vectors for gene delivery with antibacterial activity (Figure 18E).^[256] The peptide has sequence (CACWQVSRRRRG) from lactoferrin, which is an iron-binding protein from the innate immune system with anti-fungal and antibacterial properties. The hybrid nanomaterials exhibited excellent antibacterial activity for both Gram-positive and Gram-negative bacteria. Moreover, it demonstrated efficient delivery of gene encoding VEGF into wounds in vivo, leading to successful introduction of blood vessel formation.^[256] Zhang and co-authors developed AuNP-stabilized liposomes in which vancomycin was encapsulated and released in the presence of toxin from active bacteria, thus significantly inhibiting the bacterial growth.^[257] Wang et al. conjugated cationic AuNPs with AMP (LL37) and pro-angiogenic (VEGF) plasmids to form AuNPs@LL37/pDNA hybrid nanomaterials, which showed significantly improved gene transfection efficiency in keratinocytes compared with pristine AuNPs/pDNAs. Moreover, the hybrids demonstrated higher antibacterial activity than the free peptides and AuNPs alone in vitro and in vivo, and improved the expression of VEGF and accelerated diabetic wound healing.^[258]

Besides AuNPs, other nanomaterials conjugated with AMPs such as AgNPs^[259–267] and magnetic nanoparticles^[268,269] were also reported on improving the antimicrobial activity. For instance, Yuan et al. developed AMP-functionalized magnetic nanoparticles incorporated with gold-coated silver-decorated graphene oxide (Au@Ag-GO) for the simultaneous isolation, detection (based on SERS), and killing of bacteria.^[268]

4.2. Antifouling Activities

Non-fouling coating is relevant in a wide range of applications, including medical devices, immunological diagnostic, marine

coatings, biosensing and so forth.^[270–273] In the development of stable, sensitive, and selective biosensors, transducer surfaces that resist the nonspecific adsorption of proteins and unwanted adhesion of cells are of great significance and problematic challenges.^[274,275] For instance, during surface plasmon resonance analysis, the surface fouling of sensor chips may block the specific binding sites and mask the analytic signal which greatly reduce the accuracy of quantitative results. Therefore, functional materials that can prevent nonspecific protein and cell adsorption from actual complex media and meet the needs of practical applications have received increasing attention. As reported by Merrill^[276] and Whitesides and co-workers,^[277] nonfouling surfaces should be electrically neutral, hydrophilic, and possess hydrogen bond acceptors but not hydrogen bond donors.^[278] Although exceptions to these rules have been observed,^[279] many coatings including polymers with antifouling properties exhibit these features.

Two major classes of antifouling materials such as hydrophilic and zwitterionic materials have been successfully used for the development of protein/cell-resistant surfaces.^[280,281] Peptides, composed of natural amino acids, can possess high hydrogen bond donor/acceptor ability due to the carbonyl, amine, and hydroxyl groups in the peptide backbone and side chains. Some amino acids, such as Glu, Lys, and Arg normally acquire a negative or positive charge at physiological pH because of the formation of deprotonated carboxyl groups ($-\text{COO}^-$) and protonated amine groups ($-\text{NH}_3^+$). These amino acids allow for the design of peptides which are close to electrically neutral similar to zwitterionic materials. The charged carboxyl and amine groups are easy to form a layer of hydration on the surface via hydrogen bonds, which makes the peptide hydrophilic and thus capable of reducing protein adsorption through common hydrophobic interactions. In addition, peptides are usually synthesized by a solid-phase technique, and the synthetic process is rapid and convenient. Moreover, peptides are normally biocompatible in nature, which make them suitable for the synthesis of zwitterionic bio- and coating materials. Therefore, some peptide-based antifouling materials, such as hydrophilic peptoids^[282,283] and zwitterionic short peptides^[284–286] have been developed and exhibit high antifouling abilities (Table 5). For example, Jiang's group has synthesized a peptide (EKEKEKEPPPPC) that exhibited strong antifouling feature to both lysozyme and fibrinogen (Figure 19A,B).^[284,285] In order to further demonstrate the controlled cell adhesion by using this antifouling peptide instead of using PEGs,

Table 5. Antifouling peptides for biosensing.

Peptide sequences	Binding strategy	Applications and matrix	Ref.
CALNN	Thiol-gold	Maintaining stability of AuNPs and enabling subsequent detections	[139,288]
EKEKEKE zwitterionic peptides, including EKEKEKE-PPPPC	Thiol-gold	Breast cancer biomarker (BRCA1), DNA detection tested in serum	[284,285,289,290]
EKEKEKE-PPPPC	Thiol-gold	ATP sensor in 1% human whole blood	[258]
CRERERE, zwitterionic peptides	Thiol-gold	Protein-resistant self-assembled monolayer (SAM) surface for anti-fouling function	[287]
EESKSEKSGGGGC, zwitterionic peptides	Thiol-gold	Alpha-fetoprotein detection	[291]
SGKGSSGSST	Thiol-gold	Biomimetic proteophobic SAM surface	[292]

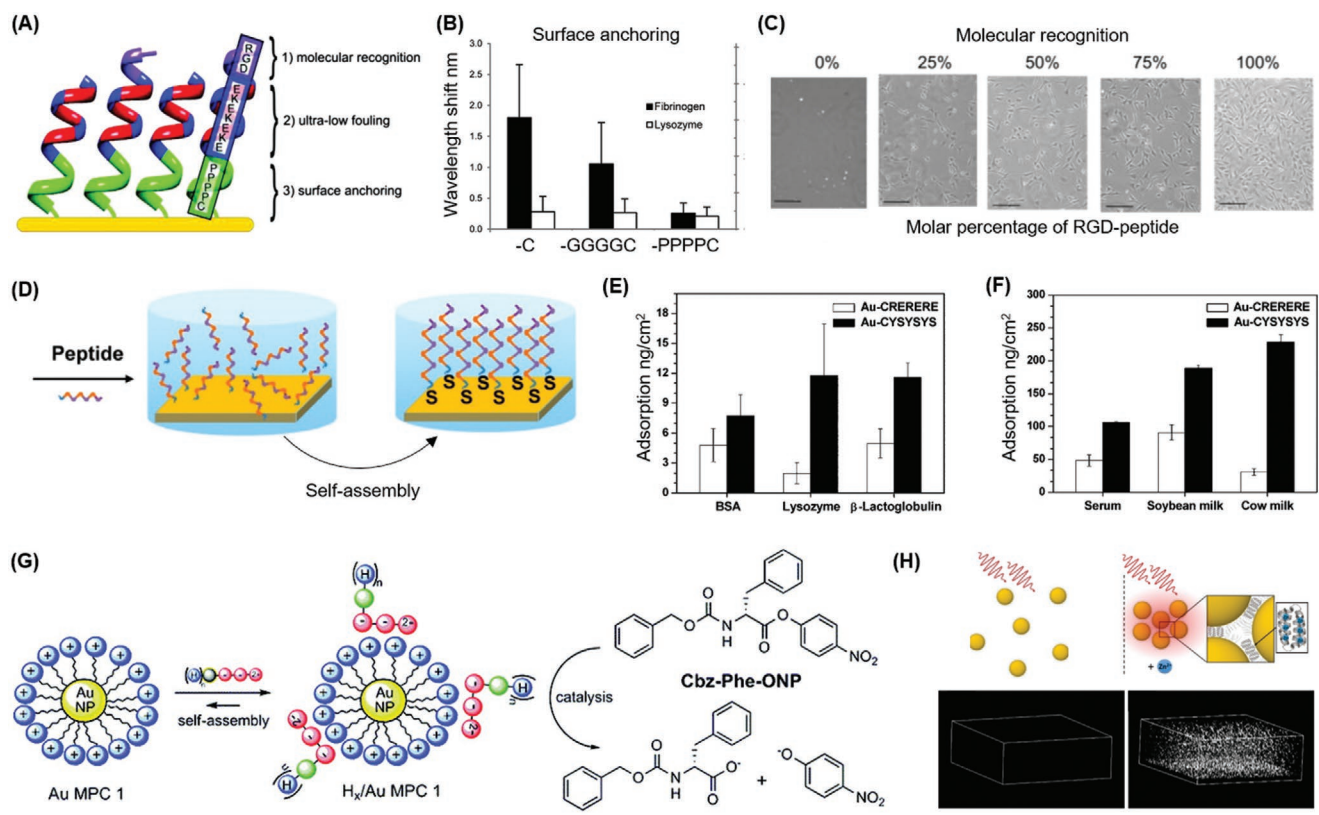


Figure 19. A) Peptide sequence of self-assembled monolayers containing molecular recognition part (RGD, purple), ultra-low fouling part (EK repeats, blue), and surface anchoring part (PPPPC, green). B) Protein adsorption tested by SPR on the anti-fouling peptide (the one containing EK repeats and PPPPC as linker) SAMs showing little attachment for both fibrinogen (black) and lysozyme (white), compared to other two. C) Cell adhesion images showing increasing cell densities cultured on peptide monolayer as percentage of RGD-peptide increased (from 0% to 100%). Reproduced with permission.^[284] Copyright 2012, American Chemical Society. D) Schematic illustration of the self-assembly process of thiolated zwitterionic peptides onto Au surface. Nonspecific proteins binding on both zwitterionic peptides and amphiphilic/non-ionic peptides SAMs with simple solution (E) and natural complex solution (F). The zwitterionic peptide (white) showed a better anti-fouling function than the amphiphilic/non-ionic peptide (black). Reproduced with permission.^[287] Copyright 2015, American Chemical Society. G) Schematic illustration of the designed peptides N-terminated with His (No: 1–3) self-assembly onto positively charged AuNPs which enabled the catalysis of transesterification by using the substrate Cbz-Phe-ONP. Reproduced with permission.^[21] Copyright 2012, American Chemical Society. H) Schematic illustration of dispersed and aggregated JR2EC-AuNPs triggered by Zn^{2+} ions (upper) and their visualizations in multiphoton-laser scanning microscopy, respectively (lower). Reproduced with permission.^[23] Copyright 2017, American Chemical Society.

cell-binding sequence RGD was added to the N-terminus of the peptide. The results of cell adhesion increased gradually as the percentage of RGD-peptide increased, indicating that the antifouling peptide was a good candidate for the control of undesirable non-specific binding (Figure 19C). Ye et al. have also reported a zwitterionic peptide with the sequence of CRERERE and an amphiphilic sequence of CYSYSYS, both of which could easily self-assembled on gold surface via thiolate-containing Cys (Figure 19D).^[287] The comparison of their antifouling performance revealed that the zwitterionic peptide possessed better resistance to both single protein and natural complex fluids than that of the amphiphilic peptide (Figure 19E,F). Although these peptides exhibited excellent antifouling performances, their applications for the construction of biosensors and assaying in complex media have rarely been reported. One exception is the pentapeptide CALNN aforementioned with excellent antifouling properties. They have been used for higher stability of modified AuNPs as well as for higher specificity of sensing performance in the detection of cTnI.^[139,157]

4.3. Other Functional Peptides

AuNP self-assembly into patterns is one of the major challenges in nanotechnology applications, especially for the assay development based on LSPR.^[293] Particular interests have been directed toward employing peptides to facilitate the assembly/synthesis process due to their chemical flexibility and versatility.^[294–300] Despite the general targeting function of peptide-gold played in gene therapy,^[20,204,301,302] peptide-AuNP conjugates have also been utilized for kinetic studies which revealed details on the effect of protease activity^[303] and aggregation progress^[304] that helps the improvement of existing assays. Most interestingly, peptide-AuNP ensembles have been demonstrated to greatly enhance the transesterification of the *p*-nitrophenyl ester of N-carboxybenzylphenylalanine (by over two orders of magnitude).^[21] Zaramella et al. reasoned that the peptide catalyst-AuNP conjugates served as a multivalent scaffold and created a local microenvironment which favored the turnover rate (Figure 19G). It showed the capability of substituting enzymatic

proteins with peptide–AuNP conjugates for catalytic applications. Most recently, Aili, Ericson, and their teams have utilized peptide–AuNP conjugates as a stimuli-responsive medium for multiphoton-induced luminescence in multiphoton microscopy, which opens up a potential way for non-invasive optical biosensing as well as imaging (Figure 19H).^[23]

5. Future Challenges and Opportunities

Realization of novel sensing/targeting strategies by using peptide–gold nanoconjugates against new types of targets is challenging but very interesting. Although many excellent peptide–AuNP based assays have been developed as discussed earlier, most of them interact with only a small part of targets redundantly. For example, most of the enzyme-responsive conjugates summarized in Table 2 target only a few catalytic reactions: proteolysis and (de)phosphorylation. Detections of many other enzymes that are critical in specific pathological processes have yet been developed using peptide–AuNPs. Opportunity remains for the detection/screening of chiral molecules/drugs with the specific designed peptide or peptide-assisted-assembly of chiral structured AuNPs (chiral plasmonics).^[24] Peptide with designed conformation would potentially provide high affinity for enantioselective detection or separation of chiral molecules, such as the reported 3D metal–organic frameworks based on tripeptide glycine (Gly)-L-His-Gly.^[29] Moreover, it is an informative approach to run simulations of molecular interactions for the design of functional peptides.^[305] Alternatively, as it is much easier to obtain dozens of mild peptide receptors rather than one with high binding affinity, proper peptide arrays can be designed from those mild peptides and utilized as one functional unity, which mimics olfactory sensing.^[306,307]

Improving sensitivity is always worthy to consider though it really is a challenge when pushed to the limits. The most direct way of improving sensitivity is to have a better peptide receptor with higher binding affinity/catalytic rate with respect to target molecules. Small ligand addition may also be required in order to boost the binding affinity, though the result is largely unpredictable. Another direction for sensitivity improvement originates from the physical properties on AuNPs. Many efforts have been adopted over years by varying the shape of AuNPs or constructing novel nano-assemblies,^[79,308,309] which aim to monitor the tiny changes of the local refractive index of the surroundings. Additionally, combinatorial approaches employing peptide–AuNPs have been used to improve the sensitivity in various detections. Despite the FRET strategy that bridges quantum dots and peptide–AuNPs as mentioned earlier,^[76,84,310] electrochemical methods have been widely explored jointly with other nanoscale materials such as carbon nanotube^[77] and silicon nanowires.^[311] Raman spectroscopy also has been used to significantly enhance the sensitivity of AuNP-based assays.^[312] Last but not least, computational tools greatly facilitate conventional approaches. Biomolecular simulation efficiently improves binding affinity between functional peptides and targets during the designing and selecting process. Raw data processing that monitors small peak shifts and eliminates unnecessary noise has been used to boost the sensitivity as well.^[70,313]

Applying functional peptide–AuNP conjugates in real samples for field tests or clinical diagnosis/imaging and therapy is another challenging but necessary move. First of all, the overall performance (referring to sensitivity, specificity, stability, etc.) is usually interfered by the complexed molecules in real samples such as serum albumin, fibrinogen, IgG, enzyme, and so forth.^[157] Hence, the majority of summarized biosensing works in this review are still limited in relatively clean aqueous conditions. Nevertheless, peptide receptors with mild affinity against target molecules may be suitable for clinical monitoring in real-time where spontaneous reversible binding is required. Stability as another important criterion in overall performance is not much affected due to the high robustness of peptides. Second, toxicity has to be considered when in/ex vivo tests are conducted. It is reported that the toxicity of peptide–AuNP conjugates can be affected by various reasons such as size, shape, surface, and environment.^[314] However, there is lack of standard database from systematic toxicity studies.^[315,316] It thus requires continuous attention as more technologies are transferred toward real tissues, organs, or in vivo.

Performance in real samples is not necessarily the only consideration as stated in previous paragraphs. When dealing with real practical applications, more issues like simplicity, cost, and eco-efficiency must be considered and they sometimes compromise one another. It is a real challenge to harmonize them according to various conditions. For trace biomolecule detection in well-equipped laboratory, performance has to be the top priority with high sensitivity and specificity, which may be time-consuming or skill-requiring. On the other hand, in the remote area, the simplicity and cost become key considerations to enable cheap, quick, user-friendly, and robust assays.^[317] In both cases, eco-efficiency is not negligible,^[318] which can be greatly helped by environmental-friendly materials and reusable assays. Although usage of functional peptide–AuNP conjugates are usually simple, cheap, and robust, efforts are still required to satisfy those key criteria simultaneously, if not all of them.

Taken together, functional peptide-gold nanomaterials have been employed in a wide range of targeting applications, and we anticipate that novel peptide design and nanotechnologies will pave the way for future application in the biomedical domain and beyond. Facing the challenges on the way to solve real/clinic sample detection with high sensitivity and specificity, cell targeting/imaging and medical therapy will be long-lasting problems to address for the medical, bioengineering, and surface and material science communities.

Acknowledgements

X.L. and Q.Z. contributed equally to this work. X.L., Q.Z., and Y.W. acknowledge financial supports from the National Natural Science Foundation of China (21605116), Zhejiang Provincial Natural Science Foundation of China (LR19H180001), the Scientific Research Fund of National Health Commission (wk-zj-1707), Public Projects of Zhejiang Province (2017C33193) and Public Projects of Wenzhou (Y20160065, Y20160067, G20170011, G20170007), and the Government of Wenzhou (RX2016005). W.K. and B.L. would like to acknowledge support from the International Graduate School (IGS) on Bionanotechnology jointly established between BOKU, Vienna, and NTU, Singapore.

Conflict of Interest

The authors declare no conflict of interest.

Keywords

biosensing, gold nanoparticles, hybrid nanomaterials, molecular interactions, peptides

Received: February 7, 2020

Revised: May 21, 2020

Published online:

-
- [1] R. Wilson, *Chem. Soc. Rev.* **2008**, 37, 2028.
- [2] D. Aili, M. M. Stevens, *Chem. Soc. Rev.* **2010**, 39, 3358.
- [3] F. Green, *Can. Med. Assoc. J.* **1925**, 15, 163.
- [4] W. P. Faulk, G. M. Taylor, *Immunochemistry* **1971**, 8, 1081.
- [5] J. H. W. Leuvers, P. J. H. M. Thal, M. V. D. Waart, A. H. W. M. Schuurs, *Fresenius' Z. Anal. Chem.* **1980**, 301, 132.
- [6] J. W. Slot, H. J. Geuze, *Eur. J. Cell Biol.* **1985**, 38, 87.
- [7] C. A. Mirkin, R. L. Letsinger, R. C. Mucic, J. J. Storhoff, *Nature* **1996**, 382, 607.
- [8] K. Saha, S. S. Agasti, C. Kim, X. N. Li, V. M. Rotello, *Chem. Rev.* **2012**, 112, 2739.
- [9] J. Zong, S. L. Cobb, N. R. Cameron, *Biomater. Sci.* **2017**, 5, 872.
- [10] K. Enander, G. T. Dolphin, L. K. Andersson, B. Liedberg, I. Lundstrom, L. Baltzer, *J. Org. Chem.* **2002**, 67, 3120.
- [11] R. Levy, N. T. K. Thanh, R. C. Doty, I. Hussain, R. J. Nichols, D. J. Schiffrin, M. Brust, D. G. Fernig, *J. Am. Chem. Soc.* **2004**, 126, 10076.
- [12] M. M. Stevens, N. T. Flynn, C. Wang, D. A. Tirrell, R. Langer, *Adv. Mater.* **2004**, 16, 915.
- [13] C. Guarise, L. Pasquato, V. De Filippis, P. Scrimin, *Proc. Natl. Acad. Sci. U. S. A.* **2006**, 103, 3978.
- [14] Z. X. Wang, R. Levy, D. G. Fernig, M. Brust, *J. Am. Chem. Soc.* **2006**, 128, 2214.
- [15] Y. W. Jun, S. Sheikholeslami, D. R. Hostetter, C. Tajon, C. S. Craik, A. P. Alivisatos, *Proc. Natl. Acad. Sci. U. S. A.* **2009**, 106, 17735.
- [16] N. Chanda, V. Kattumuri, R. Shukla, A. Zambre, K. Katti, A. Upendran, R. R. Kulkarni, P. Kan, G. M. Fent, S. W. Casteel, C. J. Smith, E. Boote, J. D. Robertson, C. Cutler, J. R. Lever, K. V. Katti, R. Kannan, *Proc. Natl. Acad. Sci. U. S. A.* **2010**, 107, 8760.
- [17] L. Maus, O. Dick, H. Bading, J. P. Spatz, R. Fiammengo, *ACS Nano* **2010**, 4, 6617.
- [18] I. Ojea-Jimenez, L. Garcia-Fernandez, J. Lorenzo, V. F. Puentes, *ACS Nano* **2012**, 6, 7692.
- [19] Y. Cheng, Q. Dai, R. A. Morshed, X. Fan, M. L. Wegscheid, D. A. Wainwright, Y. Han, L. Zhang, B. Auffinger, A. L. Tobias, E. Rincon, B. Thaci, A. U. Ahmed, P. C. Warnke, C. He, M. S. Lesniak, *Small* **2014**, 10, 5137.
- [20] J. Conde, N. Oliva, Y. Zhang, N. Artzi, *Nat. Mater.* **2016**, 15, 1128.
- [21] D. Zaramella, P. Scrimin, L. J. Prins, *J. Am. Chem. Soc.* **2012**, 134, 8396.
- [22] X. N. Li, S. M. Robinson, A. Gupta, K. Saha, Z. W. Jiang, D. F. Moyano, A. Sahar, M. A. Riley, V. M. Rotello, *ACS Nano* **2014**, 8, 10682.
- [23] J. Borglin, R. Selegård, D. Aili, M. B. Ericson, *Nano Lett.* **2017**, 17, 2102.
- [24] H. E. Lee, H. Y. Ahn, J. Mun, Y. Y. Lee, M. Kim, N. H. Cho, K. Chang, W. S. Kim, J. Rho, K. T. Nam, *Nature* **2018**, 556, 360.
- [25] N. Sewald, H.-D. Jakubke, *Peptides: Chemistry and Biology*, Wiley-VCH, Weinheim **2009**.
- [26] A. Gross, C. Hashimoto, H. Sticht, J. Eichler, *Front. Bioeng. Biotechnol.* **2016**, 3, 211.
- [27] D. Mandal, A. N. Shirazi, K. Parang, *Angew. Chem., Int. Ed.* **2011**, 50, 9633.
- [28] S. E. Wood, G. Sinsinbar, S. Gudlur, M. Nallani, C. F. Huang, B. Liedberg, M. Mrksich, *Angew. Chem., Int. Ed.* **2017**, 56, 16531.
- [29] J. Navarro-Sanchez, A. I. Argente-Garcia, Y. Moliner-Martinez, D. Roca-Sanjuan, D. Antypov, P. Campins-Falco, M. J. Rosseinsky, C. Marti-Gastaldo, *J. Am. Chem. Soc.* **2017**, 139, 4294.
- [30] J. Rabone, Y. F. Yue, S. Y. Chong, K. C. Stylianou, J. Bacsá, D. Bradshaw, G. R. Darling, N. G. Berry, Y. Z. Khimyak, A. Y. Ganin, P. Wiper, J. B. Claridge, M. J. Rosseinsky, *Science* **2010**, 329, 1053.
- [31] A. M. Smith, R. J. Williams, C. Tang, P. Coppo, R. F. Collins, M. L. Turner, A. Saiani, R. V. Ulijn, *Adv. Mater.* **2008**, 20, 37.
- [32] E. P. Holowka, V. Z. Sun, D. T. Kamei, T. J. Deming, *Nat. Mater.* **2007**, 6, 52.
- [33] P. Teng, G. M. Gray, M. Zheng, S. Singh, X. Li, L. Wojtas, A. van der Vaart, J. Cai, *Angew. Chem. Int. Ed. Engl.* **2019**, 58, 7778.
- [34] M. Amit, S. Yuran, E. Gazit, M. Reches, N. Ashkenasy, *Adv. Mater.* **2018**, 30, 1707083.
- [35] S. Zhu, R. Tian, A. L. Antaris, X. Chen, H. Dai, *Adv. Mater.* **2019**, 31, 1900321.
- [36] K. Tao, P. Makam, R. Aizen, E. Gazit, *Science* **2017**, 358, eaam9756.
- [37] M. Black, A. Trent, Y. Kostenko, J. S. Lee, C. Olive, M. Tirrell, *Adv. Mater.* **2012**, 24, 3845.
- [38] W. Li, N. B. Caberoy, *Appl. Microbiol. Biotechnol.* **2010**, 85, 909.
- [39] R. A. Houghten, C. Pinilla, J. R. Appel, S. E. Blondelle, C. T. Dooley, J. Eichler, A. Nefzi, J. M. Ostresh, *J. Med. Chem.* **1999**, 42, 3743.
- [40] M. B. Zwick, J. Q. Shen, J. Scott, *Curr. Opin. Biotechnol.* **1998**, 9, 427.
- [41] R. B. Merrifield, *J. Am. Chem. Soc.* **1963**, 85, 2149.
- [42] K. Enander, G. T. Dolphin, L. Baltzer, *J. Am. Chem. Soc.* **2004**, 126, 4464.
- [43] J. Eichler, *Curr. Opin. Chem. Biol.* **2008**, 12, 707.
- [44] M. Ciemny, M. Kurcinski, K. Kamel, A. Kolinski, N. Alam, O. Schueler-Furman, S. Kmiecik, *Drug Discovery Today* **2018**, 23, 1530.
- [45] Y. Cui, S. N. Kim, R. R. Naik, M. C. McAlpine, *Acc. Chem. Res.* **2012**, 45, 696.
- [46] Z. F. Kuang, S. N. Kim, W. J. Crookes-Goodson, B. L. Farmer, R. R. Naik, *ACS Nano* **2010**, 4, 452.
- [47] M. C. McAlpine, H. D. Agnew, R. D. Rohde, M. Blanco, H. Ahmad, A. D. Stuparu, W. A. Goddard, J. R. Heath, *J. Am. Chem. Soc.* **2008**, 130, 9583.
- [48] S. Monti, G. Barcaro, L. Sementa, V. Carravetta, H. Ågren, *Nano Res.* **2018**, 11, 1757.
- [49] S. Monti, V. Carravetta, H. Ågren, *Small* **2016**, 12, 6134.
- [50] Z. E. Hughes, M. A. Nguyen, Y. Li, M. T. Swihart, T. R. Walsh, M. R. Knecht, *Nanoscale* **2017**, 9, 421.
- [51] J. E. Dover, G. M. Hwang, E. H. Mullen, B. C. Prorok, S. J. Suh, *J. Microbiol. Methods* **2009**, 78, 10.
- [52] Q. Liu, J. Wang, B. J. Boyd, *Talanta* **2015**, 136, 114.
- [53] M. S. Inkpen, Z. F. Liu, H. Li, L. M. Campos, J. B. Neaton, L. Venkataraman, *Nat. Chem.* **2019**, 11, 351.
- [54] H. Hakkinen, *Nat. Chem.* **2012**, 4, 443.
- [55] S. Monti, V. Carravetta, H. Ågren, *Nanoscale* **2016**, 8, 12929.
- [56] X. Y. Li, F. Y. Feng, X. D. Zhou, J. M. Hu, *Nanoscale* **2018**, 10, 11491.
- [57] M. G. Ryadnov, B. Ceyhan, C. M. Niemeyer, D. N. Woolfson, *J. Am. Chem. Soc.* **2003**, 125, 9388.
- [58] D. Aili, K. Enander, L. Baltzer, B. Liedberg, *Nano Lett.* **2008**, 8, 2473.
- [59] D. Aili, K. Enander, J. Rydberg, I. Lundstrom, L. Baltzer, B. Liedberg, *J. Am. Chem. Soc.* **2006**, 128, 2194.

- [60] P. S. Ghosh, A. Verma, V. M. Rotello, *Chem. Commun.* **2007**, 2796.
- [61] P. S. Ghosh, G. Han, B. Erdogan, O. Rosado, V. M. Rotello, *J. Pept. Sci.* **2008**, *14*, 134.
- [62] N. M. Bedford, Z. E. Hughes, Z. Tang, Y. Li, B. D. Briggs, Y. Ren, M. T. Swihart, V. G. Petkov, R. R. Naik, M. R. Knecht, T. R. Walsh, *J. Am. Chem. Soc.* **2016**, *138*, 540.
- [63] B. D. Briggs, J. P. Palafox-Hernandez, Y. Li, C. K. Lim, T. J. Woehl, N. M. Bedford, S. Seifert, M. T. Swihart, P. N. Prasad, T. R. Walsh, M. R. Knecht, *Phys. Chem. Chem. Phys.* **2016**, *18*, 30845.
- [64] Q. Zhang, D. Zhang, Y. Lu, G. Xu, Y. Yao, S. Li, Q. Liu, *Biosens. Bioelectron.* **2016**, *77*, 963.
- [65] D. Wu, P. Cai, Z. Tao, Y. Pan, *Anal. Chim. Acta* **2016**, *902*, 174.
- [66] C. Lopez-Otin, J. S. Bond, *J. Biol. Chem.* **2008**, *283*, 30433.
- [67] N. N. Nemova, L. A. Lysenko, *Paleontol. J.* **2013**, *47*, 1085.
- [68] W. X. Xue, G. X. Zhang, D. Q. Zhang, *Analyst* **2011**, *136*, 3136.
- [69] G. B. Kim, K. H. Kim, Y. H. Park, S. Ko, Y.-P. Kim, *Biosens. Bioelectron.* **2013**, *41*, 833.
- [70] A. Laromaine, L. L. Koh, M. Murugesan, R. V. Ulijn, M. M. Stevens, *J. Am. Chem. Soc.* **2007**, *129*, 4156.
- [71] Y. Wang, X. H. Liu, J. L. Zhang, D. Aili, B. Liedberg, *Chem. Sci.* **2014**, *5*, 2651.
- [72] X. Liu, Y. Wang, P. Chen, Y. Wang, J. Mang, D. Aili, B. Liedberg, *Anal. Chem.* **2014**, *86*, 2345.
- [73] P. Chen, R. Selegard, D. Aili, B. Liedberg, *Nanoscale* **2013**, *5*, 8973.
- [74] X. Wang, J. Geng, D. Miyoshi, J. Ren, N. Sugimoto, X. Qu, *Biosens. Bioelectron.* **2010**, *26*, 743.
- [75] E. Chang, J. S. Miller, J. T. Sun, W. W. Yu, V. L. Colvin, R. Drezek, J. L. West, *Biochem. Biophys. Res. Commun.* **2005**, *334*, 1317.
- [76] Y. P. Kim, Y. H. Oh, E. Oh, S. Ko, M. K. Han, H. S. Kim, *Anal. Chem.* **2008**, *80*, 4634.
- [77] K. A. Mahmoud, J. H. T. Luong, *Anal. Chem.* **2008**, *80*, 7056.
- [78] S. J. Zhen, Y. F. Li, C. Z. Huang, Y. F. Long, *Talanta* **2008**, *76*, 230.
- [79] M. Oishi, A. Tamura, T. Nakamura, Y. Nagasaki, *Adv. Funct. Mater.* **2009**, *19*, 827.
- [80] Y. L. Pan, M. L. Guo, Z. Nie, Y. Huang, Y. Peng, A. F. Liu, M. Qing, S. Z. Yao, *Chem. Commun.* **2012**, *48*, 997.
- [81] X. Huang, Y. Liang, L. Ruan, J. Ren, *Anal. Bioanal. Chem.* **2014**, *406*, 5677.
- [82] B. Khalilzadeh, H. N. Charoudeh, N. Shadjou, R. Mohammad-Rezaei, Y. Omid, K. Velaei, Z. Aliyari, M. R. Rashidi, *Sens. Actuators, B* **2016**, *231*, 561.
- [83] J. Wang, S. Achilefu, M. Nantz, K. A. Kang, *Anal. Chim. Acta* **2011**, *695*, 96.
- [84] Y. Choi, Y. Cho, M. Kim, R. Grailhe, R. Song, *Anal. Chem.* **2012**, *84*, 8595.
- [85] X. Yi, H. Han, Y. Zhang, J. Wang, Y. Zhang, F. Zhou, *Biosens. Bioelectron.* **2013**, *50*, 224.
- [86] Y. C. Chuang, W. T. Huang, P. H. Chiang, M. C. Tang, C. S. Lin, *Biosens. Bioelectron.* **2012**, *32*, 24.
- [87] S. Y. Park, S. M. Lee, G. B. Kim, Y. P. Kim, *Gold Bull.* **2012**, *45*, 213.
- [88] W.-H. Chen, X.-D. Xu, H.-Z. Jia, Q. Lei, G.-F. Luo, S.-X. Cheng, R.-X. Zhuo, X.-Z. Zhang, *Biomaterials* **2013**, *34*, 8798.
- [89] D. Deng, D. Zhang, Y. Li, S. Achilefu, Y. Gu, *Biosens. Bioelectron.* **2013**, *49*, 216.
- [90] J. Hong, M. Ku, E. Lee, J.-S. Suh, Y.-M. Huh, D. S. Yoon, J. Yang, *J. Biomed. Opt.* **2014**, *19*, 051202.
- [91] Z. M. Dong, X. Jin, G. C. Zhao, *Biosens. Bioelectron.* **2018**, *106*, 111.
- [92] J. H. Choi, H. S. Kim, J.-W. Choi, J. W. Hong, Y.-K. Kim, B.-K. Oh, *Biosens. Bioelectron.* **2013**, *49*, 415.
- [93] A. Parnsubsakul, R. E. Saftiri, P. Rijiravanich, W. Surareungchai, *J. Electroanal. Chem.* **2017**, *785*, 125.
- [94] L. K. Pietersen, P. Govender, H. G. Kruger, G. E. M. Maguire, T. Govender, *J. Nanosci. Nanotechnol.* **2011**, *11*, 3075.
- [95] L. Gelens, J. B. Qian, M. Bollen, A. T. Saurin, *Trends Cell Biol.* **2018**, *28*, 6.
- [96] P. Hainaut, A. Plymoth, *Curr. Opin. Oncol.* **2013**, *25*, 50.
- [97] F. Ardito, M. Giuliani, D. Perrone, G. Troiano, L. Lo Muzio, *Int. J. Mol. Med.* **2017**, *40*, 271.
- [98] Y. Choi, N. H. Ho, C. H. Tung, *Angew. Chem., Int. Ed.* **2007**, *46*, 707.
- [99] T. Serizawa, Y. Hirai, M. Aizawa, *Mol. Biosyst.* **2010**, *6*, 1565.
- [100] S. Zhang, H. Wu, S. Huan, X. Zhang, G. Shen, R. Yu, *Anal. Lett.* **2013**, *46*, 2029.
- [101] J. Y. Piao, D. S. Chung, *Analyst* **2012**, *137*, 2669.
- [102] G. Manning, D. B. Whyte, R. Martinez, T. Hunter, S. Sudarsanam, *Science* **2002**, *298*, 1912.
- [103] J. Oishi, Y. Asami, T. Mori, J. H. Kang, M. Tanabe, T. Niidome, Y. Katayama, *ChemBioChem* **2007**, *8*, 875.
- [104] J. Oishi, Y. Asami, T. Mori, J. H. Kang, T. Niidome, Y. Katayama, *Biomacromolecules* **2008**, *9*, 2301.
- [105] J. Oishi, X. Han, J. H. Kang, Y. Asami, T. Mori, T. Niidome, Y. Katayama, *Anal. Biochem.* **2008**, *373*, 161.
- [106] J.-H. Kang, Y. Asami, M. Murata, H. Kitazaki, N. Sadanaga, E. Tokunaga, S. Shiotani, S. Okada, Y. Maehara, T. Niidome, M. Hashizume, T. Mori, Y. Katayama, *Biosens. Bioelectron.* **2010**, *25*, 1869.
- [107] Y. Asami, J. Oishi, H. Kitazaki, J. Kamimoto, J. H. Kang, T. Niidome, T. Mori, Y. Katayama, *Anal. Biochem.* **2011**, *418*, 44.
- [108] S. Gupta, H. Andresen, J. E. Ghadiali, M. M. Stevens, *Small* **2010**, *6*, 1509.
- [109] Z. X. Wang, J. Lee, A. R. Cossins, M. Brust, *Anal. Chem.* **2005**, *77*, 5770.
- [110] L. Sun, D. Liu, Z. Wang, *Anal. Chem.* **2007**, *79*, 773.
- [111] T. Li, D. Liu, Z. Wang, *Biosens. Bioelectron.* **2009**, *24*, 3335.
- [112] T. Li, X. Liu, D. Liu, Z. Wang, *Anal. Chem.* **2013**, *85*, 7033.
- [113] K. Inamori, M. Kyo, Y. Nishiya, Y. Inoue, T. Sonoda, E. Kinoshita, T. Koike, Y. Katayama, *Anal. Chem.* **2005**, *77*, 3979.
- [114] Q. Wen, Y. Gu, L.-J. Tang, R.-Q. Yu, J.-H. Jiang, *Anal. Chem.* **2013**, *85*, 11681.
- [115] W. Song, R. P. Liang, Y. Wang, L. Zhang, J. D. Qiu, *Chem. Commun.* **2015**, *51*, 10006.
- [116] S. J. Xu, Y. Liu, T. H. Wang, J. H. Li, *Anal. Chem.* **2010**, *82*, 9566.
- [117] Z. H. Wang, Z. Y. Yan, N. Sun, Y. Liu, *Biosens. Bioelectron.* **2015**, *68*, 771.
- [118] M. M. Dong, X. Liu, Q. Dang, H. L. Qi, Y. Huang, Q. Gao, C. X. Zhang, *Anal. Chim. Acta* **2016**, *906*, 72.
- [119] K. Kerman, M. Chikae, S. Yamamura, E. Tamiya, *Anal. Chim. Acta* **2007**, *588*, 26.
- [120] K. Kerman, H. B. Kraatz, *Biosens. Bioelectron.* **2009**, *24*, 1484.
- [121] F. Yi, X. Huang, J. Ren, *Anal. Chem.* **2018**, *90*, 3871.
- [122] Y. P. Kim, E. Oh, Y. H. Oh, D. W. Moon, T. G. Lee, H. S. Kim, *Angew. Chem., Int. Ed.* **2007**, *46*, 6816.
- [123] E. Hutter, D. Maysinger, *Trends Pharmacol. Sci.* **2013**, *34*, 497.
- [124] L. Yang, N. Li, K. Wang, X. Hai, J. Liu, F. Dang, *Talanta* **2018**, *179*, 531.
- [125] N. Xia, X. Wang, X. Wang, B. Zhou, *Materials* **2016**, *9*, 857.
- [126] S. Pavan, F. Berti, *Anal. Bioanal. Chem.* **2012**, *402*, 3055.
- [127] H. A. Godwin, J. M. Berg, *J. Am. Chem. Soc.* **1996**, *118*, 6514.
- [128] M. Lin, M. Cho, W. S. Choe, J. B. Yoo, Y. Lee, *Biosens. Bioelectron.* **2010**, *26*, 940.
- [129] M. B. Villiers, S. Cortes, C. Brakha, J. P. Lavergne, C. A. Marquette, P. Deny, T. Livache, P. N. Marche, *Biosens. Bioelectron.* **2010**, *26*, 1554.
- [130] T. Z. Wu, Y. R. Lo, E. C. Chan, *Biosens. Bioelectron.* **2001**, *16*, 945.
- [131] P. Fechner, F. Proll, M. Carlquist, G. Proll, *Anal. Bioanal. Chem.* **2009**, *393*, 1579.
- [132] H. H. Lu, Y. K. Rao, T. Z. Wu, Y. M. Tzeng, *Sens. Actuators, B* **2009**, *137*, 741.
- [133] S. Sankaran, S. Panigrahi, S. Mallik, *Sens. Actuators, B* **2011**, *155*, 8.
- [134] Y. Yu, Q. Cao, M. Zhou, H. Cui, *Biosens. Bioelectron.* **2013**, *43*, 137.

- [135] G. P. Anderson, K. D. King, K. L. Gaffney, L. H. Johnson, *Biosens. Bioelectron.* **2000**, *14*, 771.
- [136] T. N. Huan, V. T. T. Ha, L. Q. Hung, M. Y. Yoon, S. H. Han, H. Chung, *Biosens. Bioelectron.* **2009**, *25*, 469.
- [137] J. Wu, D. M. Crokek, A. C. West, S. Banta, *Anal. Chem.* **2010**, *82*, 8235.
- [138] M. L. Frisk, G. Y. Lin, E. A. Johnson, D. J. Beebe, *Biosens. Bioelectron.* **2011**, *26*, 1929.
- [139] Y. Wang, X. H. Liu, P. Chen, N. T. Tran, J. L. Zhang, W. S. Chia, S. Boujday, B. Liedberg, *Analyst* **2016**, *141*, 3233.
- [140] J. Zhang, I. Khan, Q. Zhang, X. Liu, J. Dostalek, B. Liedberg, Y. Wang, *Biosens. Bioelectron.* **2018**, *99*, 312.
- [141] S. Carnazza, C. Foti, G. Gioffre, F. Felici, S. Guglielmino, *Biosens. Bioelectron.* **2008**, *23*, 1137.
- [142] J. H. Gao, K. Chen, Z. Miao, G. Ren, X. Y. Chen, S. S. Gambhir, Z. Cheng, *Biomaterials* **2011**, *32*, 2141.
- [143] A. K. Vashishtha, J. M. Wang, W. H. Konigsberg, *J. Biol. Chem.* **2016**, *291*, 20869.
- [144] J. Anastassopoulou, in *Bioinorganic Chemistry*, Vol. 459 (Ed: D. P. Kessissoglou), Springer, Dordrecht **1995**, p. 209.
- [145] D. Aili, R. Selegard, L. Baltzer, K. Enander, B. Liedberg, *Small* **2009**, *5*, 2445.
- [146] D. Aili, K. Enander, J. Rydberg, I. Nesterenko, F. Bjorefors, L. Baltzer, B. Liedberg, *J. Am. Chem. Soc.* **2008**, *130*, 5780.
- [147] X. Li, Z. Wu, X. Zhou, J. Hu, *Biosens. Bioelectron.* **2017**, *92*, 496.
- [148] L. L. Liu, K. J. Franz, *J. Biol. Inorg. Chem.* **2007**, *12*, 234.
- [149] I. Sovago, K. Osz, *Dalton Trans.* **2006**, 3841.
- [150] E. Chow, J. J. Gooding, *Electroanalysis* **2006**, *18*, 1437.
- [151] S. J. Lippard, J. M. Berg, G. Klatt, *Principles of Bioinorganic Chemistry*, University Science Books, Sausalito, CA **1994**.
- [152] J. M. Slocik, J. S. Zabinski, D. M. Phillips, R. R. Naik, *Small* **2008**, *4*, 548.
- [153] J. W. Jaworski, D. Raorane, J. H. Huh, A. Majumdar, S.-W. Lee, *Langmuir* **2008**, *24*, 4938.
- [154] J. Jaworski, K. Yokoyama, C. Zueger, W.-J. Chung, S.-W. Lee, A. Majumdar, *Langmuir* **2011**, *27*, 3180.
- [155] D. L. Roy, W. Yang, X. Yin, R. Y. Lai, S.-H. Liou, D. J. Sellmyer, *J. Appl. Phys.* **2011**, *109*, 07E532.
- [156] E. R. Goldman, M. P. Pazirandeh, P. T. Charles, E. D. Balighian, G. P. Anderson, *Anal. Chim. Acta* **2002**, *457*, 13.
- [157] X. Liu, Y. Wang, P. Chen, A. McCadden, A. Palaniappan, J. Zhang, B. Liedberg, *ACS Sens.* **2016**, *1*, 1416.
- [158] J. P. Park, D. M. Crokek, S. Banta, *Biotechnol. Bioeng.* **2010**, *105*, 678.
- [159] L. M. Wei, X. Y. Wang, C. Li, X. X. Li, Y. M. Yin, G. X. Li, *Biosens. Bioelectron.* **2015**, *71*, 348.
- [160] H. Andresen, M. Mager, M. Griessner, P. Charchar, N. Todorova, N. Bell, G. Theocharidis, S. Bertazzo, I. Yarovsky, M. M. Stevens, *Chem. Mater.* **2014**, *26*, 4696.
- [161] M. Shi, J. Chen, Y. Huang, K. Hu, S. Zhao, Z.-F. Chen, H. Liang, *RSC Adv.* **2013**, *3*, 13884.
- [162] N. Xia, X. Wang, J. Yu, Y. Wu, S. Cheng, Y. Xing, L. Liu, *Sens. Actuators, B* **2017**, *239*, 834.
- [163] K. Sun, Y. Chang, B. Zhou, X. Wang, L. Liu, *Int. J. Nanomed.* **2017**, *12*, 1905.
- [164] G. van Niel, G. D'Angelo, G. Raposo, *Nat. Rev. Mol. Cell Biol.* **2018**, *19*, 213.
- [165] M. I. Ramirez, M. G. Amorim, C. Gadelha, I. Milic, J. A. Welsh, V. M. Freitas, M. Nawaz, N. Akbar, Y. Couch, L. Makin, F. Cooke, A. L. Vettore, P. X. Batista, R. Freezor, J. A. Pezuk, L. Rosa-Fernandes, A. C. O. Carreira, A. Devitt, L. Jacobs, I. T. Silva, G. Coakley, D. N. Nunes, D. Carter, G. Palmisano, E. Dias-Neto, *Nanoscale* **2018**, *10*, 881.
- [166] J. S. Schorey, Y. Cheng, P. P. Singh, V. L. Smith, *EMBO Rep.* **2015**, *16*, 24.
- [167] G. Raposo, W. Stoorvogel, *J. Cell Biol.* **2013**, *200*, 373.
- [168] A. Schneider, *J. Neural. Transm.* **2019**, *126*, 646.
- [169] T. Huang, C. X. Deng, *Int. J. Biol. Sci.* **2019**, *15*, 1.
- [170] J. Lin, J. Li, B. Huang, J. Liu, X. Chen, X. M. Chen, Y. M. Xu, L. F. Huang, X. Z. Wang, *ScientificWorldJournal* **2015**, *2015*, 657086.
- [171] R. Nedaenia, M. Manian, M. H. Jazayeri, M. Ranjbar, R. Salehi, M. Sharifi, F. Mohaghegh, M. Goli, S. H. Jahednia, A. Avan, M. Ghayour-Mobarhan, *Cancer Gene Ther.* **2017**, *24*, 48.
- [172] C. Roma-Rodrigues, L. R. Raposo, R. Cabral, F. Paradinha, P. V. Baptista, A. R. Fernandes, *Int. J. Mol. Sci.* **2017**, *18*, 162.
- [173] R. Carney, S. Hazari, T. Rojalin, A. Knudson, T. Gao, Y. Tang, R. Liu, T. Viitala, M. Yliperttula, K. Lam, *Adv. Biosyst.* **2017**, *1*, 1600038.
- [174] W. L. Liu, J. P. Li, Y. X. Wu, S. Xing, Y. Z. Lai, G. Zhang, *Biosens. Bioelectron.* **2018**, *102*, 204.
- [175] A. Ghosh, M. Davey, I. C. Chute, S. G. Griffiths, S. Lewis, S. Chacko, D. Barnett, N. Crapoulet, S. Fournier, A. Joy, M. C. Caissie, A. D. Ferguson, M. Daigle, M. V. Meli, S. M. Lewis, R. J. Ouellette, *PLoS One* **2014**, *9*, e110443.
- [176] R. Duraichelvan, B. Srinivas, S. Badilescu, R. Ouellette, A. Ghosh, M. Packirisamy, *ECS Trans.* **2016**, *75*, 11.
- [177] D. Raju, S. Bathini, S. Badilescu, R. J. Ouellette, A. Ghosh, M. Packirisamy, *J. Electrochem. Soc.* **2019**, *166*, B3001.
- [178] S. Bathini, D. Raju, S. Badilescu, A. Kumar, R. J. Ouellette, A. Ghosh, M. Packirisamy, *Research* **2018**, *2018*, 3917986.
- [179] H. Im, H. L. Shao, Y. I. Park, V. M. Peterson, C. M. Castro, R. Weissleder, H. Lee, *Nat. Biotechnol.* **2014**, *32*, 490.
- [180] C. Lee, R. Carney, K. Lam, J. W. Chan, *J. Raman Spectrosc.* **2017**, *48*, 1771.
- [181] L. Diacovich, J. P. Gorvel, *Nat. Rev. Microbiol.* **2010**, *8*, 117.
- [182] M. Hoyos-Nogues, F. J. Gil, C. Mas-Moruno, *Molecules* **2018**, *23*, 1683.
- [183] N. V. Kulagina, M. E. Lassman, F. S. Ligler, C. R. Taitt, *Anal. Chem.* **2005**, *77*, 6504.
- [184] L. C. Shriver-Lake, S. H. North, S. N. Dean, C. R. Taitt, in *Designing Receptors for the Next Generation of Biosensors* (Eds: S. A. Piletsky, M. J. Whitcombe), Springer, Berlin **2013**, p. 85.
- [185] M. S. Mannoor, S. Y. Zhang, A. J. Link, M. C. McAlpine, *Proc. Natl. Acad. Sci. U. S. A.* **2010**, *107*, 19207.
- [186] G. Palmieri, M. Balestrieri, F. Capuano, Y. T. R. Proroga, F. Pomilio, P. Centorame, A. Riccio, R. Marrone, A. Anastasio, *Int. J. Food Microbiol.* **2018**, *279*, 33.
- [187] S. Azmi, K. Jiang, M. Stiles, T. Thundat, K. Kaur, *ACS Comb. Sci.* **2015**, *17*, 156.
- [188] J. A. Jackman, E. Linardy, D. Yoo, J. Seo, W. B. Ng, D. J. Klemme, N. J. Wittenberg, S. H. Oh, N. J. Cho, *Small* **2016**, *12*, 1159.
- [189] H. J. Hwang, M. Y. Ryu, C. Y. Park, J. Ahn, H. G. Park, C. Choi, S. D. Ha, T. J. Park, J. P. Park, *Biosens. Bioelectron.* **2017**, *87*, 164.
- [190] H. J. Hwang, M. Y. Ryu, J. P. Park, *RSC Adv.* **2015**, *5*, 55300.
- [191] I. C. Baines, P. Colas, *Drug Discovery Today* **2006**, *11*, 334.
- [192] Y. Y. Li, M. R. Zhao, H. Y. Wang, *Anal. Bioanal. Chem.* **2017**, *409*, 6371.
- [193] N. Xia, B. B. Zhou, N. B. Huang, M. S. Jiang, J. B. Zhang, L. Liu, *Biosens. Bioelectron.* **2016**, *85*, 625.
- [194] M. Biyani, K. Kawai, K. Kitamura, M. Chikae, M. Biyani, H. Ushijima, E. Tamiya, T. Yoneda, Y. Takamura, *Biosens. Bioelectron.* **2016**, *84*, 120.
- [195] T. Yang, X.-X. Zhang, J.-Y. Yang, Y.-T. Wang, M.-L. Chen, *Talanta* **2018**, *177*, 212.
- [196] M. Dong, M. Li, H. Qi, Z. Li, Q. Gao, C. Zhang, *Gold Bull.* **2015**, *48*, 21.
- [197] N.-F. Chiu, C.-T. Kuo, T.-L. Lin, C.-C. Chang, C.-Y. Chen, *Biosens. Bioelectron.* **2017**, *94*, 351.
- [198] J. M. Lim, N. S. Heo, S. Y. Oh, M. Y. Ryu, J. H. Seo, T. J. Park, Y. S. Huh, J. P. Park, *Biosens. Bioelectron.* **2018**, *99*, 289.

- [199] W. W. Xiao, T. H. Li, F. C. Bononi, D. Lac, I. A. Kekessie, Y. L. Liu, E. Sanchez, A. Mazloom, A. H. Ma, J. Lin, J. Tran, K. Yang, K. S. Lam, R. W. Liu, *EJNMMI Res.* **2016**, *6*, 18.
- [200] M. Mammen, S. K. Choi, G. M. Whitesides, *Angew. Chem., Int. Ed.* **1998**, *37*, 2754.
- [201] L. Gao, M. Q. Liu, G. F. Ma, Y. L. Wang, L. N. Zhao, Q. Yuan, F. P. Gao, R. Liu, J. Zhai, Z. F. Chai, Y. L. Zhao, X. Y. Gao, *ACS Nano* **2015**, *9*, 10979.
- [202] J. D. Meyers, Y. Cheng, A.-M. Broome, R. S. Agnes, M. D. Schluchter, S. Margevicius, X. Wang, M. E. Kenney, C. Burda, J. P. Basilion, *Part. Part. Syst. Character.* **2015**, *32*, 448.
- [203] Q. Chen, H. Wang, H. Liu, S. Wen, C. Peng, M. Shen, G. Zhang, X. Shi, *Anal. Chem.* **2015**, *87*, 3949.
- [204] A. Gilam, J. Conde, D. Weissglas-Volkov, N. Oliva, E. Friedman, N. Artzi, N. Shomron, *Nat. Commun.* **2016**, *7*, 12868.
- [205] G. von Maltzahn, Y. Ren, J.-H. Park, D.-H. Min, V. R. Kotamraju, J. Jayakumar, V. Fogal, M. J. Sailor, E. Ruoslahti, S. N. Bhatia, *Bioconjugate Chem.* **2008**, *19*, 1570.
- [206] L. Hosta-Rigau, I. Olmedo, J. Arbiol, L. J. Cruz, M. J. Kogan, F. Albericio, *Bioconjugate Chem.* **2010**, *21*, 1070.
- [207] N. Lue, S. Ganta, D. X. Hammer, M. Mujat, A. E. Stevens, N. Harrison, R. D. Ferguson, D. Rosen, M. Amiji, N. Iftimia, *Nanomedicine* **2010**, *5*, 1467.
- [208] Y.-H. Kim, J. Jeon, S. H. Hong, W.-K. Rhim, Y.-S. Lee, H. Youn, J.-K. Chung, M. C. Lee, D. S. Lee, K. W. Kang, J.-M. Nam, *Small* **2011**, *7*, 2052.
- [209] X. M. Qian, X. H. Peng, D. O. Ansari, Q. Yin-Goen, G. Z. Chen, D. M. Shin, L. Yang, A. N. Young, M. D. Wang, S. M. Nie, *Nat. Biotechnol.* **2008**, *26*, 83.
- [210] A. G. Tkachenko, H. Xie, D. Coleman, W. Glomm, J. Ryan, M. F. Anderson, S. Franzen, D. L. Feldheim, *J. Am. Chem. Soc.* **2003**, *125*, 4700.
- [211] A. G. Tkachenko, H. Xie, Y. L. Liu, D. Coleman, J. Ryan, W. R. Glomm, M. K. Shipton, S. Franzen, D. L. Feldheim, *Bioconjugate Chem.* **2004**, *15*, 482.
- [212] Y. Liu, M. K. Shipton, J. Ryan, E. D. Kaufman, S. Franzen, D. L. Feldheim, *Anal. Chem.* **2007**, *79*, 2221.
- [213] Y. Liu, S. Franzen, *Bioconjugate Chem.* **2008**, *19*, 1009.
- [214] C. D. Dekiwadia, A. C. Lawrie, J. V. Fecondo, *J. Pept. Sci.* **2012**, *18*, 527.
- [215] A. Davies, D. J. Lewis, S. P. Watson, S. G. Thomas, Z. Pikramenou, *Proc. Natl. Acad. Sci. U. S. A.* **2012**, *109*, 1862.
- [216] E. Oh, J. B. Delehanty, K. E. Sapsford, K. Susumu, R. Goswami, J. B. Blanco-Canosa, P. E. Dawson, J. Granek, M. Shoff, Q. Zhang, P. L. Goering, A. Huston, I. L. Medintz, *ACS Nano* **2011**, *5*, 6434.
- [217] A. K. Nowinski, A. D. White, A. J. Keefe, S. Jiang, *Langmuir* **2014**, *30*, 1864.
- [218] M. Li, Y. Guan, A. Zhao, J. Ren, X. Qu, *Theranostics* **2017**, *7*, 2996.
- [219] X. Gao, Q. Yue, Z. Liu, M. Ke, X. Zhou, S. Li, J. Zhang, R. Zhang, L. Chen, Y. Mao, C. Li, *Adv. Mater.* **2017**, *29*, 1603917.
- [220] R. Huang, S. Harmsen, J. M. Samii, H. Karabeber, K. L. Pitter, E. C. Holland, M. F. Kircher, *Theranostics* **2016**, *6*, 1075.
- [221] R. Prades, S. Guerrero, E. Araya, C. Molina, E. Salas, E. Zurita, J. Selva, G. Egea, C. Lopez-Iglesias, M. Teixido, M. J. Kogan, E. Giralt, *Biomaterials* **2012**, *33*, 7194.
- [222] S. A. Jensen, E. S. Day, C. H. Ko, L. A. Hurley, J. P. Luciano, F. M. Kouri, T. J. Merkel, A. J. Luthi, P. C. Patel, J. I. Cutler, W. L. Daniel, A. W. Scott, M. W. Rotz, T. J. Meade, D. A. Giljohann, C. A. Mirkin, A. H. Stegh, *Sci. Transl. Med.* **2013**, *5*, 209ra152.
- [223] H. Maeda, J. Wu, T. Sawa, Y. Matsumura, K. Hori, *J. Controlled Release* **2000**, *65*, 271.
- [224] B. Oller-Salvia, M. Sanchez-Navarro, E. Giralt, M. Teixido, *Chem. Soc. Rev.* **2016**, *45*, 4690.
- [225] A. Cassini, L. D. Hogberg, D. Plachouras, A. Quattrocchi, A. Hoxha, G. S. Simonsen, M. Colomb-Cotinat, M. E. Kretzschmar, B. Devleeschauwer, M. Cecchini, D. A. Ouakrim, T. C. Oliveira, M. J. Struelens, C. Suetens, D. L. Monnet, A. M. R. C. G. Burden of, *Lancet Infect. Dis.* **2019**, *19*, 56.
- [226] M. Mahlapuu, J. Hakansson, L. Ringstad, C. Bjorn, *Front. Cell Infect. Mi.* **2016**, *6*, 194.
- [227] L. J. Zhang, R. L. Gallo, *Curr. Biol.* **2016**, *26*, R14.
- [228] M. Zaslhoff, *Nature* **2002**, *415*, 389.
- [229] K. Matsuzaki, *Biochim. Biophys. Acta, Biomembr.* **2009**, *1788*, 1687.
- [230] L. L. Wang, C. Hu, L. Q. Shao, *Int. J. Nanomed.* **2017**, *12*, 1227.
- [231] A. Raghunath, E. Perumal, *Int. J. Antimicrob. Agents* **2017**, *49*, 137.
- [232] M. Ul-Islam, A. Shehzad, S. Khan, W. A. Khattak, M. W. Ullah, J. K. Park, *J. Nanosci. Nanotechnol.* **2014**, *14*, 780.
- [233] S. M. Dizaj, F. Lotfipour, M. Barzegar-Jalali, M. H. Zarrintan, K. Adibkia, *Mater. Sci. Eng., C* **2014**, *44*, 278.
- [234] A. Azam, A. S. Ahmed, M. Oves, M. S. Khan, S. S. Habib, A. Memic, *Int. J. Nanomed.* **2012**, *7*, 6003.
- [235] O. Gordon, T. V. Slenters, P. S. Brunetto, A. E. Villaruz, D. E. Sturdevant, M. Otto, R. Landmann, K. M. Fromm, *Antimicrob. Agents Chemother.* **2010**, *54*, 4208.
- [236] M. Singh, S. Singh, S. Prasad, I. S. Gambhir, *Dig. J. Nanomater. Bios.* **2008**, *3*, 115.
- [237] K. Y. Zheng, M. I. Setyawati, D. T. Leong, J. P. Xie, *ACS Nano* **2017**, *11*, 6904.
- [238] A. M. Allahverdiyev, K. V. Kon, E. S. Abamor, M. Bagirova, M. Rafailovich, *Expert Rev. Anti-Infect. Ther.* **2011**, *9*, 1035.
- [239] Y. Y. Zhao, Y. Tian, Y. Cui, W. W. Liu, W. S. Ma, X. Y. Jiang, *J. Am. Chem. Soc.* **2010**, *132*, 12349.
- [240] A. Verma, O. Uzun, Y. H. Hu, Y. Hu, H. S. Han, N. Watson, S. L. Chen, D. J. Irvine, F. Stellacci, *Nat. Mater.* **2013**, *12*, 376.
- [241] A. S. Urban, M. Fedoruk, M. R. Horton, J. Radler, F. D. Stefani, J. Feldmann, *Nano Lett.* **2009**, *9*, 2903.
- [242] J. M. Chen, J. A. Hessler, K. Putchakayala, B. K. Panama, D. P. Khan, S. Hong, D. G. Mullen, S. C. DiMaggio, A. Som, G. N. Tew, A. N. Lopatin, J. R. Baker, M. M. B. Holl, B. G. Orr, *J. Phys. Chem. B* **2009**, *113*, 11179.
- [243] P. He, X. Y. Zhu, *Mater. Res. Bull.* **2007**, *42*, 1310.
- [244] E. Katz, I. Willner, *Angew. Chem., Int. Ed.* **2004**, *43*, 6042.
- [245] H. Khandelia, J. H. Ipsen, O. G. Mouritsen, *Biochim. Biophys. Acta, Biomembr.* **2008**, *1778*, 1528.
- [246] U. Rajchakit, V. Sarojini, *Bioconjugate Chem.* **2017**, *28*, 2673.
- [247] H. W. Gu, P. L. Ho, E. Tong, L. Wang, B. Xu, *Nano Lett.* **2003**, *3*, 1261.
- [248] H. Z. Lai, W. Y. Chen, C. Y. Wu, Y. C. Chen, *ACS Appl. Mater. Interfaces* **2015**, *7*, 2046.
- [249] A. Rai, S. Pinto, T. R. Velho, A. F. Ferreira, C. Moita, U. Trivedi, M. Evangelista, M. Comune, K. P. Rumbaugh, P. N. Simoes, L. Moita, L. Ferreira, *Biomaterials* **2016**, *85*, 99.
- [250] W. Y. Chen, H. Y. Chang, J. K. Lu, Y. C. Huang, S. G. Harroun, Y. T. Tseng, Y. J. Li, C. C. Huang, H. T. Chang, *Adv. Funct. Mater.* **2015**, *25*, 7189.
- [251] N. S. Shaligram, R. S. Singhal, *Food Technol. Biotech.* **2010**, *48*, 119.
- [252] M. Deleu, J. Lorent, L. Lins, R. Brasseur, N. Braun, K. El Kirat, T. Nylander, Y. F. Dufrene, M. P. Mingeot-Leclercq, *Biochim. Biophys. Acta, Biomembr.* **2013**, *1828*, 801.
- [253] H. Heerklotz, J. Seelig, *Eur. Biophys. J.* **2007**, *36*, 305.
- [254] Y. K. Zheng, W. W. Liu, Y. Chen, C. M. Li, H. Jiang, X. M. Wang, *J. Colloid Interface Sci.* **2019**, *546*, 1.
- [255] G. Palmieri, R. Tate, M. Gogliettino, M. Balestrieri, I. Rea, M. Terracciano, Y. T. Proroga, F. Capuano, A. Anastasio, L. De Stefano, *Bioconjugate Chem.* **2018**, *29*, 3877.
- [256] L. H. Peng, Y. F. Huang, C. Z. Zhang, J. Niu, Y. Chen, Y. Chu, Z. H. Jiang, J. Q. Gao, Z. W. Mao, *Biomaterials* **2016**, *103*, 137.
- [257] D. Pornpattananangkul, L. Zhang, S. Olson, S. Aryal, M. Obonyo, K. Vecchio, C. M. Huang, L. F. Zhang, *J. Am. Chem. Soc.* **2011**, *133*, 4132.

- [258] S. Wang, C. Yan, X. M. Zhang, D. Z. Shi, L. X. Chi, G. X. Luo, J. Deng, *Biomater. Sci.* **2018**, *6*, 2757.
- [259] P. Surwade, C. Ghildyal, C. Weikel, T. Luxton, D. Peloquin, X. Fan, V. Shah, *J. Antibiot.* **2019**, *72*, 50.
- [260] C. Zhou, H. M. Zou, M. Li, C. J. Sun, D. X. Ren, Y. X. Li, *Biosens. Bioelectron.* **2018**, *117*, 347.
- [261] D. Kim, S. J. Kwon, X. Wu, J. Sauve, I. Lee, J. Nam, J. Kim, J. S. Dordick, *ACS Appl. Mater. Interfaces* **2018**, *10*, 13317.
- [262] I. Pal, V. P. Brahmkhatri, S. Bera, D. Bhattacharyya, Y. Quirishi, A. Bhunia, H. S. Atreya, *J. Colloid Interface Sci.* **2016**, *483*, 385.
- [263] S. Mohanty, P. Jena, R. Mehta, R. Pati, B. Banerjee, S. Patil, A. Sonawane, *Antimicrob. Agents Chemother.* **2013**, *57*, 3688.
- [264] L. H. Liu, J. Yang, J. P. Xie, Z. T. Luo, J. Jiang, Y. Y. Yang, S. M. Liu, *Nanoscale* **2013**, *5*, 3834.
- [265] O. Y. Golubeva, O. V. Shamova, D. S. Orlov, T. Y. Pazina, A. S. Boldina, I. A. Drozdova, V. N. Kokryakov, *Glass Phys. Chem.* **2011**, *37*, 78.
- [266] S. Ruden, K. Hilpert, M. Berditsch, P. Wadhvani, A. S. Ulrich, *Antimicrob. Agents Chemother.* **2009**, *53*, 3538.
- [267] E. Morales-Avila, G. Ferro-Flores, B. E. Ocampo-Garcia, G. Lopez-Tellez, J. Lopez-Ortega, D. G. Rogel-Ayala, D. Sanchez-Padilla, *J. Nanomater.* **2017**, *2017*, 1.
- [268] K. S. Yuan, Q. S. Mei, X. J. Guo, Y. W. Xu, D. T. Yang, B. J. Sanchez, B. B. Sheng, C. S. Liu, Z. W. Hu, G. C. Yu, H. M. Ma, H. Gao, C. Haisch, R. Niessner, Z. J. Jiang, H. B. Zhou, *Chem. Sci.* **2018**, *9*, 8781.
- [269] W. J. Zhang, X. H. Shi, J. Huang, Y. X. Zhang, Z. R. Wu, Y. Z. Xian, *ChemPhysChem* **2012**, *13*, 3388.
- [270] C. Blaszykowski, S. Sheikh, M. Thompson, *Chem. Soc. Rev.* **2012**, *41*, 5599.
- [271] I. Banerjee, R. C. Pangule, R. S. Kane, *Adv. Mater.* **2011**, *23*, 690.
- [272] M. Krishnamoorthy, S. Hakobyan, M. Ramstedt, J. E. Gautrot, *Chem. Rev.* **2014**, *114*, 10976.
- [273] S. Jiang, Z. Cao, *Adv. Mater.* **2010**, *22*, 920.
- [274] L. Wu, X. Qu, *Chem. Soc. Rev.* **2015**, *44*, 2963.
- [275] A. Hucknall, S. Rangarajan, A. Chilkoti, *Adv. Mater.* **2009**, *21*, 2441.
- [276] E. W. Merrill, *Ann. N. Y. Acad. Sci.* **1987**, *516*, 196.
- [277] E. Ostuni, R. G. Chapman, R. E. Holmlin, S. Takayama, G. M. Whitesides, *Langmuir* **2001**, *17*, 5605.
- [278] J. L. Dalsin, P. B. Messersmith, *Mater. Today* **2005**, *8*, 38.
- [279] N. B. Holland, Y. Qiu, M. Ruegsegger, R. E. Marchant, *Nature* **1998**, *392*, 799.
- [280] C. J. Huang, N. D. Brault, Y. T. Li, Q. M. Yu, S. Y. Jiang, *Adv. Mater.* **2012**, *24*, 1834.
- [281] C. J. Huang, Y. T. Li, S. Y. Jiang, *Anal. Chem.* **2012**, *84*, 3440.
- [282] S. Lin, B. Zhang, M. J. Skoumal, B. Ramunno, X. Li, C. Wesdemiotis, L. Liu, L. Jia, *Biomacromolecules* **2011**, *12*, 2573.
- [283] H. O. Ham, S. H. Park, J. W. Kurutz, I. G. Szleifer, P. B. Messersmith, *J. Am. Chem. Soc.* **2013**, *135*, 13015.
- [284] A. K. Nowinski, F. Sun, A. D. White, A. J. Keefe, S. Jiang, *J. Am. Chem. Soc.* **2012**, *134*, 6000.
- [285] S. Chen, Z. Cao, S. Jiang, *Biomaterials* **2009**, *30*, 5892.
- [286] J. Cui, Y. Ju, K. Liang, H. Ejima, S. Lorcher, K. T. Gause, J. J. Richardson, F. Caruso, *Soft Matter* **2014**, *10*, 2656.
- [287] H. Ye, L. Wang, R. Huang, R. Su, B. Liu, W. Qi, Z. He, *ACS Appl. Mater. Interfaces* **2015**, *7*, 22448.
- [288] G. H. Zhou, Y. Z. Liu, M. Luo, Q. F. Xu, X. H. Ji, Z. K. He, *ACS Appl. Mater. Interfaces* **2012**, *4*, 5010.
- [289] M. Cui, Y. Wang, H. Wang, Y. Wu, X. Luo, *Sens. Actuators, B* **2017**, *244*, 742.
- [290] G. Wang, X. Su, Q. Xu, G. Xu, J. Lin, X. Luo, *Biosens. Bioelectron.* **2018**, *101*, 129.
- [291] M. Cui, Y. Wang, M. Jiao, S. Jayachandran, Y. Wu, X. Fan, X. Luo, *ACS Sens.* **2017**, *2*, 490.
- [292] R. Chelmowski, S. D. Köster, A. Kerstan, A. Prekelt, C. Grunwald, T. Winkler, N. Metzler-Nolte, A. Terfort, C. Wöll, *J. Am. Chem. Soc.* **2008**, *130*, 14952.
- [293] B. Sepulveda, P. C. Angelome, L. M. Lechuga, L. M. Liz-Marzan, *Nano Today* **2009**, *4*, 244.
- [294] D. Ernenwein, P. Ghosh, V. Rotello, J. Chmielewski, *J. Mater. Chem.* **2010**, *20*, 5608.
- [295] R. Nochomovitz, M. Amit, M. Matmor, N. Ashkenasy, *Nanotechnology* **2010**, *21*, 145305.
- [296] H. M. Borteh, N. J. Ferrell, R. T. Butler, S. V. Olesik, D. J. Hansford, *Appl. Surf. Sci.* **2011**, *258*, 230.
- [297] G. Zhou, Y. Liu, M. Luo, X. Li, Q. Xu, X. Ji, Z. He, *Langmuir* **2013**, *29*, 4697.
- [298] J. Del Re, A. S. Blum, *Appl. Surf. Sci.* **2014**, *296*, 24.
- [299] Y. F. Gong, X. Chen, Y. L. Lu, W. S. Yang, *Biosens. Bioelectron.* **2015**, *66*, 392.
- [300] J. Luo, Y. Cheng, Z. W. Gong, K. Wu, Y. Zhou, H. X. Chen, M. Gauthier, Y. Z. Cheng, J. Liang, T. Zou, *Langmuir* **2020**, *36*, 600.
- [301] J. Conde, A. Ambrosone, V. Sanz, Y. Hernandez, V. Marchesano, F. Tian, H. Child, C. C. Berry, M. R. Ibarra, P. V. Baptista, C. Tortiglione, J. M. de la Fuente, *ACS Nano* **2012**, *6*, 8316.
- [302] R. P. Ahwazi, M. Kiani, M. Dinarvand, A. Assali, F. S. M. Tekie, R. Dinarvand, F. Atyabi, *J. Cell. Physiol.* **2020**, *235*, 2049.
- [303] P. Free, C. P. Shaw, R. Levy, *Chem. Commun.* **2009**, 5009.
- [304] H. Andresen, S. Gupta, M. M. Stevens, *Nanoscale* **2011**, *3*, 383.
- [305] A. E. Leffler, A. Kuryatov, H. A. Zebroski, S. R. Powell, P. Filipenko, A. K. Hussein, J. Gorson, A. Heizmann, S. Lyskov, R. W. Tsien, S. F. Poget, A. Nicke, J. Lindstrom, B. Rudy, R. Bonneau, M. Holford, *Proc. Natl. Acad. Sci. U. S. A.* **2017**, *114*, E8100.
- [306] S. Brenet, A. John-Herpin, F. X. Gallat, B. Musnier, A. Buhot, C. Herrier, T. Rousselle, T. Livache, Y. X. Hou, *Anal. Chem.* **2018**, *90*, 9879.
- [307] J. S. Han, H. R. Cheng, B. H. Wang, M. S. Braun, X. B. Fan, M. Bender, W. Huang, C. Domhan, W. Mier, T. Lindner, K. Seehafer, M. Wink, U. H. F. Bunz, *Angew. Chem., Int. Ed.* **2017**, *56*, 15246.
- [308] J. R. Waldeisen, T. Wang, B. M. Ross, L. P. Lee, *ACS Nano* **2011**, *5*, 5383.
- [309] P. Chen, X. Liu, G. Goyal, N. T. Tran, J. C. S. Ho, Y. Wang, D. Aili, B. Liedberg, *Anal. Chem.* **2018**, *90*, 4916.
- [310] A. D. Quach, G. Crivat, M. A. Tarr, Z. Rosenzweig, *J. Am. Chem. Soc.* **2011**, *133*, 2028.
- [311] J.-H. Choi, H. Kim, J.-H. Choi, J.-W. Choi, B.-K. Oh, *ACS Appl. Mater. Interfaces* **2013**, *5*, 12023.
- [312] A. S. D. S. Indrasekara, B. J. Paladini, D. J. Naczynski, V. Starovoytov, P. V. Moghe, L. Fabris, *Adv. Healthcare Mater.* **2013**, *2*, 1370.
- [313] P. Chen, N. T. Tran, X. L. Wen, Q. H. Xiong, B. Liedberg, *ACS Sens.* **2017**, *2*, 235.
- [314] S. Sharifi, S. Behzadi, S. Laurent, M. L. Forrest, P. Stroeve, M. Mahmoudi, *Chem. Soc. Rev.* **2012**, *41*, 2323.
- [315] A. Pietroiusti, H. Stockmann-Juvala, F. Lucaroni, K. Savolainen, *Wiley Interdiscip. Rev.: Nanomed. Nanobiotechnol.* **2018**, *10*, e1513.
- [316] I. Fratoddi, I. Venditti, C. Cametti, M. V. Russo, *Nano Res.* **2015**, *8*, 1771.
- [317] S. C. Fernandes, J. A. Walz, D. J. Wilson, J. C. Brooks, C. R. Mace, *Anal. Chem.* **2017**, *89*, 5654.
- [318] S. J. Klaine, P. J. J. Alvarez, G. E. Batley, T. F. Fernandes, R. D. Handy, D. Y. Lyon, S. Mahendra, M. J. McLaughlin, J. R. Lead, *Environ. Toxicol. Chem.* **2008**, *27*, 1825.